



TAMPERE UNIVERSITY OF TECHNOLOGY

LUIS MIGUEL ORONA DOMINGUEZ

OPTIMIZATION AND REDESIGN OF A SPHERICAL WRIST FOR
A WATER HYDRAULIC MANIPULATOR

Master of Science Thesis

Examiner: Professor Jouni Mattila
Examiner and topic approved in the
Faculty of Automation, Mechanical
and Materials Engineering Council
meeting on 4th of May 2011

ABSTRACT

TAMPERE UNIVERSITY OF TECHNOLOGY

Master's Degree Programme in Machine Automation

ORONA, LUIS: Optimization and redesign of a spherical wrist for a water hydraulic manipulator

Master of Science Thesis, 80 pages, 11 Appendix pages

August 2011

Major: Mechatronics

Examiner: Professor Jouni Mattila

Keywords: Vane actuator, manipulator, water hydraulic, spherical wrist, WHMAN, ITER.

Robot arm manipulators have a wrist to change the orientation of its end-effector. Since the wrist is located at the end of the robot arm, as the wrist in a human arm, its weight has a big influence in the dynamics of the robot. This is because a large weight represents large inertial forces for the arm actuators.

This thesis presents the redesign and optimization of a spherical wrist for a Water Hydraulic MANipulator (WHMAN), having as a major objective reducing the size and weight of the wrist. The wrist has three actuators in order to have three degrees of freedom; these are water hydraulic rotary vane actuators.

The redesign process was divided into two parts. First the redesign of the vane actuators; for this part is explained theory regarding these actuators and the equations to calculate their characteristics are defined. Also is developed and reported an approach to define the requirements and to size the water hydraulic vane actuators. Second part is the redesign of the wrist; the components of the new wrist are shown and the improvements in the design are explained.

This mechanical redesign was validated with Finite Element Method (FEM) analyses, their results are presented. With this redesign work the wrist structure is more compact and weights less (about 50%). Also the dexterity of the WHMAN is improved by reducing the hand length on the wrist.

PREFACE

This Master of Science Thesis has been undertaken at Tampere University of Technology at the Department of Intelligent Hydraulics and Automation.

I would like to thank my supervisor Prof. Jouni Mattila and my colleagues at the office for their availability in helping me to develop this Thesis. Working with people with such experience and knowledge was always very helpful for me.

With this Master of Science thesis is concluded a personal project that I started about three years ago. The goal in this project was to obtain a Master of Science Degree from a European University. I am very glad and satisfied to have chosen Finland as the country to study; here I met great people whom I am proudly to call them friends.

I want to thank all my friends and also to a very special Russian girl, that were somehow related to this work, by advising me, encouraging me and been always positive.

Quiero dedicar este trabajo a mis padres Rafael y Alicia, ya que gracias a su apoyo pude concluir una meta más en mi vida. También quiero agradecer a mi familia y amigos por siempre contar con ellos, especialmente a mi hermana Dehira y a mis abuelos Luis y Consuelo por su apoyo durante momentos muy importantes.

Tampere, Finland August 2011

Luis Miguel Orona Domínguez

TABLE OF CONTENTS

1. INTRODUCTION	1
1.1. Background	1
1.2. Scope of the work	5
2. THEORETICAL BACKGROUND	6
2.1. Hydraulic Vane Actuators	6
2.1.1. Design Parameters	7
2.1.2. System Characteristics	8
2.2. Actuator Flexibilities in the Control System	11
2.3. Wrist of Robot Manipulator	13
2.4. Finite Element Method theory	15
2.4.1. A comparison between solving a problem with formulas and with Finite Element Method (FEM)	18
3. DESIGN REQUIREMENTS	23
3.1. General Requirements: Wrist	23
3.2. Specific requirements: Water hydraulic vane actuator	24
3.2.1. Design Requirements previously defined	24
3.2.2. Analysis of load, torque and moment of inertia based on current 3D models	25
3.2.3. Design Criteria	27
4. VANE ACTUATOR NEW DESIGN	30
4.1. Sizing of the vane actuators	30
4.1.1. Nature of the design	30
4.1.2. Characteristic of the current vane actuators in the wrist	32
4.1.3. Optimum Design based on the requirements	33
4.2. Materials review	38
4.3. Mechanical components of the new vane actuator design	39
4.3.1. Chamber	40
4.3.2. Shaft	42
4.3.3. Bearings	43
4.3.4. Side sealings	44
4.3.5. Bearing housings	44

4.3.6.	Fluid passages	45
4.3.7.	Seals on the vane actuators	46
4.3.8.	Valve block	48
4.4.	Comparison between new and current vane actuator designs	48
5.	NEW WRIST DESIGN	50
5.1.	Wrist of the WHMAN	50
5.2.	Mechanical design and breakdown of the wrist	51
5.2.1.	Link four	53
5.2.2.	Link five	54
5.2.3.	Link six	54
5.3.	Some improvements in the new wrist design	55
5.4.	Comparison between new and current wrist design	56
6.	STRUCTURAL VALIDATION OF THE WRIST COMPONENTS	59
6.1.	Finite element analysis	59
6.2.	Structural validation of the main components in the vane actuator	59
6.2.1.	Chamber and vanes FEM structural analysis	59
6.2.2.	Shaft and vanes FEM structural analysis	62
6.3.	Structural validation of the wrist links	67
6.3.1.	Link 6 structural analysis	67
6.3.2.	Link 5 structural analysis	70
6.3.3.	Link 4 structural analysis (only for the modified components)	73
7.	CONCLUSIONS	77

ABBREVIATIONS AND NOTATION

α_t	Angle of twist
Δp	Pressure difference across the vanes
ε	Strain vector
θ	Motion range
ν	Poisson's ratio
σ	Stress vector
σ_y	Yield strength
τ	Shear stress
τ_{max}	Maximum shear stress
τ_{xz}	Shear stress in the x-z plane
ω	Angular speed
ω_h	Hydraulic natural frequency
ω_n	Closed-loop system natural frequency
ω_{res}	Lowest structural resonance frequency
ω_s	Mechanical natural frequency
A	Cross sectional area
a_1	Offset distance
b	Chamber length
B	Bulk modulus
B_e	Element strain-displacement vector
c	Outer radius of the shaft
$C1$	External shaft radius 1
$C2$	External shaft radius 2
C_{int}	Internal shaft radius
C_n	External shaft radius n, n is any integer
D	Material matrix
D_v	Radian volume
E	Young modulus
F	External load
F_a	Axial force
F_r	Radial force
G	shear modulus
I	Moment of inertia
J	Polar moment of inertia
$J5$	Joint five
$J6$	Joint six
$J7$	Joint seven
K	Stiffness matrix
K^e	Element stiffness matrix
K_h	Hydraulic torsion stiffness
K_s	Mechanical torsion stiffness

L	Length of the shaft
$L1$	Shaft length 1
$L2$	Shaft length 2
L_d	Linear deformation
L_n	Shaft length n, n is any integer
m	mass
P_o	Equivalent static load
Q	Fluid flow
Q_d	Displacement vector
r	Radius
$R1$	Chamber radius
$R2$	Shaft radius
T_e	Torque applied to one end of the shaft
T_o	Theoretical output torque of the vane actuator
V	Volume capacity
V_L	Volume of the pipe
Y_o	Calculation factor of a bearing

CMM	Cassette Multifunctional Mover
DOF	Degree Of Freedom
DRM	Divertor Region Mock-Up
DTP2	Divertor Test Platform 2
FEM	Finite Element Method
FOS	Factor Of Safety
IHA	Department of Intelligent Hydraulics and Automation
POM	PolyOxyMethylene
SCEE	Second Cassette End-Effector
SR	Stiffness Ratio
TUT	Tampere University of Technology
UHMW-PE	Ultra High Molecular Weight Polyethylene
VTT	Technical Research Centre of Finland
WHMAN	Water Hydraulic MANipulator

1. INTRODUCTION

1.1. Background

This work continues the developing of a Water Hydraulic MANipulator (WHMAN) suitable for developing remote handling maintenance tasks in the experimental reactor ITER. The ITER is an international project that aims to demonstrate the feasibility of producing commercial energy from fusion. It is a joint project between European Union, USA, China, Japan, South Korea, Russia Federation and India.

Figure 1 shows the reactor that is based on the ‘tokamak’ concept, which is a device that uses a magnetic field to confine plasma in the shape of a torus or doughnut.

One large source of energy to the world is the sun, and it produces energy by fusion. In the sun, plasma is created by the fusion of two light Hydrogen atoms that produces a heavier element Helium. Due to the fusion, the core of our sun reaches temperatures of 15 000 000° Celsius [1]. Basically the idea of the ITER project is to create plasma on earth and from it generate electricity.

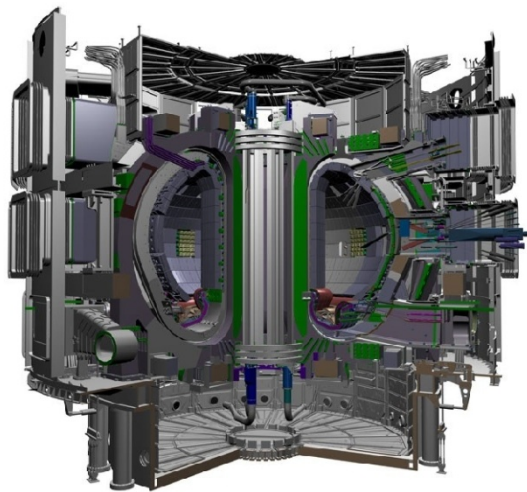


Figure 1: ITER based on the tokamak concept [1].

In the last century fusion science has found that the most efficient fusion reaction to be produced in the laboratory is between two Hydrogen isotopes: Deuterium (D) and Tritium (T). However, it requires the tremendous temperature of 150 000 000 °C (ten times more than at the core of the sun) to take place [1], this is why the plasma is confined in the shape of a torus away from the walls.

The ITER is not yet a power plant, is still an experimental reactor in which key technologies like plasma heating, control, diagnostics and remote handling for the development of future fusion power plants will be tested.

The ITER reactor is a huge machine composed of numerous parts, made of different materials which have specific functions. The Vacuum Vessel shown in Figure 2 has at the bottom of it the Divertor shown in Figure 3 and Figure 4.

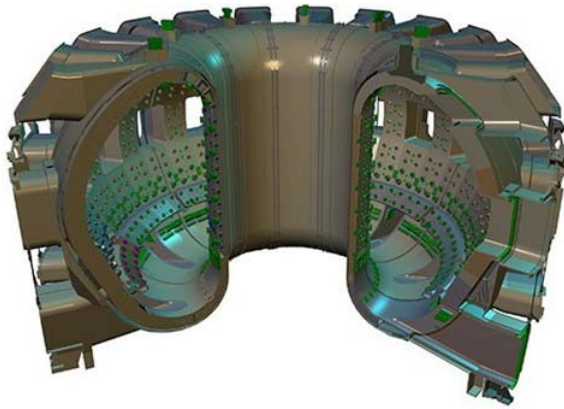


Figure 2: Vacuum Vessel [1].

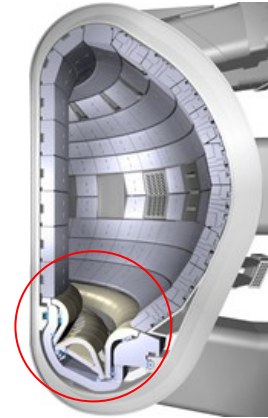


Figure 3: Divertor in the Vacuum Vessel [1].

As mention in [1] the Divertor is one of the key components in the ITER machine. Its function is to extract heat and Helium ash produced during the fusion process. It is built up of 54 remotely removable Cassettes like the one shown in Figure 5; each of them has three plasma facing components and weighs about 10 tons. For more information about the ITER machine and its subsystems see [1].

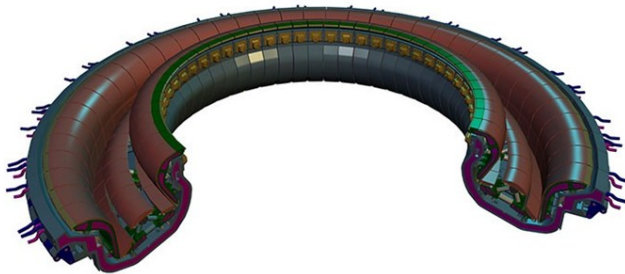


Figure 4: Divertor [1].

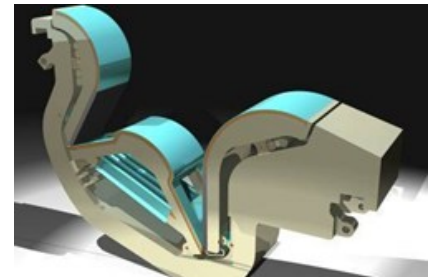


Figure 5: Cassette [1].

Teleoperated robots are needed to place and remove the Cassettes on the Divertor, during the assembly of the reactor and during the maintenance of it. At the Department of Intelligent Hydraulics and Automation (IHA) in the Tampere University of Technology (TUT), have been developed remote handling manipulators to perform these tasks, for example the CMM (Cassette Multifunctional Mover) with the SCEE (Second Cassette End Effector) and the WHMAN (Water Hydraulic Manipulator). Figure 6 shows the 3D models of these robots.

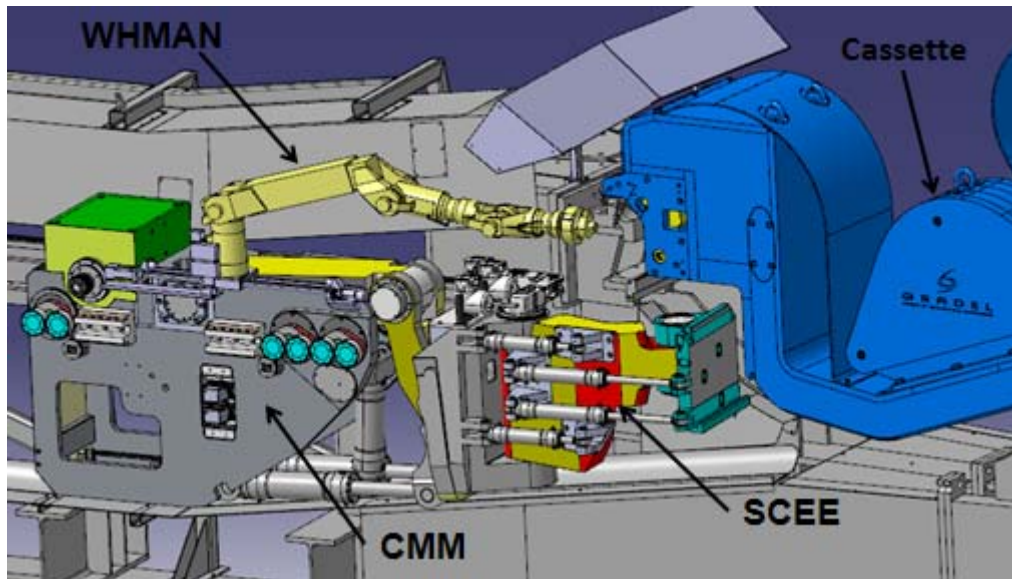


Figure 6: Teleoperated robots.

These robots have the general requirement of manipulate heavy loads in a very limited space with high accuracy. This is why the main actuators for the robots are hydraulic actuators. Since hydraulics systems may have leakages, the used of oil is not allowed due to the risk of contamination. The hydraulic fluid use is demineralised water which does not represent a risk of contamination and moreover is not affected by the radiation.

The prototypes of these robots are being tested in the full-scale Divertor Region Mock-up (DRM), which is in the Divertor Test Platform 2 (DTP2) facility, located in VTT the Technical Research Centre of Finland in Tampere, Finland (Figure 7).



Figure 7: Divertor Region Mock-up [2].

This Thesis is focused in the WHMAN, which is a 6 DOF robot arm. A water hydraulic rotary actuator to actuate the joints of the WHMAN was developed in [3] later the same author developed the wrist for the WHMAN. Afterwards in [4] was developed

the arm which combined with the wrist constitute what is known as the WHMAN shown in Figure 8.

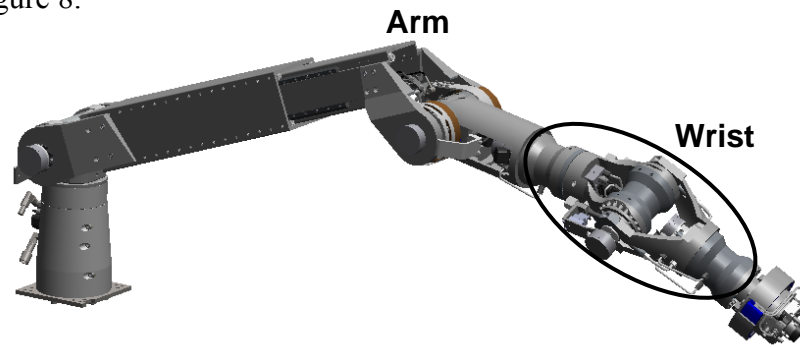


Figure 8: WHMAN.

The requirements of manipulating heavy loads in a limited space with high accuracy can be translated in to have small, strong and stiff actuators mounted in light and stiff structures; their assembly (actuators and structures) is the robot.

One of the main difficulties of having a stiff actuator that means large actuator and vice versa, is to design the smallest actuator with sufficient stiffness for the specific application. The problem is in defining the requirements (how stiff the actuators need to be) which leads the application of different design criteria. In general the experience of the designer is very important to establish the requirements. As seen in Figure 8, for example, the wrist constitutes a big part of the robot structure, and represents a heavy load at the end of the manipulator which affects the dynamic properties of it. The wrist is big, heavy and robust because its actuators are very large due to they were sized to meet certain stiffness requirements. Figure 9 shows a closer view of the actuators in the wrist.

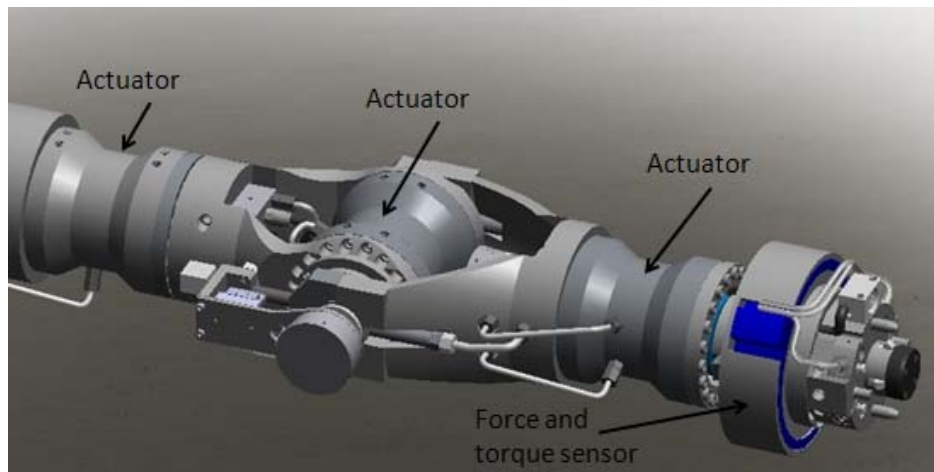


Figure 9: Wrist of the WHMAN.

The development to lock the second Cassette in the DRM shows that exist a collision between the WHMAN and the blanket module of the DRM. The collision is shown in Figure 10. Three solutions to avoid the collision were proposed [5]: a) to change the insertion angle of the tool, or b) to modify the tool used in that operation or c) to shorten the length of the WHMAN.

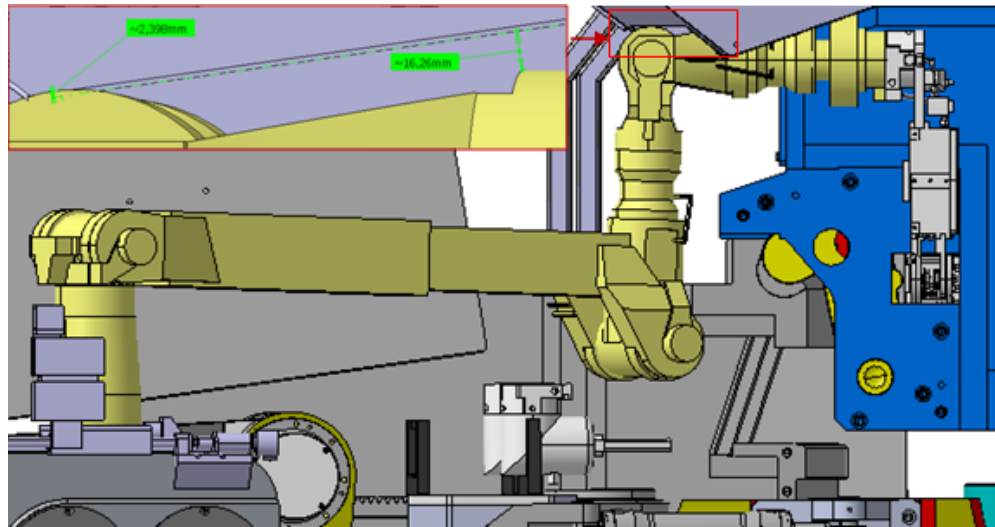


Figure 10: Collision between WHMAN and the blanket module in the DRM [5].

Even if there are other easier solutions than modify the WHMAN structure to avoid this collision, a redesign of the wrist that will make it smaller and lighter, will help to avoid this collision as well as to have a more dexterous and reliable manipulator.

1.2. Scope of the work

The main objective of this Thesis is the mechanical redesign and optimization of the wrist for the WHMAN. The mechanical redesign includes the redesign of the water hydraulic vane actuators and the structural redesign of the wrist, focused in reducing the size and weight of the overall wrist.

Since the size of the wrist is proportional to the size of the actuators, one of the key objectives in this work is to define the requirements for the hydraulic rotary vane actuators to be met in terms of torque, mechanic and hydraulic stiffness among others and based on them resize the actuators.

Also an easier and efficient way for the assembly and construction of the wrist and actuators is aim of this work.

Chapter 2 describes some theoretical background of the vane actuator and the equations that describe it. There is also an explanation of the relation between the mechanical design of the vane actuator and the design of the control system. Also theory regarding the wrist of a manipulator is presented. Finally theory of the validation of mechanical designs using Finite Element Method (FEM) is explained. Proposed method was used to validate the new mechanical designs introduced in this Thesis.

Third chapter presents the general requirements for the wrist and the specific requirements for the water hydraulic rotary vane actuators. The definition of the latter ones is a very important task to be developed since based on them the actuators will be resized. Chapters 4 and 5 present the mechanical redesign of the water hydraulic rotary vane actuator and the mechanical redesign of the wrist respectively.

In Chapter 6 is presented the structural validation of the new mechanical designs and finally the conclusions are in Chapter 7.

2. THEORETICAL BACKGROUND

This chapter presents the technical and theoretical background used in this Thesis. Section 2.1 presents the theory regarding the hydraulic vane actuator used later in Chapter 4 to develop the new design. Section 2.2 explains the relation between the mechanical characteristics of the vane actuator and the control system, which is used in Chapter 3 to develop the requirements. Section 2.3 describes some basic theory about the function of the wrist in robot manipulators. Finally Section 2.4 presents some theory regarding the Finite Element Method (FEM) analysis, this method is used later in Chapter 6 to validate the new mechanical designs of the water hydraulic vane actuator and the wrist.

2.1. Hydraulic Vane Actuators

The hydraulic vane actuator (rotary actuator) is a hydraulic device used in many fields when rotary actuation is needed. As an example, Figure 11 shows a typical vane actuator. One of the main characteristics of these actuators is that they produce high torque at low angular speed, making possible the direct connection of the actuator to the system (without any transmission).

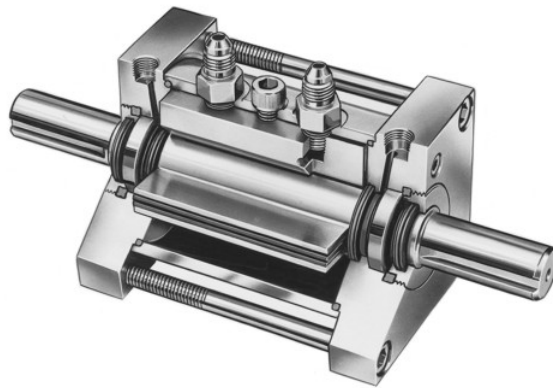


Figure 11: Rotary vane actuator [6].

Typically there are two designs for vane actuators; one-vane and double-vane, illustrated in Figure 12. The single-vane actuator has a cylindrical chamber where a vane connected to a shaft rotates in an arc of about 280° [7]. Two ports for the fluid flow (input and output) are separate by a vane on the chamber. The double-vane actuator has two diametrically opposed vanes in the shaft and in the chamber. This construction provides twice the torque (in comparison to a single-vane actuator of the same size) at the expense of lower motion range typically 135° - 140° . In both designs, differential pressure applied across the shaft vane or vanes, rotates the shaft until its vane(s) and chamber vane(s) meets.

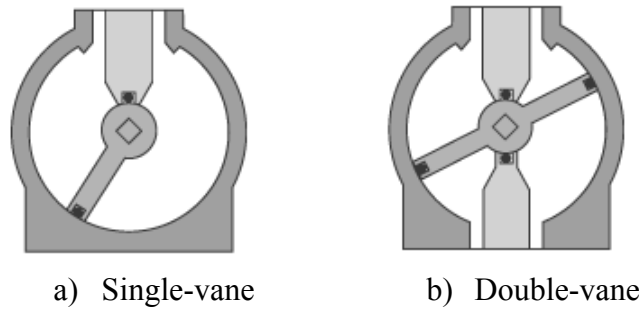


Figure 12: Cross section of single-vane and double-vane actuators [7].

In general, a vane actuator can be considered as a system which has Design Parameters (inputs to the system) and System Characteristics (outputs of the system) as shown in Figure 13, from now on all refers to hydraulic single-vane actuators.

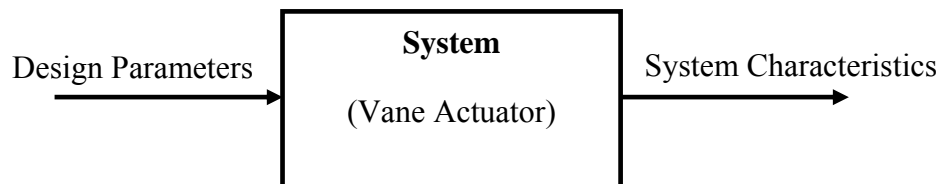


Figure 13: System Representation.

2.1.1. Design Parameters

Following are listed the design parameters used in the redesign of the vane actuators:

Main design parameters

- Chamber radius ($R1$)
- Shaft radius ($R2$)
- Chamber length (b)

Shaft design parameters

- Internal shaft radius (C_{int})
- External shaft radius 1-minimum ($C1$)
- Shaft length 1 ($L1$)
- External shaft radius 2 ($C2$)
- Shaft length 2 ($L2$)

Figure 14 (chamber of the vane actuator) and Figure 15 (shaft of the vane actuator) shows these design parameters. There can be more design parameters, e.g. more for the chamber, but for the purposes of defining the size of an optimal vane actuator for the wrist, these are enough. Depending on the design, the value for C_{int} , $C2$ and $L2$ can be zero or also there can be C_n and L_n , where n is any integer number.

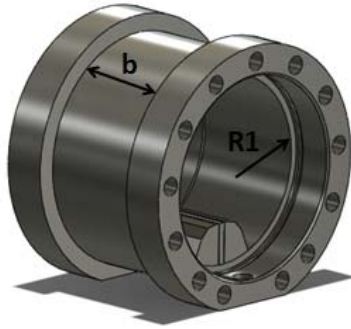


Figure 14: Chamber of the Vane Actuator.

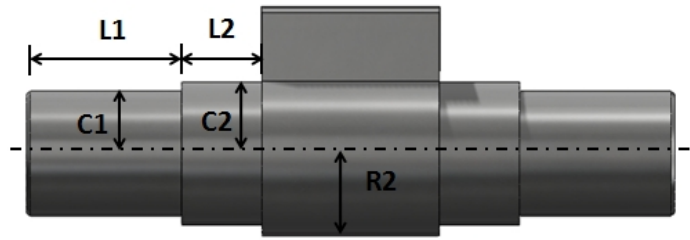


Figure 15: Shaft of the Vane Actuator.

2.1.2. System Characteristics

The system characteristics are the outputs of the system; these must match with the requirements. Below are listed the system characteristics used in the redesign of the vane actuator:

- Torque (T)
- Angular speed (ω)
- Shaft Factor Of Safety (Shaft FOS)
- Mechanical Torsion Stiffness (K_s)
- Hydraulic Torsion Stiffness (K_h)
- Stiffness Ratio (SR)

Following are the equations for the system characteristics.

Torque

In order to understand better how the torque is computed, first is needed to define some other characteristics of the vane actuator regarding its size.

Cross-sectional area:

$$A = \pi(R1^2 - R2^2) \quad (1)$$

Volume capacity:

$$V = A \cdot b \quad (2)$$

Radian volume:

$$D_v = \frac{V}{2 \cdot \pi} \quad (3)$$

Finally, the theoretical output torque is given by:

$$T_o = D_v \cdot p = \frac{1}{2} (R1^2 - R2^2) \cdot b \cdot \Delta p \quad (4)$$

Where: Δp = pressure difference across the vanes.

Angular speed

The angular speed is given by:

$$\omega = \frac{Q}{D_v} = \frac{2 \cdot Q}{(R1^2 - R2^2) \cdot b} \quad (5)$$

Where: Q = the fluid flow.

Shaft factor of safety

This is the relation between the yield strength of the material and the shear stress on the material generated by external loads.

$$FOS = \frac{\sigma_y}{2 \cdot \tau} \quad (6)$$

Where: σ_y = yield strength

τ = shear stress, and is defined as [8]:

$$\tau = \frac{2 \cdot T_e \cdot C_1}{\pi \cdot [(C_1)^4 - (C_{int})^4]} \quad (7)$$

Where: C_1 and C_{int} = design parameters

T_e = torque applied to one end of the shaft

Mechanical Torsion Stiffness

The mechanical torsion stiffness is the relation between the torque acting on the shaft and the angular deformation (angle of twist) of the shaft due to the applied torque.

$$K_s = \frac{T_e}{\alpha_t} \quad (8)$$

Where: α_t = angle of twist

Since the angle of twist also depends on the torque applied, when Equation (8) is expanded, can see that the mechanical torsion stiffness does not depends on the torque, only depends on the size of the shaft, Equation (9) shows this.

$$K_s = \frac{1}{\frac{2}{\pi \cdot G} \cdot \sum_{i=1}^n \left[\frac{L_i}{(C_i)^4 - (C_{int})^4} \right]} \quad (9)$$

Where: C_i , L_i and C_{int} = design parameters
 G = shear modulus

The mechanical torsion stiffness defined in Equation (9) is for the case when only one end of the shaft is subjected to torque. When both ends of the shaft are subjected to external torque, half of this torque is applied to each end of the shaft, which means that the mechanical torsion stiffness will be twice and the angular deformation will be half.

Hydraulic Torsion Stiffness

The hydraulic torsion stiffness is defined as [9]:

$$K_h = \frac{4 \cdot D_v^2 \cdot B}{D_v \cdot \theta + V_L} \quad (10)$$

Where: D_v = Radian volume
 B = Bulk modulus of the fluid
 V_L = Volume of the pipe
 θ = Motion range

Since the hydraulic torsion stiffness depends on the position of the vane, the formula presented is to calculate the minimum torsion stiffness. The volume of the pipe (line that connects the valve with the actuator) is sometimes neglected since this volume is much smaller than the volume of fluid inside the actuator.

Stiffness ratio

This is a relation between the mechanical and hydraulic torsion stiffness. This ratio is an important criterion for the design of the vane actuator.

$$SR = \frac{K_s}{K_h} \quad (11)$$

Where: K_s = Mechanical torsion stiffness
 K_h = Hydraulic torsion stiffness

The equations used for sizing the water hydraulic vane actuator according to the requirements have now been defined.

2.2. Actuator Flexibilities in the Control System

Since the main objective of this Thesis is the redesign of a robot wrist, which includes the redesign of the actuators on it, in this subchapter is explained the relation between the mechanical design of the vane actuator with the design of the control system. In Figure 16, is shown the basic diagram of a control system.

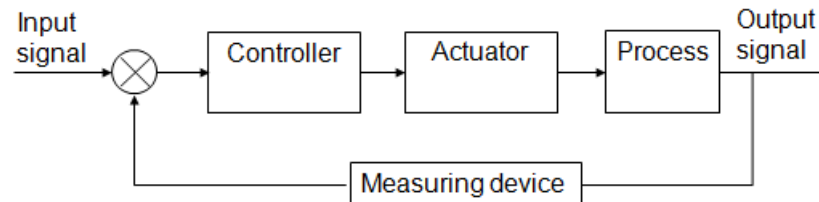


Figure 16: Control System Diagram.

The controller sends a signal to the actuator and based on it the actuator modifies a variable in the process (e.g. the opening of a valve or the position of a linkage in a mechanism among others). In the case of robot actuators, they actuate joints connected by links in an open kinematic chain like the one shown in Figure 17.

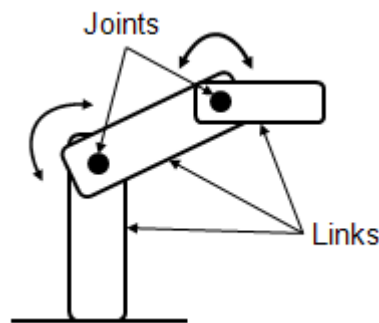


Figure 17: Open kinematic chain.

The actuators in most cases are electric, pneumatic or hydraulic devices constructed of mechanical parts. These actuators are specified by certain characteristics for example: nominal voltage, nominal pressure, efficiency, accuracy, speed, dimensional characteristics among others.

From the control engineering point of view the stiffness/flexibility of the system is very important, in this case we focus on the flexibility of the actuator. When the equations of the dynamic model to be controlled are developed, many times assumptions about ignoring the flexibilities of the actuators are made to have a simpler model (lower order). However, often if the actuator is not stiff enough this assumption is invalid and flexibilities have to be taken into account. This will make the equations of higher order, adding complexity to the design of the control system. To understand better this, the stiffness of an actuator is presented as an example.

Let's assume there is an actuator and its shaft is connected to a disk with inertia as shown in Figure 18a. A control system forces the actuator to rotate to place the disk in different positions (e.g. 90° from its original position).

In this example, the stiffness of the actuator is related to its shaft because it is not completely rigid (is flexible). The shaft stiffness (K_s) in this case is like a torsion spring constant (Figure 18b) and can be calculated with Equation (9).

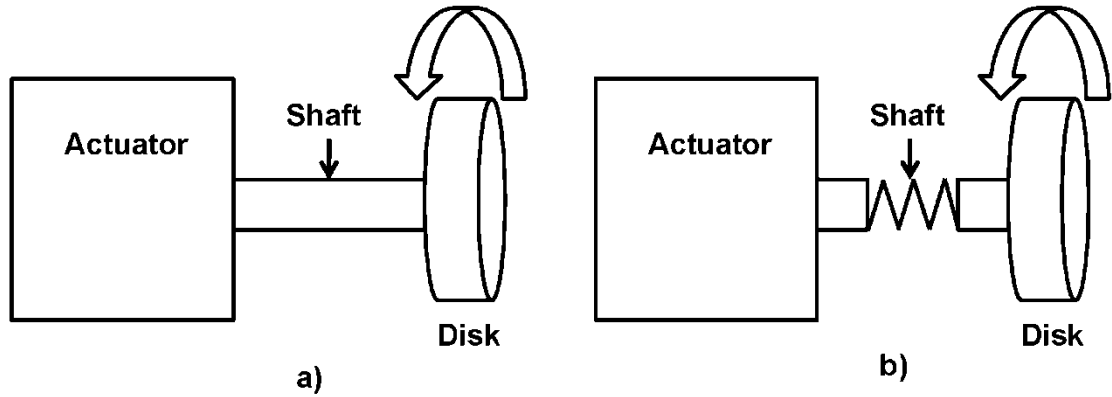


Figure 18: Actuator-Disk System

The disk of radius r and mass m has a moment of inertia I , Equation (12). The natural frequency of the shaft, in this example is the natural frequency of the actuator and can be computed with Equation (13).

$$I = \frac{mr^2}{2} \quad (12)$$

$$\omega_s = \sqrt{\frac{K_s}{I}} \quad (13)$$

The flexibility effects the actuator has can be ignored only if it is sufficiently stiff, this is, only if its natural frequency (ω_s) is bigger in comparison with the natural frequency of the closed-loop system (ω_n).

How much bigger has to be ω_s compared with ω_n is sometimes difficult to establish, for this will be use a rule of thumb mentioned in [10], shown in Equation (14). This rule establish that the lowest structural resonance frequency ω_{res} (in the example ω_s) has to be at least two times bigger than the closed-loop natural frequency of the system in order to ignore (unmodeled) the effect of the structural flexibilities of the actuator, in developing the control system.

$$\omega_{res} \geq 2 \cdot \omega_n \quad (14)$$

Where: ω_{res} = Lowest structural resonance frequency

ω_n = Closed-loop natural frequency of the system

In Equation (14) the closed-loop natural frequency (ω_n) of the system has to be assumed or calculated based on certain specifications for the control system (e.g. by specifying the bandwidth and overshoot), then ω_{res} is calculated. After this the lowest structural resonance frequency on the system is identified and the value of ω_{res} is assigned to it. In this example ω_s is equal to ω_{res} , then from Equation (13) the value of the shaft stiffness (K_s) is calculated, and finally with Equation (9) the radius or length of the shaft is computed (one has to be defined since there still are two unknowns in one equation). With this procedure, an actuator which is stiff enough that allows to ignore its flexibilities is designed.

There can be two approaches for the use of Equation (14), the first one already explained in the last paragraph, can be considered the mechanical approach. The second one can be considered as the control approach, and is when the system is already built and the task is just to control it. In this case, the flexibilities in the system are calculated, then the lowest is assigned to ω_{res} , with Equation (14) but now in the form of Equation (15) the closed-loop natural frequency (ω_n) of the system is calculated. This frequency is related to the bandwidth of the system, also the value of ω_n limits the magnitude of the gains in the control system [10].

$$\omega_n \leq \frac{1}{2} \omega_{res} \quad (15)$$

In many cases it is hard to define the value for the lowest structural resonance natural frequency because it varies depending on the configuration/position of the system and thus several natural frequencies can be computed. In this case the worst scenario (lowest structural stiffness and highest moment of inertia value) has to be compared with the closed-loop natural frequency of the system.

2.3. Wrist of Robot Manipulator

At least six degrees of freedom (DOF) in a robot manipulator are required in order to move an object freely in the space. The first three degrees of freedom are used for manipulating the position of the end effector, and the last three degrees of freedom for changing the orientation of it. Because of this, the first three joints and its corresponding links are called the arm (or major links) and the assembly of the last three joints and links is called the wrist (or minor links) [11].

There are many configurations for a robot arm and for a wrist; two common configurations for robot wrists are the spherical wrist shown on Figure 19 and the non-spherical wrist on Figure 20. In the spherical wrist, all its three joint axes intersect at a single point called the wrist center, this makes possible to decouple the position from the orientation during the kinematic analysis of the manipulator [12]. In the case of the non-spherical wrist, its three axes do not intersect at a single point because it has an offset distance (a_1).

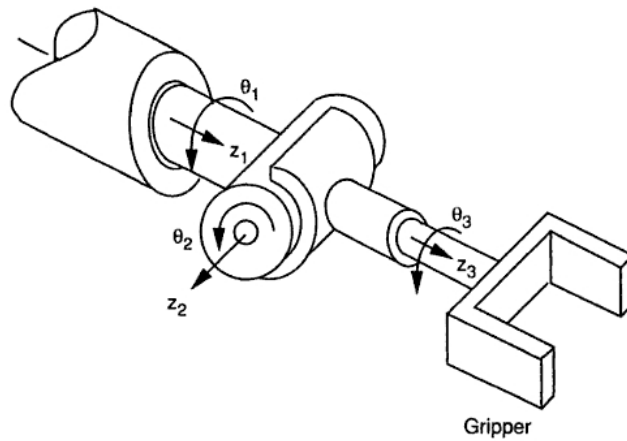


Figure 19: Spherical wrist configuration [13].

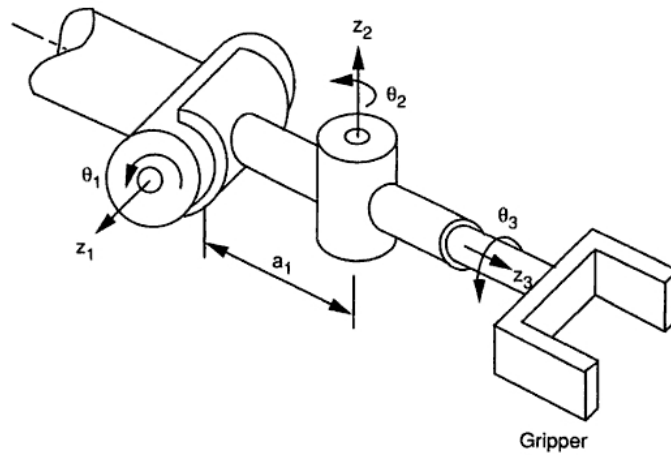


Figure 20: Non-spherical wrist configuration [13].

In a spherical wrist, the distance between the second joint axis and the end effector measured along the third joint axis as shown on Figure 21, it is called the hand length [14]. If the hand length is zero, meaning that the three axes of the wrist intersect at the tool tip of the robot arm; the reachable workspace becomes the dexterous workspace. In practice is very hard to design a zero hand length spherical wrist due to mechanical constrains. A comparison between the reach ability of a zero hand length and a non-zero hand length spherical wrists is developed in [14], the results shows that the hand length reduces the accessibility region of the wrist.

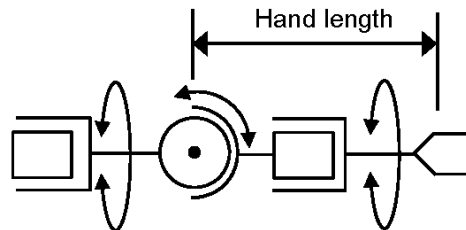


Figure 21: Hand length in the spherical wrist.

The way the wrist changes the orientation of the end effector is by a suitable sequence of three rotations (one rotation with each joint), this sequence of rotations is

known as Euler angles, this is way sometimes the wrist of a robot manipulator is called Euler angle wrist. Following are presented the characteristic identified in [13] that in practice a good wrist design should have:

1. Three degrees of freedom
2. Spherical motion
3. Large workspace (in this case large angular orientation range)
4. Remote drive capability
5. Compact size, light weight, and low inertia
6. High accuracy and repeatability
7. High mechanical stiffness
8. Low manufacturing cost
9. Rugged and reliable design

In this work, effort is put especially to fulfill the point number five. This because due to the wrist is located at the end of the arm, a heavy wrist will increase the inertia load for the actuators in the arm affecting the dynamic properties of the manipulator. Normally to avoid this, mechanical transmissions are use to actuate the joints which allow to install the actuators away from the wrist. Unfortunately, this is not possible for the design of the WHMAN wrist because direct actuation for the links is being used due to the nature of the actuator (low speed and high torque). Direct actuation has some pros for example the system is much simpler due to the lack of mechanical transmissions (no gear boxes). But the actuators become part of the links increasing the weight of it; this is why small and lighter actuators have to be designed.

2.4. Finite Element Method theory

The structures and mechanical components are validated using theory of mechanics of materials. This branch of the mechanics studies the relationships between the external loads applied to a body and the intensity of the internal forces acting within the body. This subject also studies the deformations of the body and its stability when is subjected to external forces.

In the design of structures or machines, it is necessary to determine if the components on them will work according to what is expected. From the mechanical point of view, in order to know this, first is necessary to use the principles of statics to determine the forces acting on and within its members. After this, the stresses and deformations are calculated based on these forces, the size (shape) of the member, and the characteristics of the material. Then by computing a factor of safety (FOS), it is possible to conclude if the members of the structure or machine are being correctly designed. The FOS is the relation between the stress which makes the material start yielding (for ductile materials) or start fracturing (for brittle material) and the maximum

stress on the member due to external forces. Usually a factor of 1.5 or 2 is used meaning that the part can hold 1.5 times or 2 times the maximum stress calculated.

When an external force is applied to a body in equilibrium, internal forces which try to keep the equilibrium will be generated. The intensity of these forces acting over an area is the stress. When the force acts normal to the area the stress generated is called normal stress and when acts tangent is called shear stress.

Since the stress depends on the external loads and the shape of the part (length, width, cross section among others), parts with complex shapes are difficult to analyze applying formulas (by pen and paper). In such cases is used the finite element method (FEM), which is a numerical method that divides the part that is being analyzing in several smaller elements and after that is calculated the stresses, deformations, strains, etc. for each smaller element.

The procedure regarding how is computed the stresses on a body (subjected to external loads) using finite element method is explained. Consider the bar in Figure 22a which is subjected to an external load F . The first step is to divide the bar into smaller finite elements as shown in Figure 22b. This is also known as the meshing of the part.

In this case, the bar is divided into two elements; each element is delimited by two nodes. One key point to understand here is that the stress is calculated for each element while the displacement is calculated for each node. This example is an one dimensional problem since the nodes can only move along the horizontal axis. Due to node 1 is at the fix point of the bar its displacement is zero, this is known as a boundary condition.

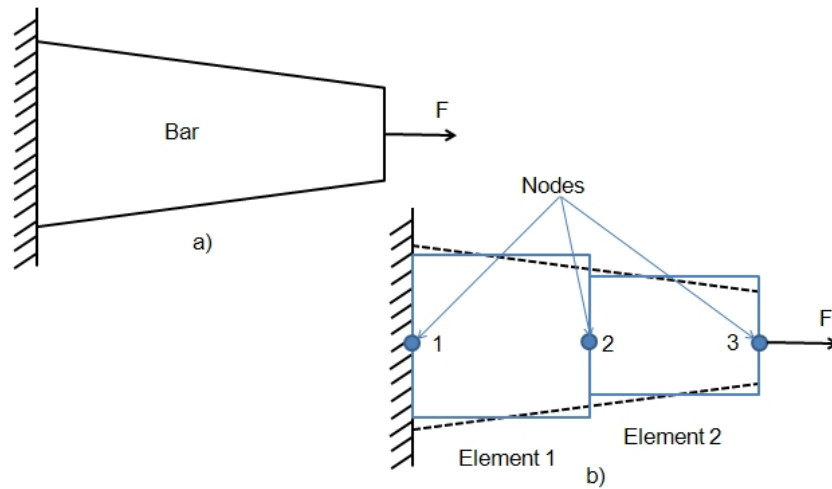


Figure 22: Finite element modeling of a bar (one dimension).

After dividing the body, the stiffness matrix (k^e which depends on the properties of the material and shape of the element) is calculated for each element and with these, the stiffness matrix of the whole body is assembled. Then by applying Equation (16) the displacement vector is computed. In this case K and F are known.

$$KQ_d = F \quad (16)$$

Where: K = stiffness matrix assembled from all the k^e

Q_d = displacement vector (displacement for each node)

F = force vector (external load) that is being applied

After this, the strain is calculated with the following formula:

$$\varepsilon = B_e Q \quad (17)$$

Where: ε = strain vector

B_e = element strain-displacement matrix

Finally, the stresses on each element are computed with Equation (18):

$$\sigma = D\varepsilon \quad (18)$$

Where: σ = stress vector, it contains the stress in each element

D = the material matrix

The material matrix is defines as:

$$D = \frac{E}{(1+\nu)(1-2\nu)} \begin{bmatrix} 1-\nu & \nu & \nu & 0 & 0 & 0 \\ \nu & 1-\nu & \nu & 0 & 0 & 0 \\ \nu & \nu & 1-\nu & 0 & 0 & 0 \\ 0 & 0 & 0 & 0.5-\nu & 0 & 0 \\ 0 & 0 & 0 & 0 & 0.5-\nu & 0 \\ 0 & 0 & 0 & 0 & 0 & 0.5-\nu \end{bmatrix} \quad (19)$$

Where: E = Young modulus of the material

ν = Poisson's ratio of the material

In the case of 2 and 3 dimensional problems, the material matrix shown in Equation (19) is used. For the one dimensional problem, Young's modulus is used instead.

$$\sigma = E\varepsilon \quad (20)$$

The previous explanation intends to shows with the mechanics of material terminology how a problem using finite element method is solved. Since this method is numerical, and uses approximation is not an exact method, the results obtained with FEM may vary with respect to the ones obtained by formulas. The idea in using FEM is that a computer solves the problem while the user provides the require information like boundary conditions (e.g. supports), external forces, properties of the material, etc. and interpret the results. For more information about the finite element theory see [15]. Following is presented an example that compares the results obtained by formulas with the ones obtained using FEM.

2.4.1. A comparison between solving a problem with formulas and with Finite Element Method (FEM)

A shaft that is subjected to torque on one end and fixed from the other end is shown in Figure 23. The shaft has a length L of 20 cm and a radius c of 30mm. The idea in this example is to calculate the stress, deformation and factor of safety in the shaft, cause by the torque applied which in this case is 500Nm. The shaft is made of stainless steel AISI 316, the material properties are presented in Table 1. First the problem is solved using formulas from the mechanics of materials theory, then by using finite element method, after this the results are compared.

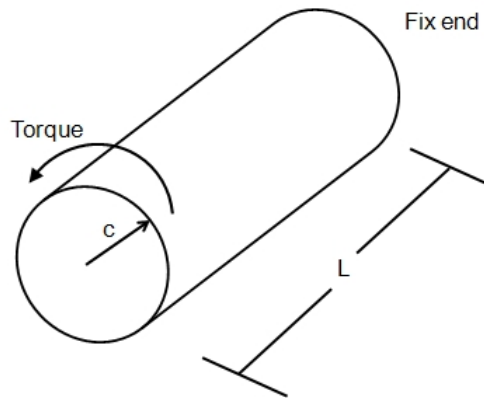


Figure 23: Shaft subjected to a torque.

Table 1: AISI 316 Material properties

Material	Elastic Modulus	Poisson's ration	Yield strength
AISI 316	193 GPa	0.29	205 MPa

The stress on the shaft due to the torque applied is a shear stress and can be calculated with the following formula [8]:

$$\tau_{max} = \frac{Tc}{J} \quad (21)$$

Where: τ_{max} = maximum shear stress in the shaft, which occurs at the outer surface

T = resultant internal torque. In this case the torque applied

J = polar moment of inertia of the cross-sectional area, Eq. (22)

c = outer radius of the shaft

$$J = \frac{\pi}{2} c^4 \quad (22)$$

To calculate the deformation in the shaft due to the torque applied, in this case angular deformation, it is used the following formula [8]:

$$\alpha_t = \frac{TL}{JG} \quad (23)$$

Where: α_t = angle of twist of one end of the shaft with respect to the other end (in radians)

L = length of the shaft

G = the sear modulus of elasticity, Eq. (24)

$$G = \frac{E}{2(1 + \nu)} \quad (24)$$

Where: E = the Young modulus of the material

ν = the Poisson's of the material

The factor of safety is calculated with the formula in Equation (6). The shear stress to be use is the one from Equation (21). Now that everything is being defined (formulas, properties of the material, size and shape of the part and the external load) is possible to calculate the stress, deformation and the factor of safety. The results are presented in Table 2, where also are presented the results from the FEM analysis, this to make a comparison of results.

The problem is now solved using the FEM, it was used SolidWorks Simulation to calculate the results. In Figure 24 is shown the 3D model of the shaft, at one end the torque of 500 Nm is applied (purple arrows) at the opposite end is fix (green arrows). Figure 25 shows the meshing of the shaft, as can be seen it is divided in many triangular elements.

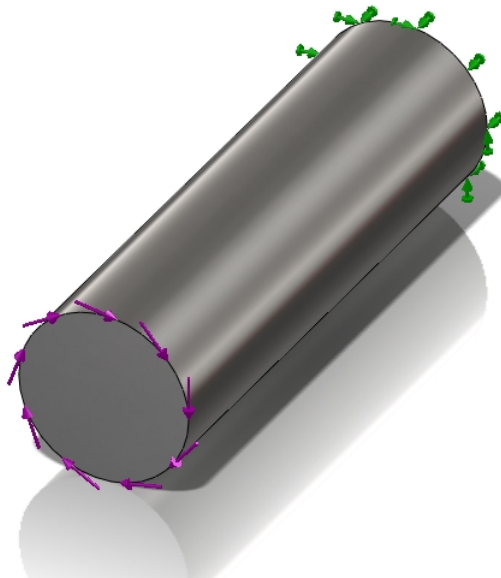


Figure 24: 3D model of the shaft.

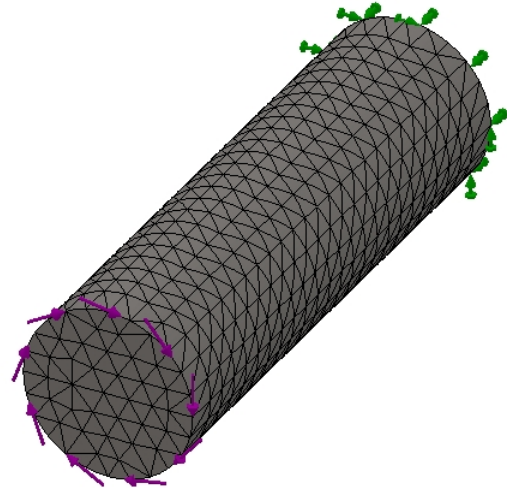


Figure 25: Meshing of the shaft.

Following is presented the shear stress distribution plot (τ_{xz} based on the coordinate system of the part), as can be seen the values of the stresses are symmetrical, the only difference is the sing minus, this means that the shear stress on one half of the parts is in one direction while in the other half is in the opposite direction.

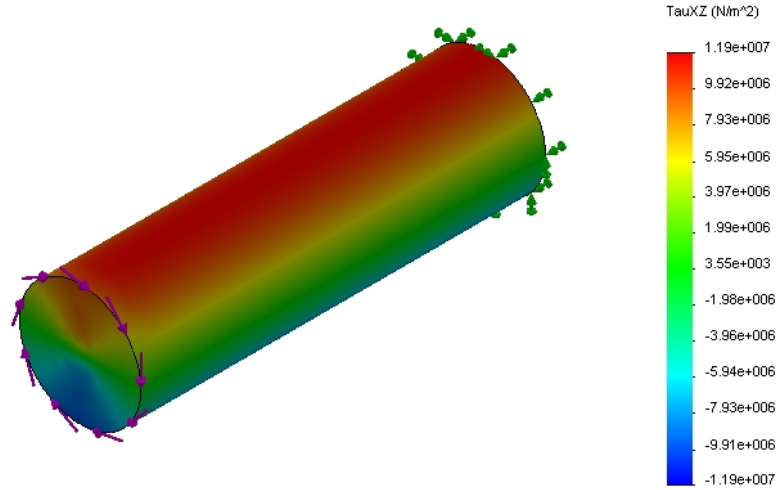


Figure 26: Shear stress distribution.

Figure 27 shows the plot of the deformation (displacement) of the shaft (in x direction based on the coordinate system of the part). As seen from the figure, the deformation is given in meters while the deformation calculated with the formula in Equation (23) is an angular deformation in radians. The user of the FEM software has to interpret the results, in this case, needs to apply the following formula to change from angular to linear deformation (or vice versa).

$$L_d = c \cdot \alpha_t \quad (25)$$

Where: L_d = the linear deformation

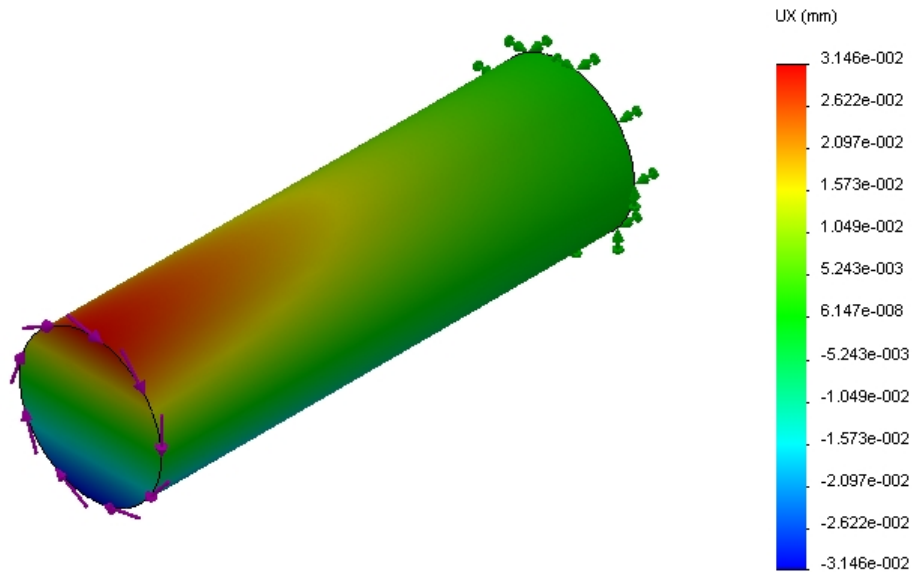


Figure 27: Displacement.

Finally Figure 28 shows the plot of the factor of safety distribution. This plot shows the behavior of the shaft, the minimum stress is at the axis passing through the center of the shaft, this area has the highest FOS. The highest shear stress is at the outer surface of the shaft having the minimum FOS (color red).

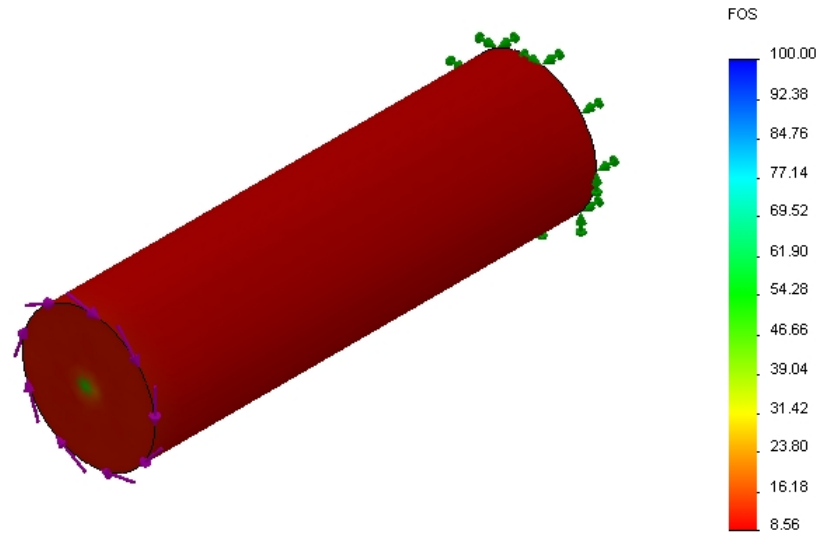


Figure 28: FOS distribution.

The results obtained with both methods are shown in Table 2. Since the FEM is not an exact method there can be some small differences. With the FEM, the maximum stress is bigger than with the formulas.

Table 2: *Comparison of the results*

Calculation Method	Maximum shear stress	Displacement	FOS
Formulas	11.79 MPa	1.05e-3rad / 3.15e-2 mm	8.69
FEM	11.90 MPa	3.14e-2 mm	8.56

One of the biggest benefits of the use of FEM is that complex structures can be analyzed. For example, Figure 29 shows the shear stress distribution for the shaft from the previous example, but now the shape of the shaft has changed (it has three holes) as seen from the figure. It is not possible to analyze this shape by using analytical formulas, at least not in an easy way, and in the case of the FEM it took about the same time as in the previous example to compute the results. This is why FEM is a useful engineering tool nowadays for analyzing structure and machine components.

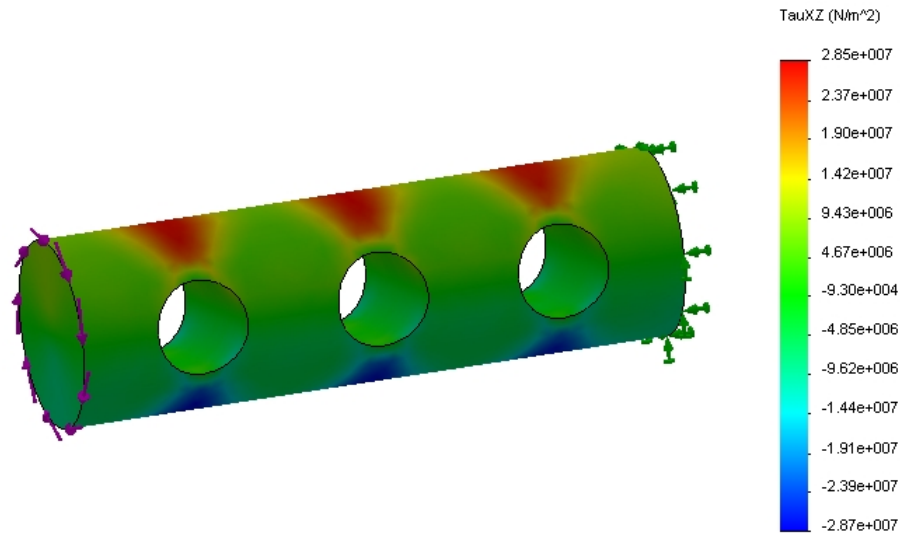


Figure 29: Shaft with holes.

Special care has to be taken when it is trying to solve complex problems. The scenario for the analysis (3D models, loads, materials, boundary conditions, etc) needs to represent the real system accurately in order to obtain good results, with which later will be make engineering decisions. Also is very important to have an idea of the behavior of the parts being analyzing, this is, an idea of the results in order to be sure that the analysis was successfully performed.

3. DESIGN REQUIREMENTS

The requirements presented in this chapter, are divided into two types: general requirements for the wrist and specific requirements for the water hydraulic vane actuator (values for the requirements are specified).

The general requirements are easy to define (and sometime hard to meet) since they just imply what the system needs to fulfill. The specific ones are difficult to define since values for the system characteristics has to be set, in many cases good guesses are used as requirements, especially at the beginning of the project when there is not many information. It is pretended that by meeting the specific requirements, some of the general requirements will be fulfilling.

The requirements defined in this chapter are based on requirements previously defined, current designs and new design criteria.

3.1. General Requirements: Wrist

In Chapter 2.3, characteristics of a good wrist design were mentioned; some of them are now used as general requirements. Also the requirements for the WHMAN defined in [4] are taken into account. Since the WHMAN is a teleoperated manipulator, the requirements are defined based on the characteristics of a force feedback remote handling manipulator and not based on industrial robot requirements. Table 3 shows the general requirements for the WHMAN wrist.

Table 3: *General requirements WHMAN wrist*

Requirement	Comments
3 Degrees of Freedom (DOF)	For remote handling the manipulator must have 6DOF and 3 have to be provided by the wrist.
Spherical Motion	For easier kinematic analysis.
Large workspace	Large angular orientation range, since the configuration of the wrist uses direct actuation, the motion range for each link is defined by the motion range of the actuator.
Compact size, light weight and low inertia	This will be achieving by having small size actuators and the use of strong and light materials (e.g. aluminum) on the links.
Medium to low backlash	Due to the direct actuation of the links, the backlash is minimal.
Sufficient mechanical stiffness	It is important to define a value for what is considering sufficient stiffness.

Radiation tolerant	Due to the seals are affected by the radiation, conventional materials cannot be used [4]. Avoid the use of digital electronics. In this case for the resolver that measures the position of the vane actuator shaft.
Low manufacturing cost	Each actuator in the wrist should be different because different loads are applied to them. However, by making a common design for all the wrist actuators, the number and complexity to manufacture the parts will be reduced as well as the testing of the actuators.
Rugged and reliable design	An easy to assembly and easy to maintain design.

3.2. Specific requirements: Water hydraulic vane actuator

3.2.1. Design Requirements previously defined

The requirements used to develop the water hydraulic vane actuator in [3] and the requirements used in [4] which concern the actuators of the wrist are summarized in Table 4.

Table 4: *Requirements from [3] and [4]*

Requirement	Value
Torque	≥ 500 Nm
Motion range	280°
Working nominal pressure	210 bar
Nominal flow rate	6.8 liters/min
Components Factor Of Safety (FOS)	≥ 1.5
Payload in [3]	50 kg
Payload in [4]	100 kg

In the case of the payload of 100 kg is in worst case at a distance of 0.45 m and the load of 50 kg at a distance of 1 m. In Table 5 is presented this information as well as the moment of inertia computed with these values.

Table 5: *Loads and moments of inertia*

	Reference [3]	Reference [4]
Payload	50 kg	100 kg
Distance	1 m	0.45 m
Moment of inertia	$50 \text{ kg}\cdot\text{m}^2$	$20.25 \text{ kg}\cdot\text{m}^2$

3.2.2. Analysis of load, torque and moment of inertia based on current 3D models

Since the values of payload in Table 4 and Table 5 are estimates based on the payload weight scenarios that the WHMAN will handle, in the following analysis is determined the torques and moments of inertia that the wrist of the WHMAN will be subjected. This analysis is based on 3D models of the current wrist and the 3D model of the heaviest tool, the hydraulic jack shown in Figure 30.

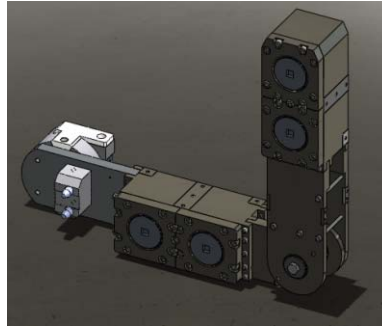


Figure 30: Hydraulic jack.

Current WHMAN spherical wrist configuration has three actuators. Figure 31 shows the corresponding joints that each actuator of the wrist will actuate.

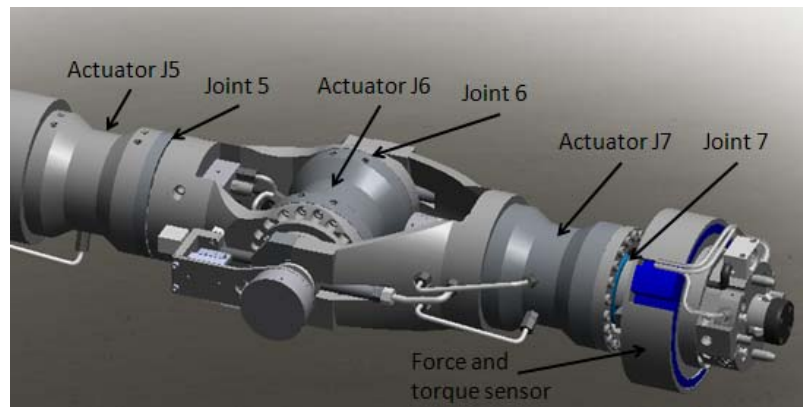


Figure 31: Current wrist.

In Figure 32 is presented the load and torque requirements for the actuator J7, basically the payload for this actuator is just the force/torque sensor (Figure 31) and the hydraulic jack.

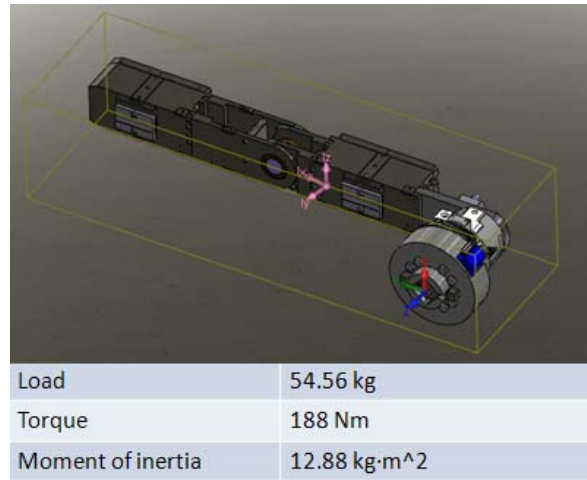


Figure 32: Load for actuator J7.

Figure 33 presents the load and torque requirements for the actuator J6, for this actuator the load is also the one for actuator J7 plus the weight of the actuator J7 and part of the wrist structure as can be seen from the figure. Due to the moment of inertia varies depending on the configuration and load in the manipulator, Figure 33 shows the configuration is which the moment of inertia was identified to be the highest.

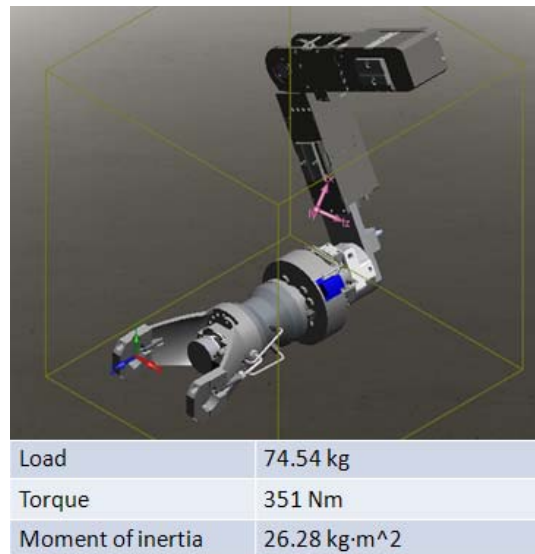


Figure 33: Load for actuator J6.

Figure 34 presents the load and torque requirements for the actuator J5, for this actuator the load is also the one for actuator J6 plus the weight of the actuator J6 and part of the wrist structure as can be seen from the figure.

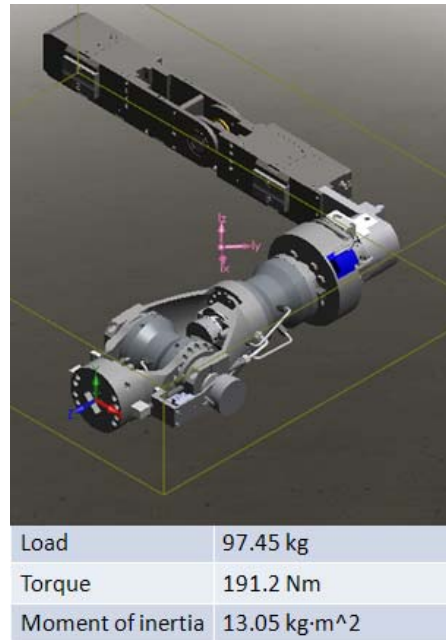


Figure 34: Load for actuator J5.

All WHMAN wrist components cannot be easily modeled exactly as they are. This is taken into account and compensated by designing the actuators using values of load, torque and moment of inertia higher than the ones obtained in this analysis. How big the values will be in comparison with the ones obtained in this analysis represents how robust the design of the actuator will be. In Table 6 is summarized the loads, torques and moments of inertia for each actuator based on the current 3D models of the wrist.

Table 6: Load, torques and moments of inertia based on current 3D models

	Actuator J5	Actuator J6	Actuator J7
Load	54.56 kg	74.54 kg	97.45 kg
Torque	188 Nm	351 Nm	191.2 Nm
Moment of inertia	12.88 kg·m ²	26.28 kg·m ²	13.05 kg·m ²

The values presented on Table 6 depend mainly on the size of the vane actuators and links of the wrist. With the redesign of the wrist, the actuators and links will be smaller and lighter making the values on Table 6 to decrease.

3.2.3. Design Criteria

In this section the theory presented in Chapter 2.2 will be used to develop the requirements for the hydraulic vane actuator. There are two types of flexibilities in the hydraulic vane actuator: the hydraulic and the mechanic. These flexibilities are defined by their natural frequencies. The formulas to compute the hydraulic and mechanical natural frequencies are presented in Equations (26) and (27) respectively.

$$\omega_h = \sqrt{\frac{K_h}{I}} \quad (26)$$

$$\omega_s = \sqrt{\frac{K_s}{I}} \quad (27)$$

Where: ω_h = Hydraulic natural frequency
 ω_s = Mechanical natural frequency
 K_h = Hydraulic torsion stiffness
 K_s = Mechanical torsion stiffness
 I = Moment of inertia

Because the moment of inertia is a factor which will define the natural frequencies, and since this, varies depending on the configuration and load in the manipulator, is needed to define a value that will help to have a good actuator design.

As recommended in [10], the value of the moment of inertia should be the maximum of the range of values that I take on. From Table 5 there are two values for the moment of inertia: 20.25 kg·m² and 50 kg·m², from the analysis performed in the previous section, the maximum value (in Table 6) is 26.28 kg·m².

Because the larger the moment of inertia is, the lower the hydraulic and mechanical natural frequencies will be. If a big moment of inertia is chosen to establish the requirements for the actuators, the manner to increase the hydraulic and mechanical natural frequencies is by increasing the hydraulic and mechanical torsional stiffness respectively; this means a large size actuator design.

If a small moment of inertia is chosen, there is the risk that the natural frequencies will be less than the theoretical values, due to bigger moments of inertia presented in the system, making that the flexibilities in the actuator have influence in the dynamics of the system. Based on the previous statements a value for the moment of inertia is defined, this is the first design criterion for the design of the actuators.

Design criterion 1: Moment of inertia $I = 40 \text{ kg}\cdot\text{m}^2$.

If the desired bandwidth of the system (WHMAN) is around 1 to 2.5 Hz, and since the closed-loop natural frequency of the system can match the bandwidth, this leads us to formulate the second design criterion.

Design criterion 2: Closed-loop natural frequency $\omega_n = 2.5 \text{ Hz}$

The lowest structural resonance frequency in the actuator is the hydraulic one shown in Equation (26); based on the rule of thumb in Equation (14), the hydraulic natural frequency in the actuator must be then $\omega_h \geq 5 \text{ Hz}$.

With the value of the hydraulic natural frequency and the moment of inertia proposed the hydraulic stiffness is computed. To calculate the mechanical stiffness and based on this design the shaft, a third design criterion was established.

Design criterion 3: Stiffness ratio $SR \geq 10$: $K_s \geq 10K_h$

With these three design criteria and the first five requirements in Table 4, it is possible to redesign the hydraulic vane actuators. After trying to fulfill the requirements and follow the design criteria, it was noticed that the design criterion 3 is hard to fulfill when is require a reduction of size in the actuators. This is why it was proposed a new design criterion.

Design criterion 3N: Mechanical natural frequency: $\omega_s \geq 2\omega_h$

Still the stiffness ratio was considered as a requirement (as reference), and was calculated during the redesign of the actuators since is a good parameter to visualize the relation between the two flexibilities in the vane actuators.

The maximum torque in Table 6 is 351 Nm, this torque is the minimum to hold the load but is not enough to move it. This is why a higher value for the torque, the same as in Table 4 ($\geq 500\text{Nm}$) is defined to be the torque requirement. Finally Table 7 summarizes the design requirements for the vane actuators in the wrist.

Table 7: Design requirements for wrist actuators

Requirement	Value
Torque	$\geq 500 \text{ Nm}$
Motion range	280°
Working nominal pressure	210 bar
Nominal flow rate	6.8 liters/min
Components Factor Of Safety (FOS)	≥ 1.5
Stiffness Ratio (reference)	10
Mechanical natural frequency ($I = 40 \text{ kg}\cdot\text{m}^2$)	$\geq 10 \text{ Hz}$
Hydraulic natural frequency ($I = 40 \text{ kg}\cdot\text{m}^2$)	$\geq 5 \text{ Hz}$

With the requirements for the vane actuator defined, it is possible to proceed with the redesign of the actuators. Next chapter shows the redesign process of the vane actuators for the wrist.

4. VANE ACTUATOR NEW DESIGN

This chapter describes the redesign process of the vane actuators for the WHMAN wrist. First with the theory described in Chapter 2.1 and the requirements, the design parameters (Chapter 2.1.1) for an optimal vane actuator design were computed. To calculate these parameters, some design tools like the sensitivity matrices were used.

After defining the design parameters, the 3D models of all the components required to have a functional vane actuator are developed. The mechanical breakdown of the components designed is also presented in this chapter. Finally a comparison between the current and the new actuator design is shown.

4.1. Sizing of the vane actuators

The equation used to define the basic size of the vane actuators is the one to calculate the theoretical output torque in Equation (4). Because the output torque depends on the three main design parameters (the internal radius of the chamber, the external radius of the shaft and chamber length) is not an easy task to calculate an optimum relation between these parameters, because there are many combinations which can produce the torque required.

By analyzing the nature of the design is easy to obtain some starting values (ranges), and from them try to meet the requirements (output torque, hydraulic and mechanical natural frequencies among others).

4.1.1. Nature of the design

The nature of the design in this case refers to analyze different configurations of the main design parameters that produce different values of torque, and try to locate the new design close to the configuration that is more suitable for the application in terms of size and shape.

In this case, this analysis is graphical and its major objective is to define ranges of values for the three main design parameters, then with these ranges calculate an optimum relation of these parameters. Figure 35 shows the values in a graphical way of the main design parameters for five different designs.

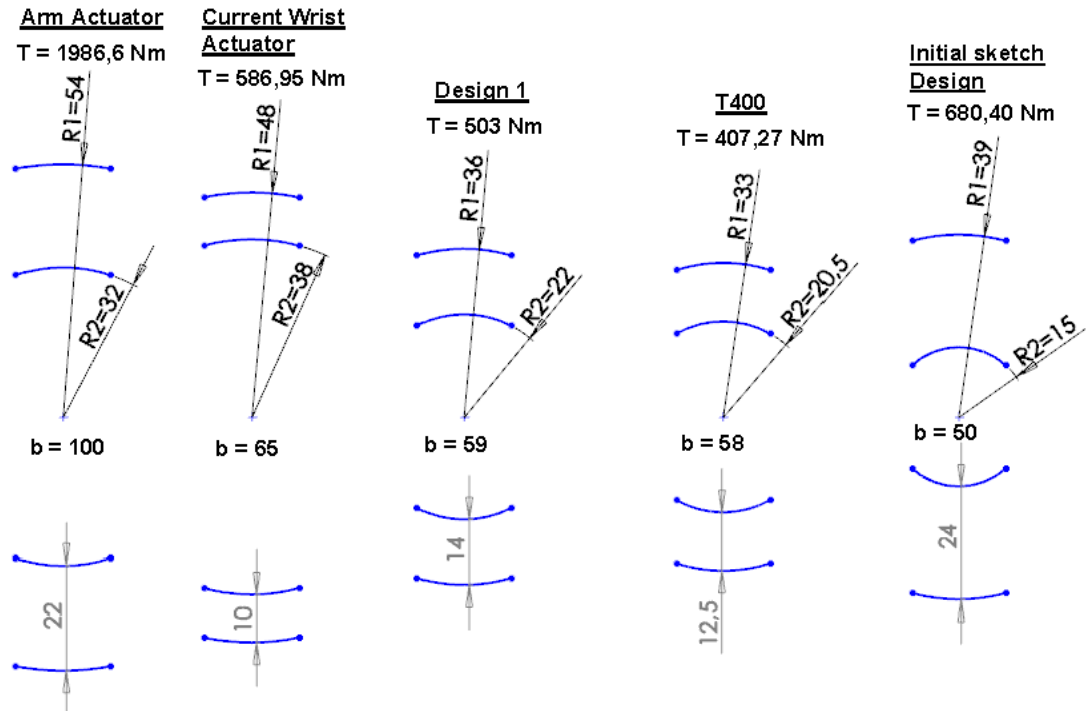


Figure 35: Different design configurations.

Arm Actuator

Design configuration of the two single-vane actuators in the arm of the WHMAN.

Current Wrist Actuator

Design of the current actuators in the wrist, as seen in Figure 35 the shaft (R2) is bigger than the shaft of the arm actuator, this is also other of the reasons why is necessary a redesign in the actuators for the wrist.

Design 1

This was the first proposal for the redesign of the actuators, this design was developed just thinking in the minimum torque requirement which is 500 Nm. Design 1 will be considering as minimum torque design.

T400

This design configuration was developing thinking in having a large reduction in the size of the actuators. However as seen in Figure 35, there is not a big difference in size between this design and Design 1. T400 will be considering as the low torque design.

Initial sketch Design

This design is presented in [4] as an initial sketch to redesign the wrist. Initial sketch Design will be considering as the high torque design.

With the minimum, low and high torque designs and by analyzing the nature of the design, the following ranges for the values of the main design parameters are defined.

Table 8: *Ranges for the main design parameters*

Design parameter	Symbol	Range (in mm)	Current Wrist Actuators (mm)
Internal radius of the chamber	R1	33-39	48
External radius of the shaft	R2	15-22	38
Chamber length	b	50-59	65

From Table 8 can be seen that the values of the main design parameters in the current wrist actuators are much larger than the ranges proposed.

4.1.2. Characteristic of the current vane actuators in the wrist

The characteristics of the current wrist actuators are presented in Table 9, these characteristic are compared with the requirements in Table 7. It is possible to see the opportunity areas to improve the vane actuators designs.

Table 9: *Comparison between current vane actuators designs and requirements*

	Design Requirement	Current Design Actuators J5 and J7	Current Design Actuator J6
Torque (Nm)	≥ 500	586.95	586.95
Angular speed (rad/min)	-	243.29	243.29
Shaft Factor Of Safety (FOS)	≥ 1.5	23.40	49.45
Stiffness Ratio	10	32.85	47.07
Mechanical natural frequency (Hz)	≥ 10 ($I = 40 \text{ kg}\cdot\text{m}^2$)	31.61	37.844
Hydraulic natural frequency (Hz)	≥ 5 ($I = 40 \text{ kg}\cdot\text{m}^2$)	5.516	5.516

The current actuators are quite large because they were designed to have a very high value of mechanical natural frequency, which means have a large value of mechanical torsion stiffness (big shaft diameter) as can be seen in Figure 35 (current wrist actuator R2). The fact that the shaft of the current actuators is quite large was already known, but in Table 9 is presented a quantified measure of how large the current shaft is (stiffness ratio or mechanical natural frequency).

4.1.3. Optimum Design based on the requirements

Having defined the equations for the design of the vane actuator (Section 2.1), the requirements and design criteria (Section 3.2.3), the ranges for the main design parameters (Table 8) as well as having identified the opportunities areas to reduce the size of the vane actuators for the wrist (Table 9), an optimal design which fulfill the requirements and follow the criteria can be calculated.

The first step is to define a set of initial values for the three main design parameters, calculate the torque and adjusts the values based on the requirements. To know the effect of changing the value of any of the design parameters on the value of the system characteristics; for example to know how the torque will change if the internal chamber radius changes, was used the sensitivity matrix which shows a quantified measure of the influence of each design parameters on each system characteristic.

To make a complete sensitivity matrix, which includes all the system characteristics in Section 2.1.2 and all the design parameters in Section 2.1.1, it is needed to define values for the shaft design parameters. From the analysis performed in [3] to design a vane actuator and from the current shaft designs (arm actuators and wrist actuators) it was observed that the shaft of the actuators must has three sections on each side of the shaft, as shown in Figure 36. One section is for the arrangement for fluid passages, other is for the bearing assembly and the third one is for the application (connection with the link). Initial values for the radius and length of these sections were defined based on the value of the external shaft radius (R_2), the seals for the fluid passages and the bearings.

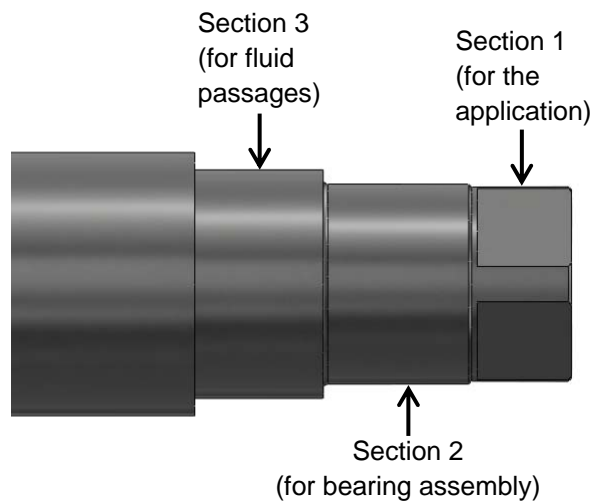


Figure 36: Different sections of the shaft.

The sizing of the bearings is based on the bearing forces created by the pressure force on the shaft. Because the bearing forces depend on the three main design parameters, it is then logical to add the bearing forces in the sensitivity matrix (as an extra system characteristic) because they represent the size of the bearings which in turns determines the size of some components of the actuators. Due to the bearing

forces vary depending on the position of the shaft, this is, vary depending the position of the shaft vanes with respect to the chamber vanes, the maximum bearing force is when there is an angle of 180 degrees between the vanes.

Equation (28) calculates the maximum bearing force acting on one bearing, this is why is divided by two.

$$Bearing_Force_{max} = \frac{(R1 + R2)b \cdot \Delta p}{2} \quad (28)$$

Where: $R1$ = internal shaft radius

$R2$ = external shaft radius

b = chamber length

Δp = pressure difference across the vane

Once all the design parameters are defined as well as the extra system characteristic (max. bearing force), is possible to develop the sensitivity matrix. Table 10 shows the sensitivity matrix for the design of the actuators J5 and J7 (these actuators are equal).

Table 10: Normalized sensitivity matrix for actuators J5 and J7

		Design parameters									
		Chamber Radius R1 (mm)	Shaft Radius R2 (mm)	Chamber length (mm)	Internal shaft radius (mm)	Ext. shaft radius 1 Min. (mm)	Shaft length 1 (mm)	Ext. Shaft radius 2 (mm)	Shaft length 2 (mm)	Ext. Shaft radius 3 (mm)	Shaft length 3 (mm)
Normalized Sensitivities	Actual values	41	23	50	5.5	17.5	10	17.5	27	20	22.5
Torque (Nm)	604.80	2.9	-0.9	1.0	0.0	0.0	0.0	0.0	0.0	0.0	0.0
Angular speed (rad/sec)	236.11	-2.9	0.9	-1.0	0.0	0.0	0.0	0.0	0.0	0.0	0.0
Shaft Safety Factor	4.066	-2.9	0.9	-1.0	-0.04	3.0	0.0	0.0	0.0	0.0	0.0
Mechanical Torsion Stiffness (Nm/rad)	2.2E+5	0.0	0.0	0.0	-0.04	0.8	-0.2	0.2	-0.54	1.1	-0.26
Hydraulic Torsion Stiffness (Nm/rad)	4.93+4	2.9	-0.9	1.0	0.0	0.0	0.0	0.0	0.0	0.0	0.0
Stiffness Ratio	4.537	-2.9	0.9	-1.0	-0.04	0.8	-0.2	2.2	-0.54	1.1	-0.26
Bearing Force (N)	3600	.65	.36	1	0.0	0.0	0.0	0.0	0.0	0.0	0.0

How to use the sensitivity matrix is explained next. In the sensitivity matrix, there is a value for each intersection between one design parameter and one system characteristics. This value can be one of the three cases shown in Table 11.

Table 11: Cases for the values in the sensitivity matrix

Case	Value	Example	Meaning
1	Zero	0.0	There is no relation between the design parameter and the system characteristic.
2	Positive	2.9	If the design parameter increases by 1% the system characteristic will increase by 2.9% and vice versa.
3	Negative	-0.9	If the design parameter increases by 1% the system characteristic will decrease by 0.9% and vice versa.

Following are summarized the relation between the design parameters and system characteristic obtained from the sensitivity matrix. This relation can be noticed from the equations in Chapter 2.1, but with the sensitivity matrix is easy to appreciate; besides quantified relations are presented.

- The torque depends only on the main design parameters as shown in Table 12.
- The angular speed also depends only on the main design parameters as shown in Table 13 the relation is exactly the opposite than with the torque.
- The shaft safety factor and stiffness ratio are the system characteristic that depends on main and shaft design parameters.
- The mechanical torsion stiffness depends only on the shaft design parameters.
- The hydraulic torsion stiffness depends only on the main design parameters.
- The bearing force depends only on the main design parameters and increase if any of these parameters increases.

Table 12: Relation between torque and design parameters

Design parameters		Torque
Internal chamber radius (R1)	Increase	Increase
External shaft radius (R2)	Increase	Decrease
Chamber length (b)	Increase	Increase

Table 13: Relation between angular speed and design parameters

Design parameters		Angular speed
Internal chamber radius (R1)	Increase	Decrease
External shaft radius (R2)	Increase	Increase
Chamber length (b)	Increase	Decrease

Since the sensitivity matrix is a linearization around the actual values shown in the sensitivity matrix, if there is a large change in these values, the matrix has to be calculated again to kept sufficient accuracy.

The sensitivity matrix for the actuator J6 is not presented since gives almost the same information shown in Table 10; there are just little differences in the values for the mechanical torsion stiffness and stiffness ratio. This is because actuator J6 holds the load with both ends of the shaft, while actuators J5 and J7 only with one end.

An optimum design was calculated by adjusting the values of the design parameters based on the sensitivity matrix. The value of the chamber length (design parameter b) was defined to be 50mm (half of the arm actuators, Figure 35) since this value gives a small shape to the actuators. The other design parameters were then calculated and adjusted using the sensitivity matrix.

To define the shaft design parameters the size of commercial seals and bearings were also taken into account. Finally Figure 37 shows a comparison between the optimal design and the designs presented in Figure 35. Table 14 shows the design parameters for the vane actuators optimal designs.

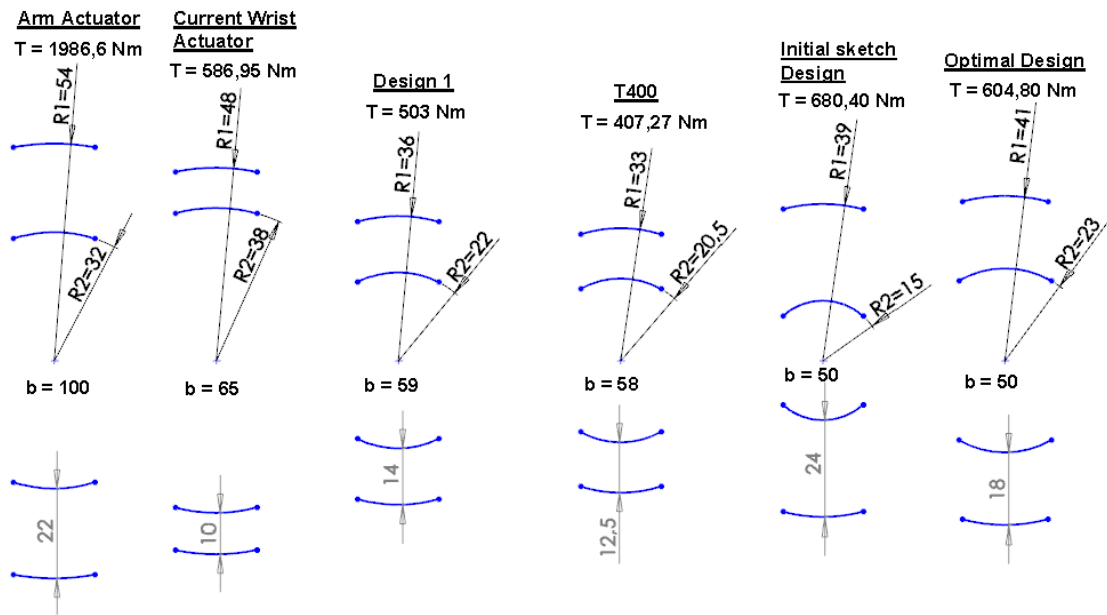


Figure 37: Comparison between optimal design and designs in Figure 35.

Table 14: *Optimal vane actuator designs*

Design parameters	Actuators J5 and J7	Actuator J6
Chamber radius (R1)	41mm	41mm
Shaft radius (R2)	23mm	23mm
Chamber length (b)	50m	50m
Internal shaft radius (C _{int})	5.5mm	5.5mm
External shaft radius 1 min. (C1)	17.5mm	17mm
Shaft length 1 (L1)	10mm	20mm
External shaft radius 2 (C2)	17.5mm	17.5mm
Shaft length 2 (L2)	27mm	23.5mm
External shaft radius 3 (C3)	20mm	20mm
Shaft length 3 (L3)	22.5mm	22.5mm

Table 15 presents a comparison between the characteristic of the optimal designs and current designs. The torque, angular speed and hydraulic natural frequency have similar values. The shaft factor of safety, stiffness ratio and mechanical natural frequency (mechanical torsion stiffness) were decreased to reasonable values.

Table 15: *Comparison between optimal vane actuators designs and current designs*

	Design Requirement	Optimal Design Actuators J5 and J7	Current Design Actuators J5 and J7	Optimal Design Actuator J6	Current Design Actuator J6
Torque (Nm)	≥ 500	604.8	586.95	604.8	586.95
Angular speed (rad/min)	-	236.11	243.29	236.11	243.29
Shaft Factor Of Safety (FOS)	≥ 1.5	4.06	23.40	7.44	49.45
Stiffness Ratio	10	4.53	32.85	7.7	47.07
Mechanic natural freq. (Hz)	≥ 10 ($I = 40 \text{ kg}\cdot\text{m}^2$)	11.90	31.61	16	37.844
Hydraulic natural freq. (Hz)	≥ 5 ($I = 40 \text{ kg}\cdot\text{m}^2$)	5.58	5.516	5.58	5.516

From Table 15 can be seen that the new designs are being reduced in size due to a reduction in the external radius of the shaft, making to have lower mechanical torsion stiffness. Because of this, also the internal radius of the chamber has to be decreased in order to meet the torque requirement.

The output theoretical torque was aiming to have a value close to 600 Nm even if the requirement states that has to be just bigger than 500 Nm. Higher theoretical output torque allows the system to work at lower pressure level having less internal leakages in the actuators.

With the design parameters defined it is possible to develop the components that will constitute the hydraulic vane actuators. Even as to define the numbers in Table 14 required a lot of effort and a good enough understanding of the system, at this point they are just numbers that define the basic size and shape of the actuator and its shaft.

The next step is to define and develop all the required parts and components to build a functional hydraulic vane actuator; calculate the bearings and seals as well as develop the 3D models for the components.

4.2. Materials review

Before showing the components of the new design of vane actuators, this section reviews the materials for the actuators and for the wrist structure. Because this is a continuation in the development of the WHMAN, the material selection for the components is already developed ([3] and [4]). A material assessment for the selection of the materials for the vane actuators and links of the WHMAN arm is developed in [4].

Following is presented a brief material assessments since basically the materials used for the new actuators and wrist are the same than those used in the arm of the WHMAN.

The two main materials employed are stainless steel and aluminum, because of their tensile strength and corrosion resistance as well as lightness in the case of the aluminum. The stainless steel has four categories (Austenitic, Martensitic, Ferritic and Duplex) based on its microstructure [4], each of these categories has different properties regarding corrosion resistance, weldability, magnetic properties, heat treatable and strength properties.

Based on these properties duplex stainless steel was chosen, it has a very good corrosion resistance and high strength properties. Also austenitic stainless steel is used in parts which are subjected to low stress because this category has excellent corrosion resistance properties but modest strength and is easier to be processed. The properties of the different stainless steels used are shown in Table 16.

Table 16: *Properties of different stainless steels [4] and [16]*

Stainless steel	Yield strength [MPa]	Tensile strength [MPa]	Modulus of elasticity (E) [GPa]	Shear modulus (G) [GPa]	Poisson's ratio (ν)	Density (ρ) [kg/m³]
1.4404 (AISI 316)	280	570	200	77	0.3	8000
1.4410 (Duplex)	590	830	200	77	0.3	7800
1.4462 (Duplex)	510	750	200	77	0.3	7800

The links of the wrist are mostly of aluminum EN AW-7075-T6, this is a special aluminum used in aerospace applications because has excellent strength properties combined with light weight. These material properties make to have a stiff and lighter robotic structure. Also some components of the vane actuators are made of this aluminum. The properties of the aluminums used are shown in Table 17.

Table 17: *Properties of aluminum alloys [4] and [16]*

Aluminum	Thickness [mm]	Product form	Yield strength [MPa]	Tensile strength [MPa]
EM AW-6082-T6	<100	Plate	240	295
EN AW-7075-T6	<100	Plate	360	460
Modulus of elasticity		E	70 GPa	
Shear modulus		G	27 GPa	
Poisson's ratio		ν	0.3	
Density		ρ	2700 kg/m ³	

The values presented in the previous tables were used in the design process and in the finite element analysis for the validation of the parts.

4.3. Mechanical components of the new vane actuator design

This section presents and describes the components of the vanes actuators that were designed. There are two different types of actuators for the wrist; the actuator for joints 5 (J5) and 7 (J7) and the actuator for joint 6 (J6).

As mention in Chapter 4.1.3 the difference is that actuators J5 and J7 support the load with only one end of the shaft, while actuator J6 does it with both ends. In Chapter 3.1 was mentioned that in order to have a low manufacturing cost, the complexity in the amount of different parts to be constructed has to be low, this is why all the parts for the two designs are equal except for the shaft.

In Figure 38, the vane actuator J5 is shown as an exploded view, can be seen the main components that constitute this vane actuator, those components are described in the following sections.

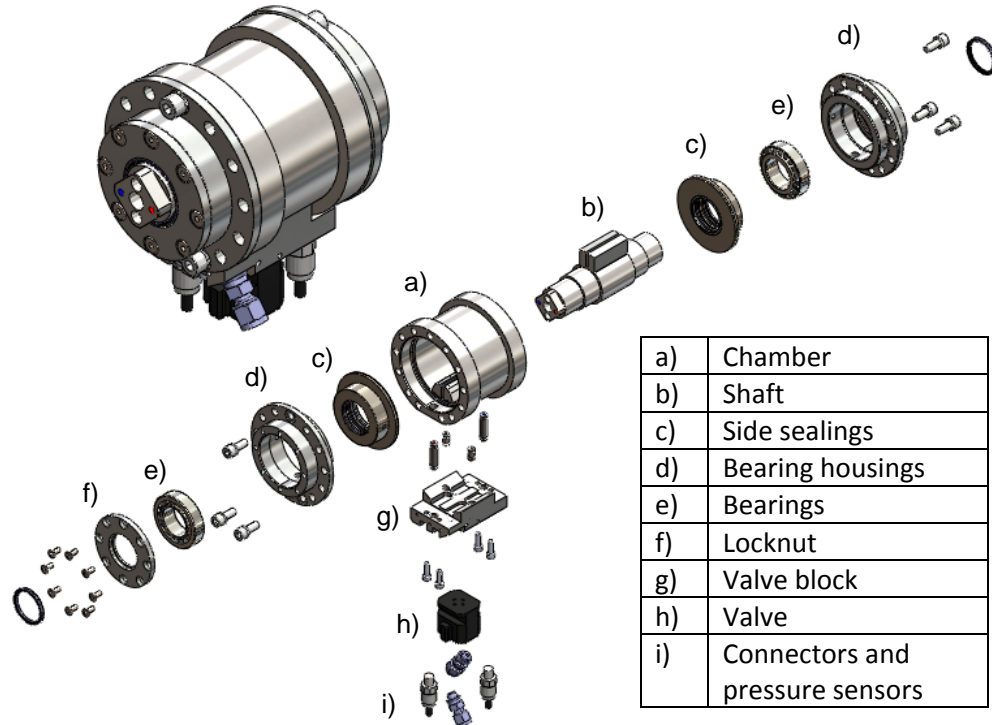


Figure 38: Exploded view of the vane actuator J5.

4.3.1. Chamber

The first component developed was the chamber of the actuator and after that its vanes. In the previous design the vanes for the chamber were welded to it, in this new design the idea is to have a bolted connection between the chamber and vanes, the solution for this connection was based on a bolted vane actuator developed by the author of [4].

The chamber is the main component of the vane actuator because other components are assembled in it. Basically, it has two main parts the “chamber” for the fluid and the bearing surfaces. In the latter the bearing housings (described in Chapter 4.3.5) are mounted, this part of the chamber is subjected to bearing forces (caused by pressure forces on the shaft) while the chamber for the fluid is just subjected to pressure forces. Figure 39 shows the chamber design and its parts.

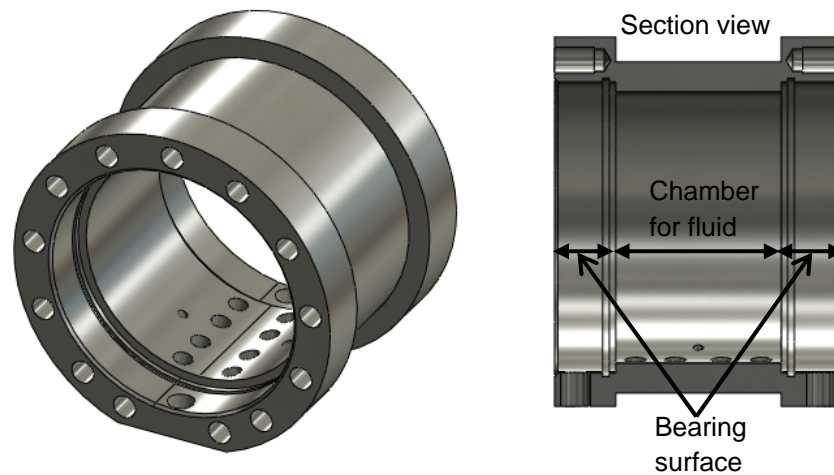


Figure 39: Chamber of the vane actuators.

The material for the chamber is duplex stainless steel 1.4462 because its tensile strength and due to as already mentioned has very good corrosion resistance. Based on the FEM analysis, this same material was chosen for the vanes of the chamber. There is no need to use as in the previous design duplex stainless steel 1.4410 (which has higher tensile strength) for the vanes. Eight socket bolts are used to fix the vanes to the chamber. These bolts have an unthreaded cylindrical shoulder which helps to place the vanes in the correct position and to have a more rigid assembly. In Figure 40 is shown the chamber and vanes assembly as well as the bolted connection.

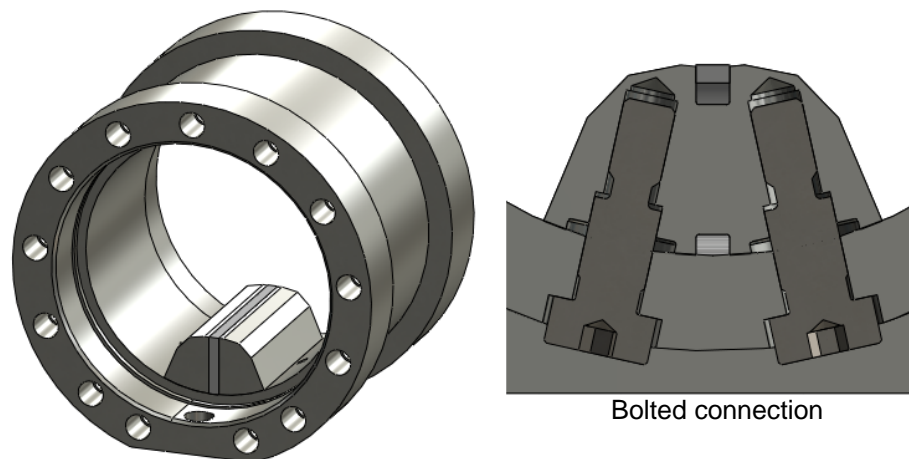


Figure 40: Chamber and vanes assembly.

The chamber has thirteen threaded holes on each side, for the bolts that keep the parts in the assembly jointly. The number and size of bolts are very important and has to be carefully calculated and analyzed because there is metal to metal sealing between the chamber and other component called side sealing (to be described in Chapter 4.3.4). This metal to metal sealing requires a strong and tight assembly between these two parts in order to work correctly, this tightness is provided by the bolts.

4.3.2. Shaft

The shaft is a very important component in the vane actuator, to it is connected the load that the actuator has to move, also the shaft determines the mechanical torsional stiffness of the actuators. As mentioned previously this is the only component that is different between the actuators J5-J7 and the actuator J6.

In this case was also developed a bolted connection between the shaft and vanes on it. This was quite challenging due to the small size of the shaft and vanes and because they are subjected to high pressure forces. The material for the shaft and vanes is stainless steel 1.4410 which also has good corrosion resistance properties and higher tensile strength than the material for the chamber.

In the shaft there are fluid passages, these have the objective of provide fluid to the actuators, by using these fluid passages the used of flexible hoses is eliminated. This type of fluid passages is utilized throughout the entire WHMAN.

Figure 41 shows the shaft for the actuators J5 and J7, also shows the fluid passages on the shaft (marked in red and blue) as well as the shaft and vanes assembly.

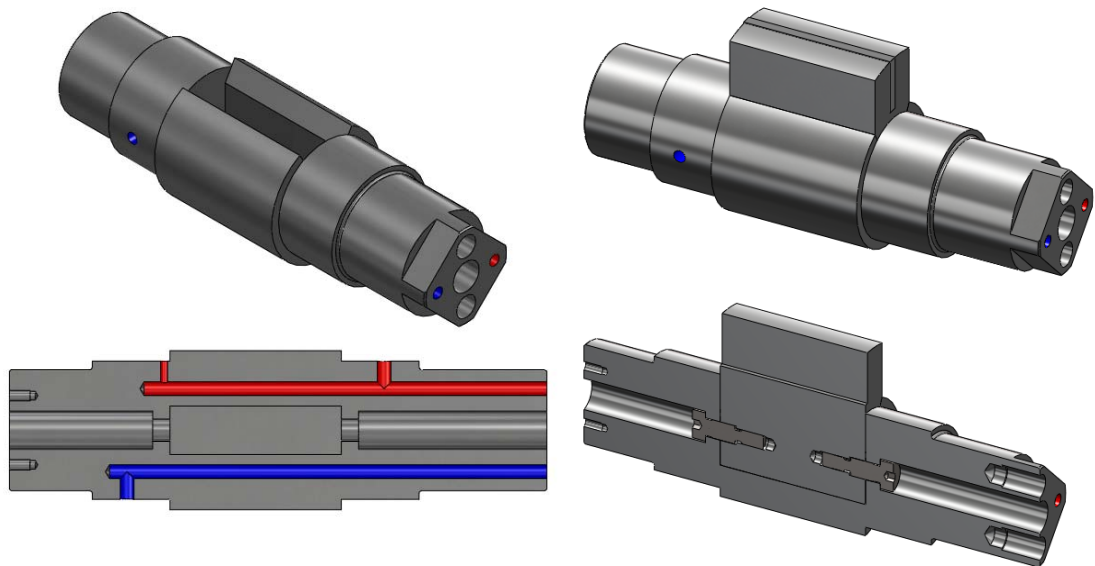


Figure 41: Shaft and vanes for actuators J5 and J7.

The shaft for the actuator J6 is shown in Figure 42 in a similar arrangement than the previous figure. The main difference with respect to the previous shaft is in the section one (Figure 36) that is for the application.

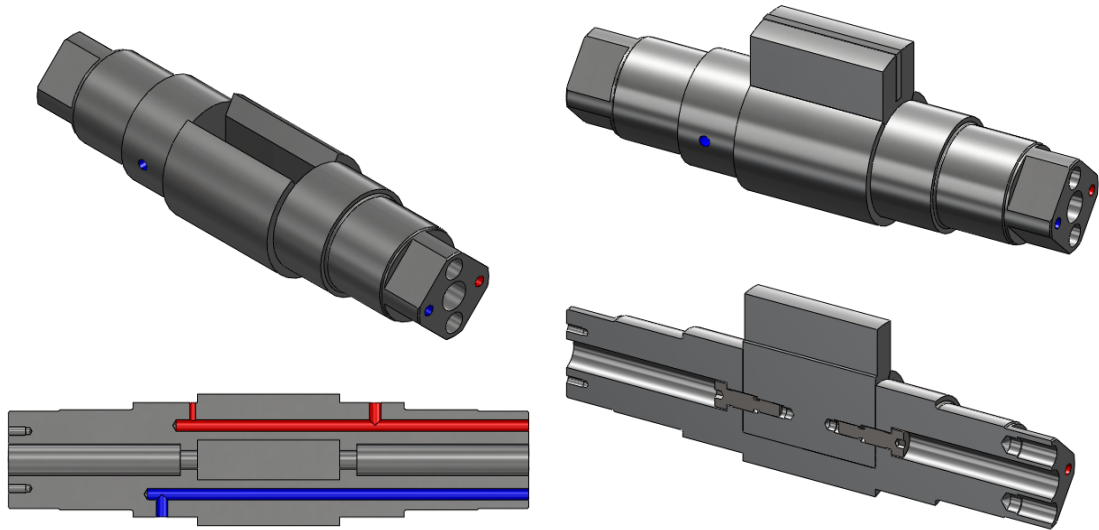


Figure 42: Shaft and vanes actuator J6.

4.3.3. Bearings

The bearings are a very important part of the design because the bearing arrangement supports the entire load applied to the shaft, this load is basically the one applied at the end(s) of the shaft plus the pressure force acting on it. The latter is much bigger than the first one.

The bearings used in the new designs are of the same type as the bearings used in previous designs which are tapered roller bearings. This is because these bearings are suitable for the accommodation of combined loads (radial and axial), which are presented in the shaft of the vane actuators. The following equation is used to calculate the equivalent static load on tapered roller bearings [17].

$$P_o = 0.5F_r + Y_oF_a \quad (29)$$

Where: P_o = Equivalent static bearing load

F_r = Radial load

F_a = Axial load

Y_o = Calculation factor specified for each bearing

The bearings are calculated based on this equivalent static load. Since the axial load is very small when comparing with the radial load this makes the equivalent static load smaller than the radial load, in this case a design rule in [17] says that the equivalent static load is then equal to the radial load.

The radial load is produced by the pressure on the shaft; this is called bearing force the formula to calculate it was shown in Equation (28). By multiplying this bearing

force (in this application equal to the equivalent static bearing load) with a safety factor for the bearing, the static load rating required for the bearing is calculated.

Besides meeting the static load rating requirement the bearing must meet dimensional requirements based on the space allowed to it. In Table 18 is shown the characteristics of the chosen bearings, each vane actuator has a pair of this tapered roller bearing.

Table 18: *Bearing selected for the actuators*

Bearing selected	Internal diameter	External diameter	Thickness	Static load rating	Safety factor
SKF 32007 X/Q	35mm	62mm	18mm	54000N	1.6

4.3.4. Side sealings

These are the side covers for the fluid chamber. The corner seal and the seals for the fluid passages are installed on these components. This is a very important part for the fluid passages within the actuator which transfers the fluid between a rotating part and a static part. The vane actuator has two identical side sealings, one at each side of the chamber.

The material for this part is duplex stainless steel 1.4410 the same as for the shaft. This is because this material is mainly used in applications where parts will be subjected to large loads and will be in contact with water. Figure 43 shows the side sealings with the seals.

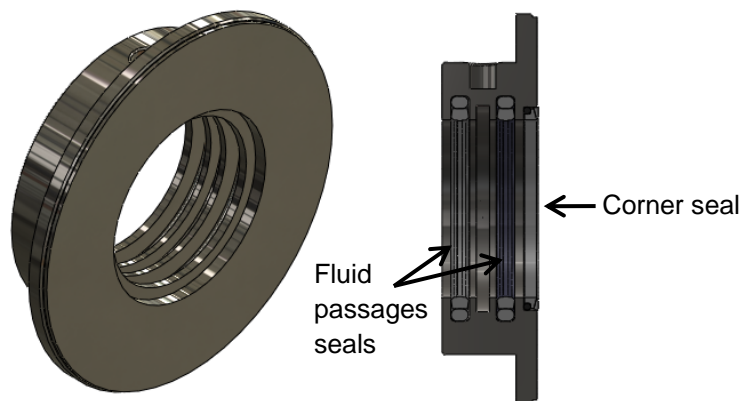


Figure 43: Side sealings.

4.3.5. Bearing housings

As its name implies, on these parts are mounted the bearings and also the side sealings, with these components the chamber assembly is closed. They are the interface between the vane actuator and the links structures of the wrist. The material for these parts is aluminum 7075-T6 due to its high tensile strength combined with lightness.

There are two different bearing housings; one that is a one piece design and other that is two pieces design (needs a bearing locknut to tight the bearing assembly). This design for the bearing arrangement was developed in [4] for the vane actuators in the arm of the WHMAN. It was used also here for the new designs since helps to reduce the time to adjust the shaft as well as reduce the possibility for a loosened bearing. Figure 44 shows the one piece design and Figure 45 shows the two pieces design of bearing housings.

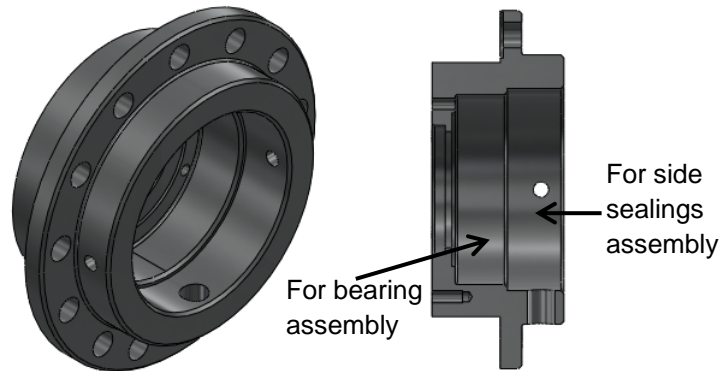


Figure 44: One piece bearing housing.

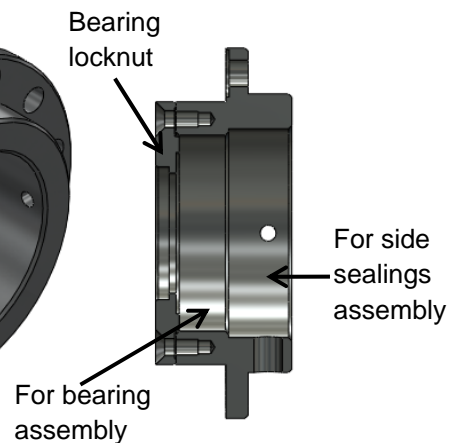


Figure 45: Bearing housing.

4.3.6. Fluid passages

Fluid passages are a key part of the vane actuator design. Normally in hydraulic systems flexible hoses are used to transfer the fluid from the pump to the actuators, in this application this is not allowed due to three main reasons. The first reason is due to the large motion range (270°) of the vane actuators, there will be long and loose hoses that could clog. The second reason is that, due to the flexibility of the hoses, the hydraulic stiffness of the actuators is reduced. Finally the third reason is that the irradiative conditions in which the WHMAN will operate affect the hoses.

There are some commercial solutions to implement fluid passages which are called rotary unions (rotary coupling or swivel joint [18]) but the use of rotary unions will increase the size of the robot structure.

By analyzing the principle of the operation of these rotary unions it is noticed that the implementation of the fluid passages to vane actuators is the best option, since many components that these rotary unions have (like the housing, bearings and shaft), are already in the actuator. Some modifications in the side sealings for the incorporation of the fluid passages seals (shown in Figure 43) and also in the shaft are needed. By doing this the vane actuator becomes a rotary union suitable for transfer fluid throughout the robot structure.

Figure 46 shows the fluid passages within the vane actuator and the bearing arrangement described in the previous section.

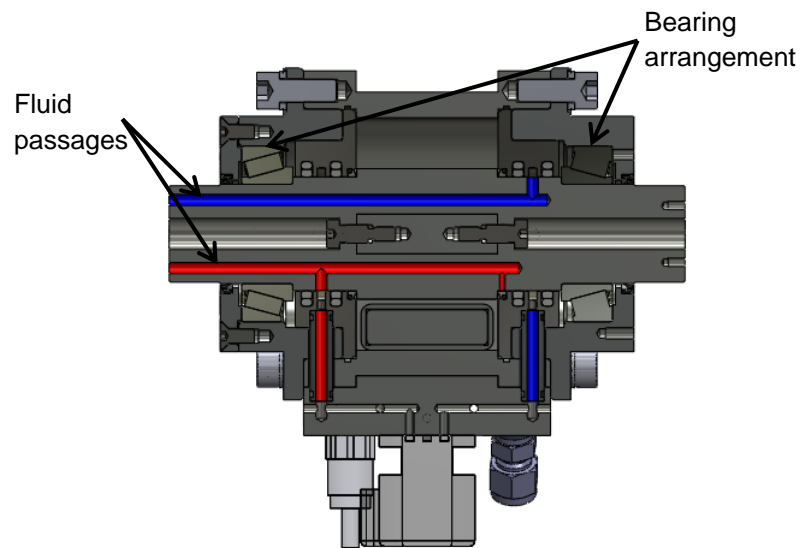


Figure 46: Fluid passages.

4.3.7. Seals on the vane actuators

The seals on hydraulics actuators play a very important role because its performance depends greatly on them. Leakages will decrease the efficiency of the actuators and in this case will reduce the output torque. Having a tighter seal assembly will reduce the leakages, but will increase the wear of the seal and also there will be torque losses due to the increased friction.

To find an optimum balance between friction, seal wear and leakages is a demanding task especially in water hydraulic applications; because the viscosity of the water is lower than the viscosity of the oil.

There are several types of seals on the vane actuators: vane seals (chamber vanes and shaft vanes), corner seals one on each side sealing (Figure 43), and the seals for the fluid passages, Figure 47 shows these seals and its locations on the vane actuators. The fluid passages seal and corner seals are at both sides of the shaft, but were named only in one side to keep a clear image.

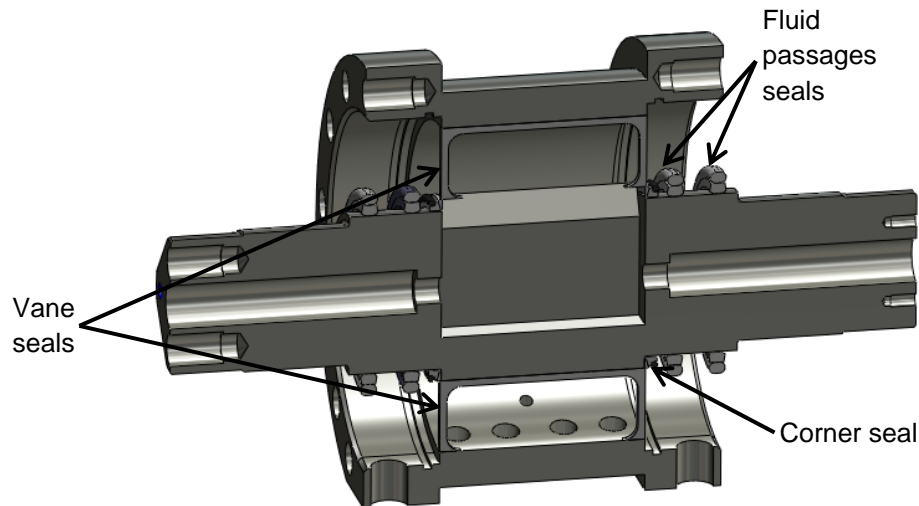


Figure 47: Different seals on the vane actuator.

The fluid passage seals are commercial solutions for applications of this kind; the material for these seals is polyethylene. The solutions for the corner seals and vane seals are based on the ones developed for the arm actuators in [4].

The corner seal consists of three parts; the actual seal, a support ring and an O-Ring. Because the force to push the seal against the shaft is produced by the supply pressure, the O-Ring is used as an elastic energizing element to activate the seal during operation at low pressure levels. The material of this seal is PolyOxyMethylene (POM). The support ring is in charge of making that the corner seal acts always in the right direction, the material for the support ring is stainless steel.

The vane seals consist of three parts in the case of the shaft vane seal. These are; the actual seal, an O-Ring and a core plate. For the chamber vane seal, it consists only of two parts; the actual seal and the O-Ring, in this case the vanes act like a core plate. Also the O-Rings are used as an energizing element. The material for vane seal is Ultra High Molecular Weight Polyethylene (UHMW-PE). As mentioned before the seal solutions for the corner seals and vane seals were based on the current solutions on the arm actuators. The study for the new sealing solutions is not included in this Thesis.

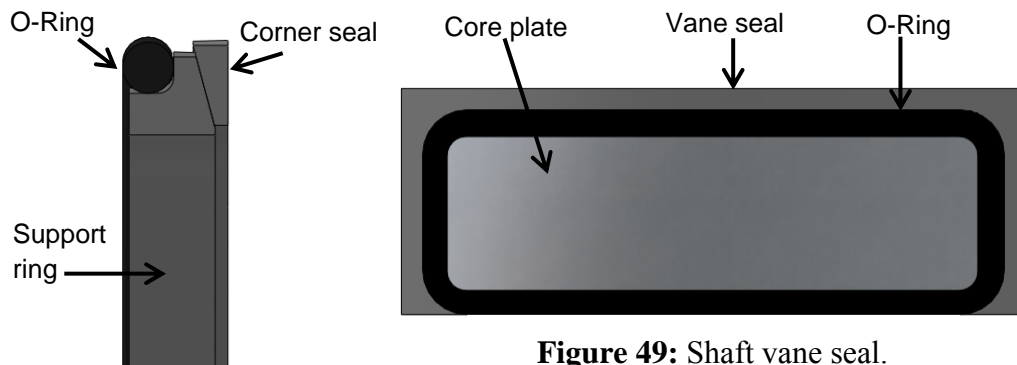


Figure 49: Shaft vane seal.

Figure 48: Corner seal.

4.3.8. Valve block

This block is the interface between the valve and the vane actuator. It connects the fluid from the fluid passages to the valve and the fluid from the valve to the chamber of the actuator. The connectors for the pipes and the pressure sensors are assembled in this block. The material for the valve block is duplex stainless steel 1.4410.

The valve block (shown in Figure 38) is one of the most complex parts of the actuator since it has many holes (fluid passages) and because it hosts and connects many components.

There are other components like bolts, washers, connectors and more seals which are important but not relevant in this breakdown of the vane actuator components.

4.4. Comparison between new and current vane actuator designs

At the end of Chapter 4.1.3, there was a comparison between the characteristics of the new actuators design and the current designs. This section presents a comparison of the size, shape and weight (based on 3D models) of these actuators.

With the objective to create a better idea besides the numbers shown in Table 14 and Table 15 regarding the size reduction of the new actuators, the overall dimensions of the actuators are compared. Figure 50 shows the isometric view of both actuators.

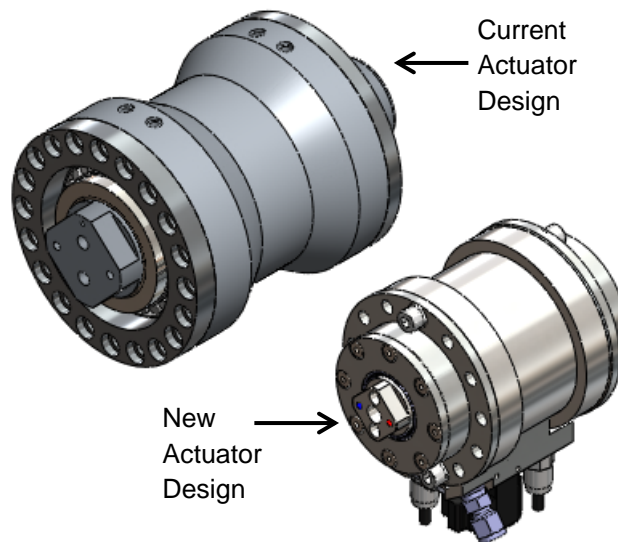


Figure 50: Isometric view comparison.

In the new design, the valve block (and the components assembled in it) is part of the actuator, while in the current design this block is on the wrist structure. The reduction in the size of the shaft can be seen from Figure 51.

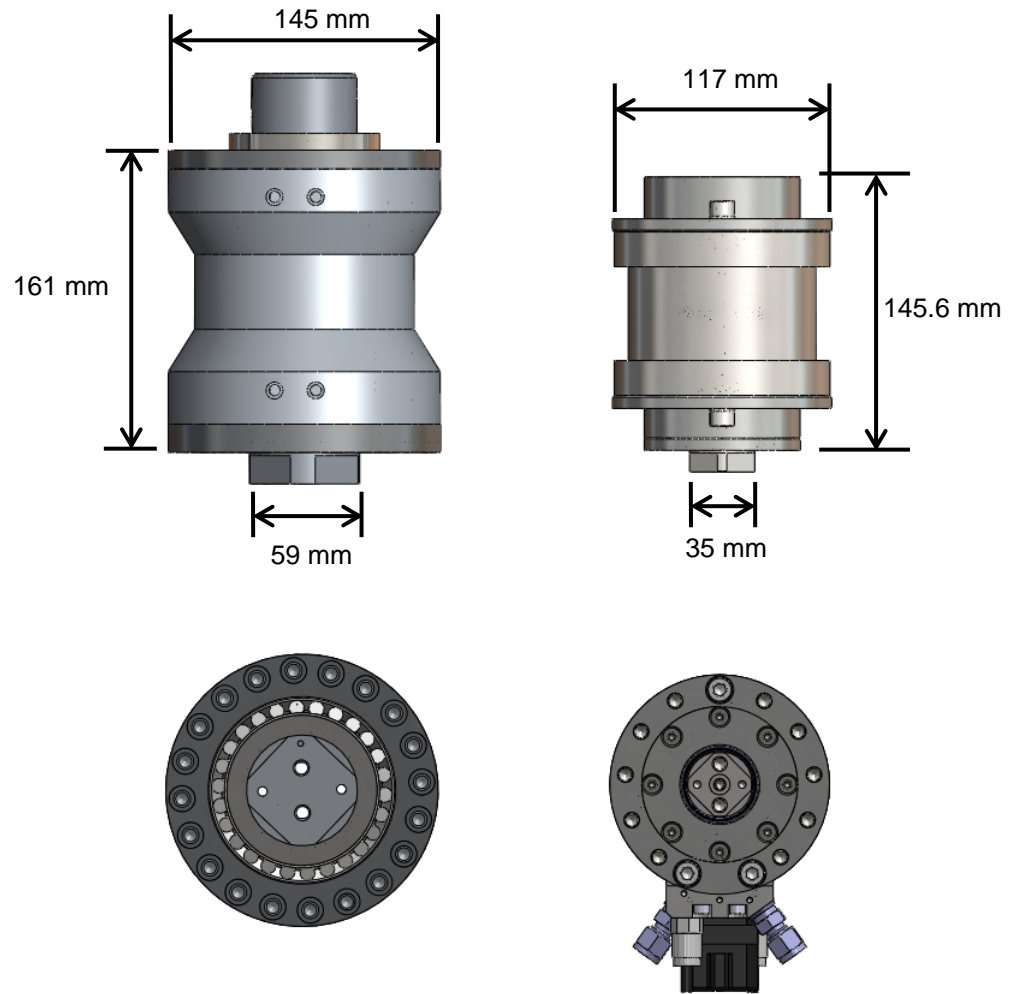


Figure 51: Overall dimensions of the new and current actuators.

The weight of the current actuator is about 13.5 kg and the weight of the new actuator is about 6.6 kg, a reduction around half of the weight was achieved. Even as these values are based on the 3D models, they are good enough for the estimation of the reduction ratio of the weight. With the new vane actuators a new wrist for the WHMAN was designed, next chapter shows the development of the wrist.

5. NEW WRIST DESIGN

This chapter presents the new design for the wrist of the WHMAN, first the WHMAN and its wrist are described in terms of robotics structures. Then the breakdown of the wrist components is presented including a comparison between the new and the current wrist designs.

5.1. Wrist of the WHMAN

As mentioned in Chapter 2.3, 6 DOF are required to move on object freely in space; most of the 6 DOF robot manipulators have six joints. The first three joints and its links are the arm of the manipulator which are labeled joints 1, 2 and 3, the last three joints and links, constitute the wrist and are labeled joints 4, 5 and 6. There are two main joint designs for robot structures, revolute joint and prismatic joint shown in Figure 52. The revolute joint provides rotational motion between the links of the robot while the prismatic joint creates linear motion.

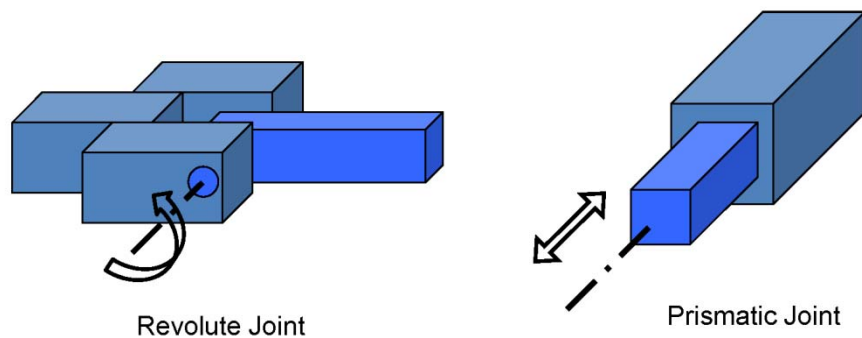


Figure 52: Most common configurations of robot joints.

In the case of the WHMAN it has 7 joints in total, the first four joints are part of the arm structure (joints 1 to 4), the first two constitute the base and shoulder of the arm and are revolute joint type. The third joint is prismatic and is located between the shoulder and the elbow. The last arm joint is the elbow which is revolute. The design of these joints as well as the arm structure is described in [4].

The last three joints (5, 6 and 7) and links are the wrist of the manipulator; the current wrist has a spherical configuration and all the joints are revolute type. In Figure 53 are identified and named the joints and links of the WHMAN with the current wrist.

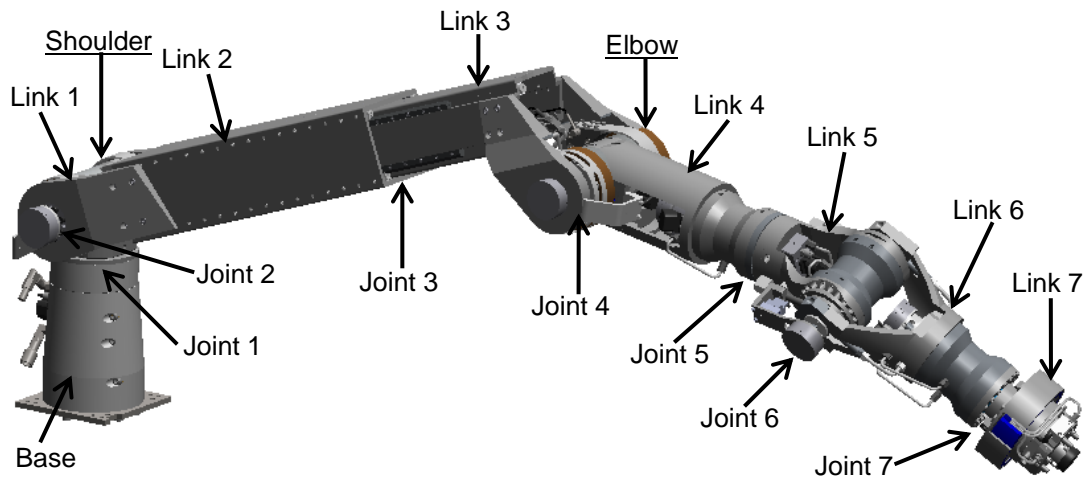


Figure 53: WHMAN (with current wrist).

The new wrist was designed to also have a spherical configuration; because as mentioned in Chapter 2.3, this configuration reduces the complexity of the kinematic analysis of the robot since there are already solutions for it.

Because direct actuation of the joints is being used for all the joints in the WHMAN, this same principle is used for the new wrist design. This decreases the complexity of the links because there are no gear, belt or chain transmissions inside the structure.

The main objective of this redesign work was to decrease the overall size and weight of the wrist of the WHMAN. By resizing the vane actuators and made them smaller (previous chapter) this objective is largely achieved, but also the design of the links is very important to enhance this objective.

5.2. Mechanical design and breakdown of the wrist

Due to the new wrist design has the same configuration as in current design (spherical), uses the same type of actuators as well as direct actuation of the joints; it looks very similar to the current wrist. One change on the new wrist is that by using the new actuators, there are no valve blocks on the wrist structure, all valve blocks are now integrated into the actuators as seen in Figure 51.

The new design was developed in thinking to have an easier way for the assembly of the wrist as well as to have easier access to the actuators valves in case they need to be replaced. Also the way to implement the fluid passages in the wrist is somewhat different; this new manner is similar to the fluid passages implemented throughout the arm of the manipulator.

The new 3 DOF spherical wrist design is shown in Figure 54. In the Figure is identified the common point where the three axis of the actuators intersect called the wrist center located in the middle of the shaft actuator of joint 6 (actuator J6). Also the hand length for the wrist is shown, which is basically the length of the link 6.

One of the major design constrains to have a compact wrist design are the resolvers that measure the angular position of actuators shafts and the hydraulic valves and

connectors for the water pipe lines. The resolver of actuator J7 makes the hand length of the wrist to increase due to its large size that requires a large space between the resolver and the actuator J6 in order to avoid collisions during the motion of link 6.

The nature of the wrist design when direct actuation of the joints is being implemented makes to have a large wrist design in comparison to the wrist of industrial robot manipulators. In the latter ones, transmissions are used for the actuation of the joints making possible to place the wrist actuators on the arm structure.

In the WHMAN configuration, the wrist constitutes part of link four, the link five and the link six.

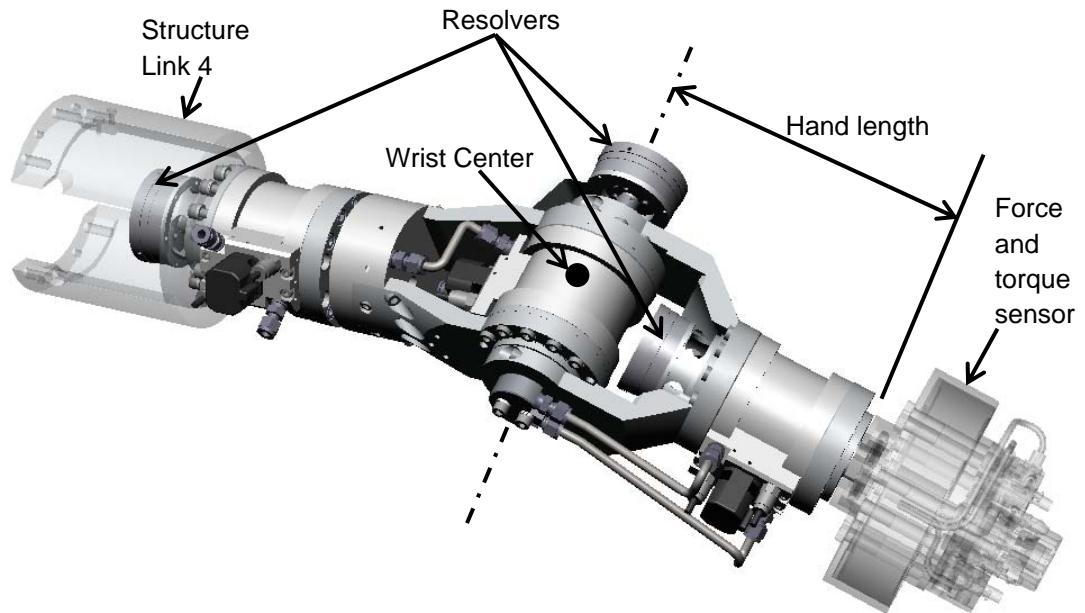


Figure 54: New wrist design for the WHMAN.

The possibility of eliminating the last actuator of the wrist (actuator J7) was evaluated in order to have a smaller and simpler wrist design like the wrist in many industrial robots. This idea was discarded due to the following two main reasons; the first one is that the wrist will become a 2DOF wrist consequently the WHMAN will be a 5DOF manipulator and according to the requirements for a force-reflecting remote handling manipulator shown in [4] robots of this kind must have 6DOF.

The second reason, which is very important is regarding the ability of the manipulator to complete the required tasks with a 2DOF wrist. Industrial robots with this 2DOF wrist, used symmetric tools for the tasks (e.g. welding tool, glue dispenser among others) which is basically a pin that is symmetric and the rotation of the last wrist joint does not have any effect on its orientation, that is why in those applications a 5DOF robot arm will perform the task without problems. Since the hydraulic jack (Figure 30) which actually is the heaviest tool for the WHMAN, is a not symmetric tool, it is required a 6DOF robot arm to manipulate it. Based on the previous reasons the last actuator is required on the wrist configuration.

5.2.1. Link four

The link four is the connection between the manipulator arm and the wrist; it is constituted by the actuator of joint four (in the arm) and the actuator of joint five (in the wrist) and the structure that connects them which is actually the link.

In the previous design there are some pneumatic valves for the WHMAN tool exchanger in the link five of the manipulator. Now those valves were relocated to this link. The material of the link structure is aluminum 6082-T6 as in the previous design. Figure 55 shows this new designed link.

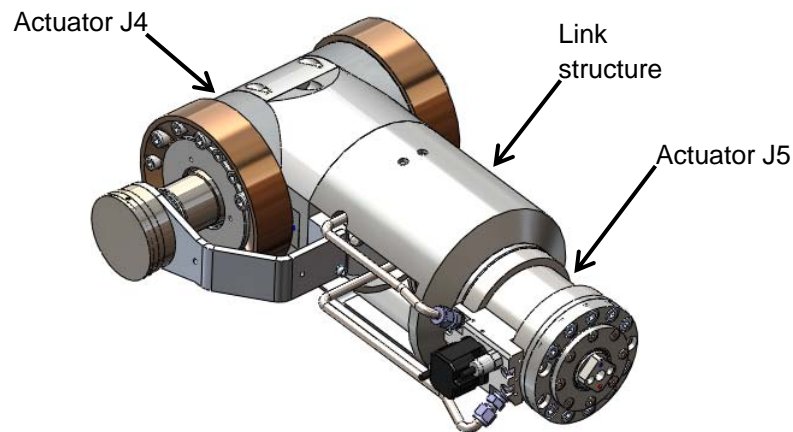


Figure 55: Link four of the WHMAN.

The exploded view of the link four is presented in Figure 56 without showing the actuator J4 since there are no changes on it. The vane actuators for joints 5 and 7 have a bolted head cover; this part is used to hide the head of the bolts to give better aesthetics to the manipulator.

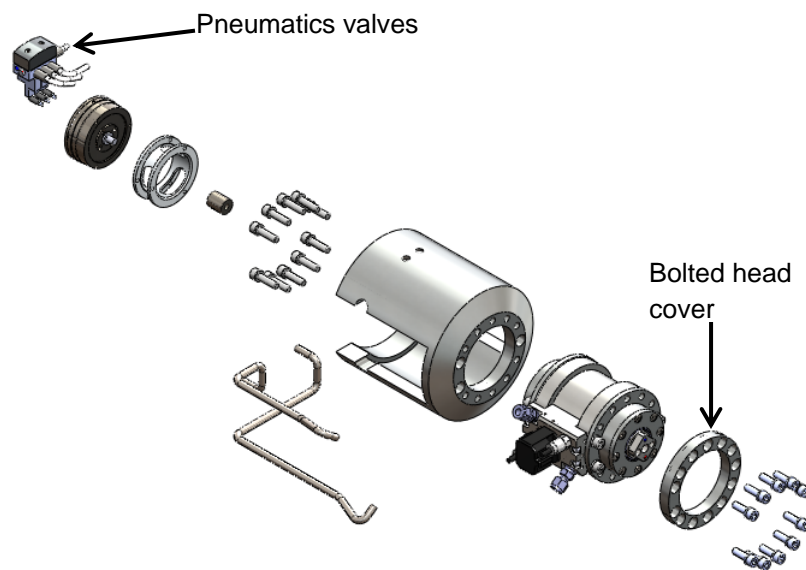


Figure 56: Exploded view sub-assembly link four.

5.2.2. Link five

This link consists of four main parts; the base of the link, two equal side parts and the vane actuator. In the base of this link, is made the connection of the fluid passages coming from the previous link through the shaft of the actuator. The base is made of duplex stainless steel 1.4462 because according to the structural analysis it is subjected to high stresses on the bolted connection. Another reason about using stainless steel is because it has fluid passages lines on it. The side parts are made of aluminum 7075-T6 in order to have a lighter structure.

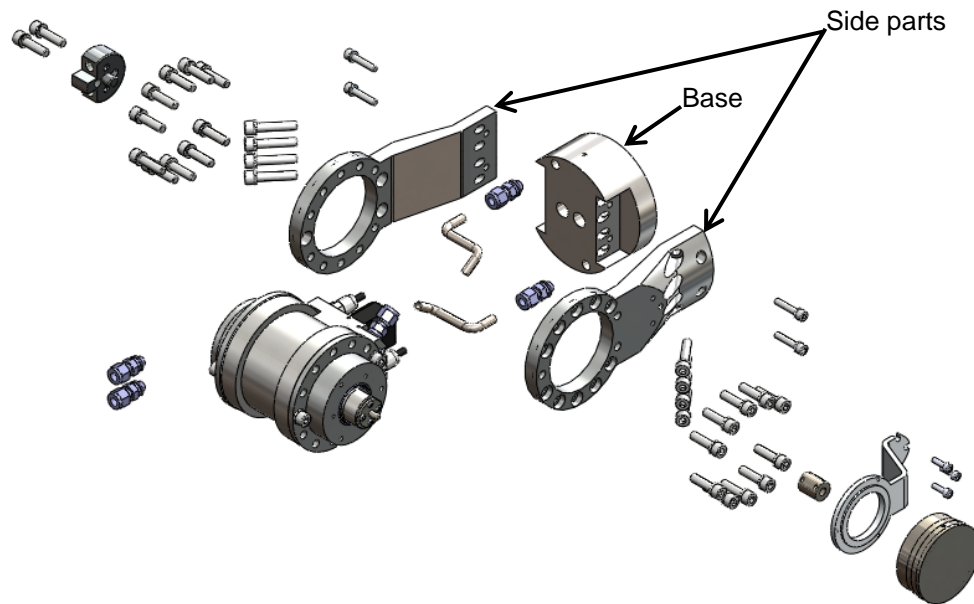


Figure 57: Exploded view link five.

The bolts used to attach the side parts to the base are different solution compared with the current design; this change was developed in order to facilitate the assembly process between this link and link four. Basically, the assembly will be performed by first attaching the base of this link to the shaft of actuator J5 (in link four) and then assembly on it at the same time the actuator and sides.

5.2.3. Link six

This is the last part of the wrist, which is connected to the force/torque sensor module. It consists basically of only the link structure and the vane actuator. Since this link represents the hand length of the robot manipulator, much effort was put into redesign of the link structure in a way to reduce the hand length. As mentioned before one of the biggest constraints is the big size of the resolver which has to be assembled along the axis of the shaft.

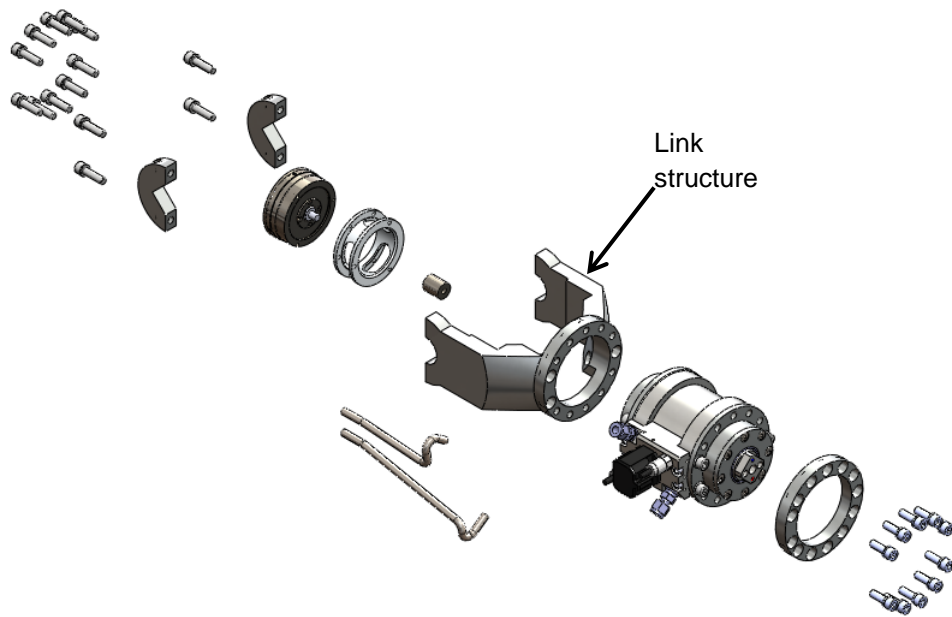


Figure 58: Exploded view link six.

As seen from Figure 56 and Figure 58, exactly the same actuator is being used. The material of the link structure in this case is aluminum 7075-T6.

5.3. Some improvements in the new wrist design

In the current wrist design, link structures have to be attached to each actuator in order to close the assembly of the actuator; this is because the actuator side covers constitute the link structures.

In the new design, the side covers (called bearing housings) are fixed to the actuator during the assembly process of it, but only with three bolts. There are other ten bolts for the attachment of the actuator with the links. The fact of fix the side covers to the actuators with three bolts will facilitate the assembly of the wrist. One example of this shown in Figure 59 presents a comparison between current design and new design of actuator J6.

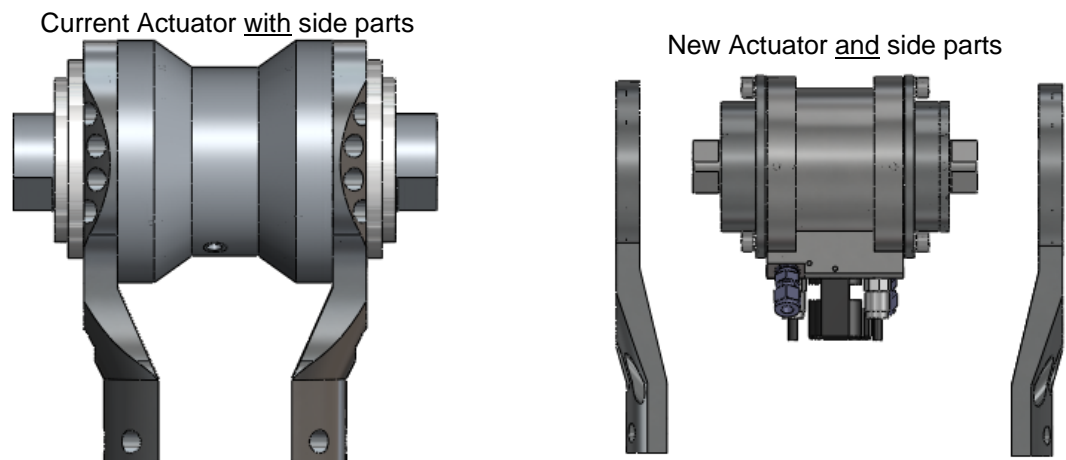


Figure 59: Assembly comparison between current and new actuator J6.

As seen from these figures the side parts of the link structure in the case of the current design are also components of the actuator assembly while in the new design the actuator is assembled as a unit.

With this change it is possible to have a spare actuator and with this will be easy and fast to repair the wrist in case one actuator fails. Also this will help in case it is needed to provide maintenance for the actuators and keep the manipulator working.

The greater use of this idea is if all the actuators are exactly the same because then is needed only one type of spare actuator, unfortunately this was not possible in the new design. Even a lot of effort was put to have only one actuator design this was not achieved, the major challenge is in the design of the shaft which actually is the only different component in the new design. To implement this idea, there has to be two different types of spare actuators.

Another improvement is that now there is easy access to the hydraulics valves at least for actuators in joints 5 and 7. The valve in the actuator of joint 6 is more difficult to reach, but can be accessed by removing some components, this is now easier due to the improvements in the assembly process. Also there are fewer bolts on the wrist for the connection of the actuators to the link structures, which make easier and faster the assembly of the wrist.

5.4. Comparison between new and current wrist design

This section presents a comparison of the two wrist designs, as mentioned previously both designs look similar.

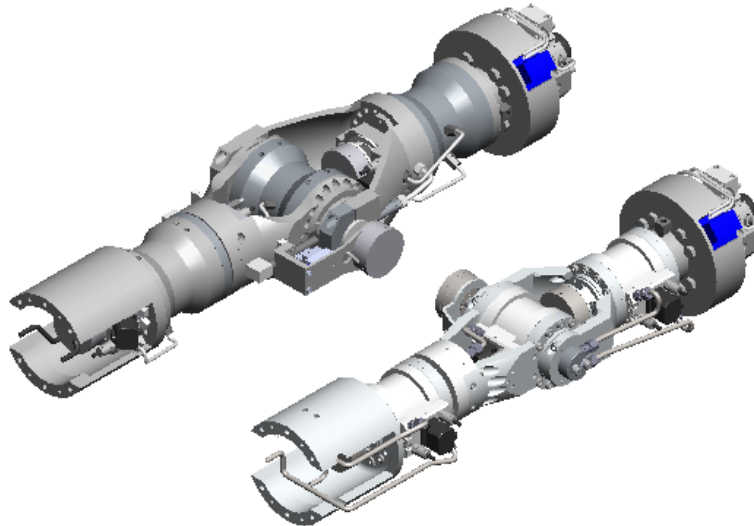


Figure 60: Isometric view of the wrists (left current, right new).

The next figure shows the hand length of both designs, as it can be seen decreased 95 mm, it is expected that with this the dexterity of the manipulator will increase. This can be known by developing simulations of the manipulator's tasks with the new wrist design, but this is out of the scope of this thesis work.

Also with these type of simulations can be determined if the distance between the axis of joint 4 and the axis of joint 6 (see Figure 53) which is basically the length of link 4 plus the length of link 5 has to be modified. The reduction in the hand length is accompanied with a reduction in the reachable space of the manipulator if the distance mentioned previously (lengths of links 4 and 5) remains the same. The easiest way to increase this distance is by increasing the length of the link 4 structure (Figure 55).

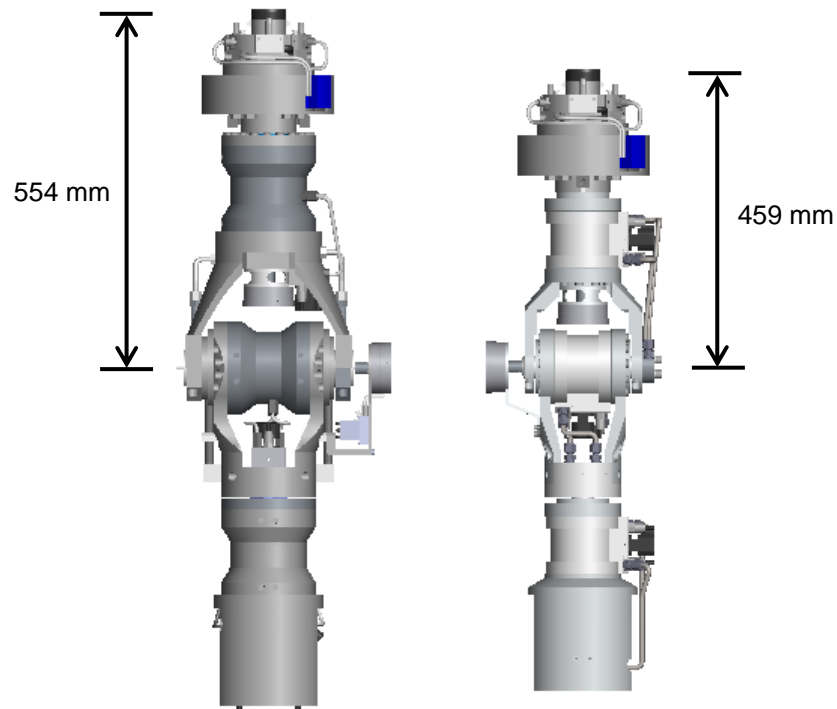


Figure 61: Hand length of the wrists.

Again as with the actuators the weight of each design is compared. Based on the 3D models in Figure 61, the weight of the current wrist is about 59.6 kg and the weight of the new wrist design is 29.5 kg. The mass reduction of fifty percent obtained with the actuators remains also as a reduction of the wrist assembly. This roughly means that the weight of each redesign component was reduced by half. Finally is presented a last figure where is possible to appreciate the reduction in size of the link structures.

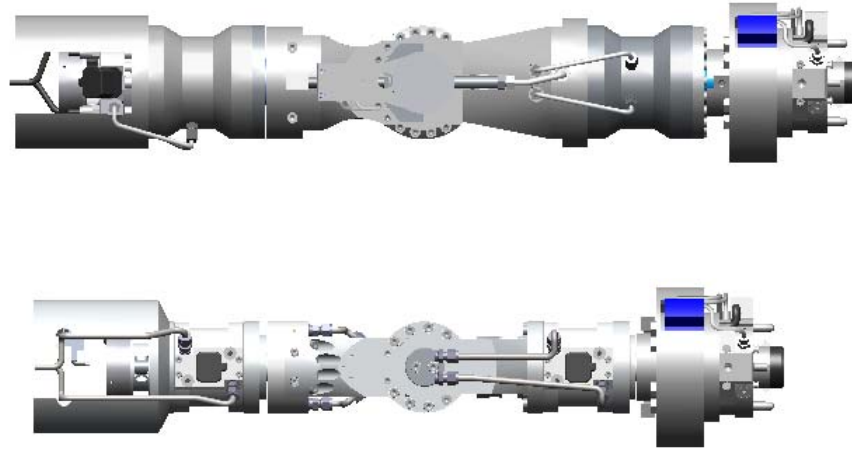


Figure 62: Side view comparison.

The next chapter presents the analyses to validate the components to the wrist and actuators. During the analysis performed some modifications were done to the components of the wrist in order to fulfill the requirements.

6. STRUCTURAL VALIDATION OF THE WRIST COMPONENTS

This chapter presents the results from the FEM analysis developed for the validation of the redesign parts. First, the results from the analysis performed on the main components of the vane actuator (chamber and shaft) are shown. After this, the results for the validation of the wrist links are presented.

6.1. Finite element analysis

All the parts and components were modeled using SolidWorks, and since in this software is also possible to develop finite element analysis with a functionality called SolidWorks Simulation (formerly called COSMOWorks), it was decided to develop all the simulations using this software.

The results for each component are shown in the following manner; first is shown the meshed 3D model of the components (assemblies) with the external loads and restraints. Then is presented a table with the names and materials for each component in the analysis, also in the same table are the values of the external forces. Following the table are shown the result plots for the stress distribution, the factor of safety (FOS) and the deformation obtained from the simulations. Finally, a table is used to summarize the FEM analysis results.

6.2. Structural validation of the main components in the vane actuator

As seen from the exploded view of the water hydraulic vane actuator in Figure 38, it has many parts and components. Analyses were developed for almost all the parts, but the results of the two main ones, which are the chamber (with the vanes) and shaft (with the vanes) are presented in this section.

6.2.1. Chamber and vanes FEM structural analysis

Figure 63 shows the chamber and vanes 3D models, with the external loads applied which are the pressure and bearing forces, the restraints (boundary conditions) in this case are the holes for the bolts.

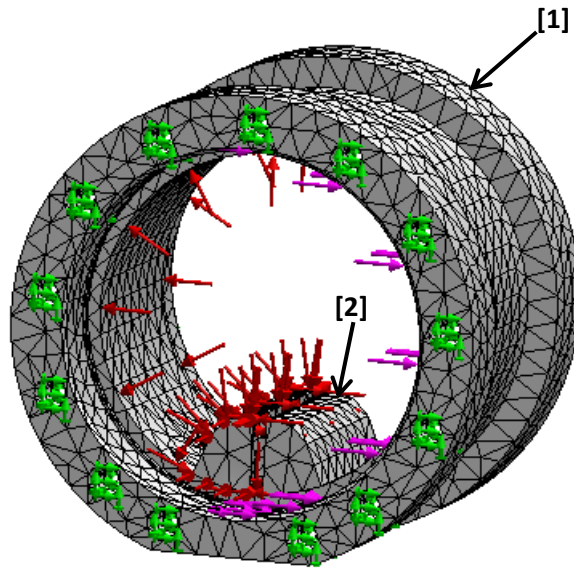




Figure 63: Meshed model with external loads and constraints (Chamber and vanes).

Table 19 defines the materials used for the components in this analysis and the external loads applied. The pressure force is equal to the maximum working pressure in the system. The maximum bearing force is calculated based on Equation (28), as mentioned earlier this pressure force has different values depending on the position of the actuator's shaft. When the volume of fluid at higher pressure increase (meaning that the shaft has moved, and the angle between the chamber's vanes and the shaft's vanes had increase) the bearing force decrease, also the stress on the chamber walls decreases due to the same pressure is applied to a bigger area. This is why the worst case load scenario is when there is an angle of 180° between the chamber and shaft vanes, the one shown in Figure 63. Other scenarios where also simulated but as expected had lower stress values than the worst case.

Table 19: *Materials for the components and external loads (Chamber and vanes)*

No.	Part Name	Material	Yield Strength [MPa]
1	Chamber	1.4462	510
2	Chamber vanes	1.4462	510
Load Name		Value	Symbol
Pressure		21 MPa	
Bearing force		33600 N	

The following 3 figures show the stress distribution plot, the deformation plot and the factor of safety plot for this analysis.

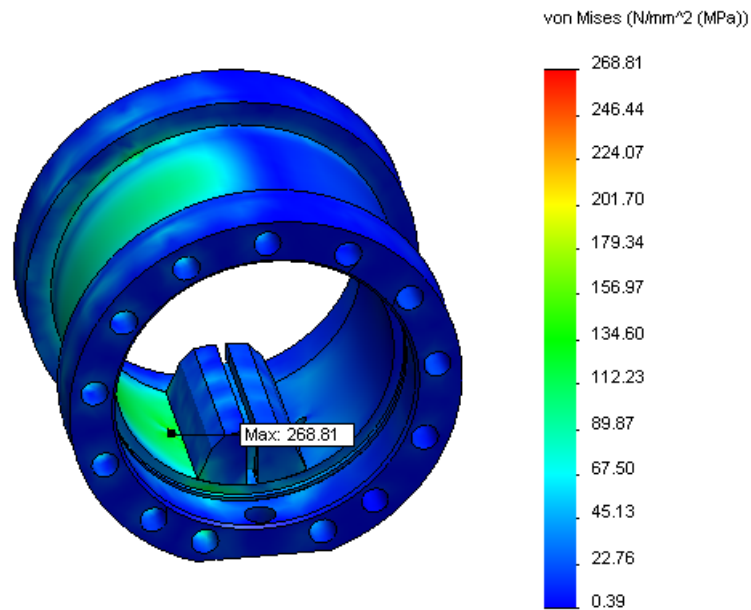


Figure 64: Stress distribution on chamber and vanes.

The highest stress is on the hole (on the pressure side) where the fluid goes into the chamber. In the bolted connection is generated a higher stress in comparison to other zones but still lower than the maximum.

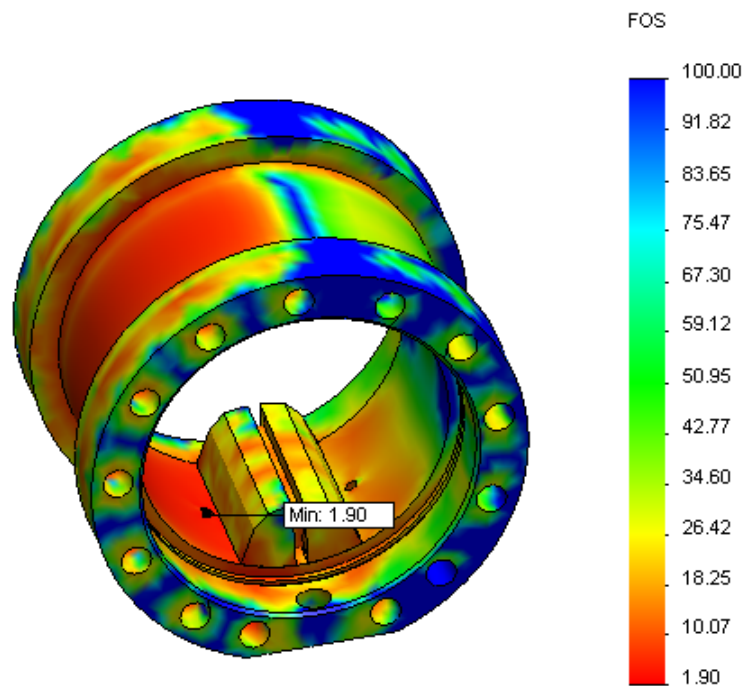


Figure 65: Factor of safety on chamber and vanes.

The lowest FOS is located exactly in the same place as the maximum stress because both components are of the same material, the minimum FOS is 1.90.

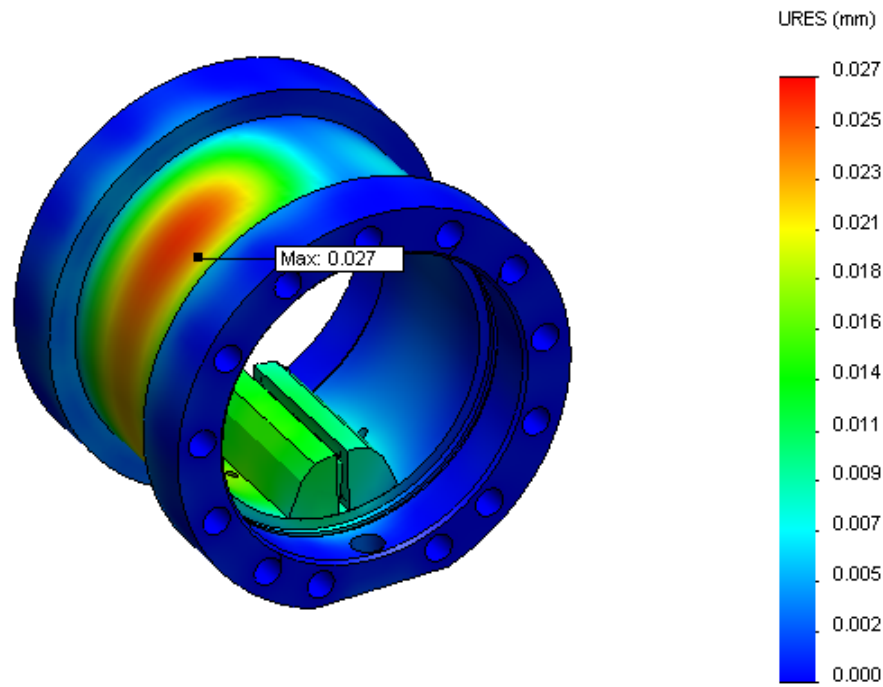


Figure 66: Deformation on chamber and vanes due to the applied loads.

The maximum deformation is due to the pressure applied to the chamber and is 0.027 mm. Table 20 presents a summary of the previous results.

Table 20: Summary of the chamber and vanes FEM analysis results

No.	Part Name	Material	Yield Strength [MPa]	Max. stress [MPa]	FOS	Max. Deformation [mm]
1	Chamber	1.4462	510	269	1.90	2.75e-2
2	Chamber vanes	1.4462	510	196	2.6	1.59e-2

6.2.2. Shaft and vanes FEM structural analysis

As mentioned before the shaft is the only component that is different between the two new actuators design, because of this difference there are two designs. The validation of the two shaft and vanes assemblies is presented next.

First is shown the validation of the shaft for the actuators in joints 5 and 7. Next figure shows the meshed model, external load and boundary conditions.

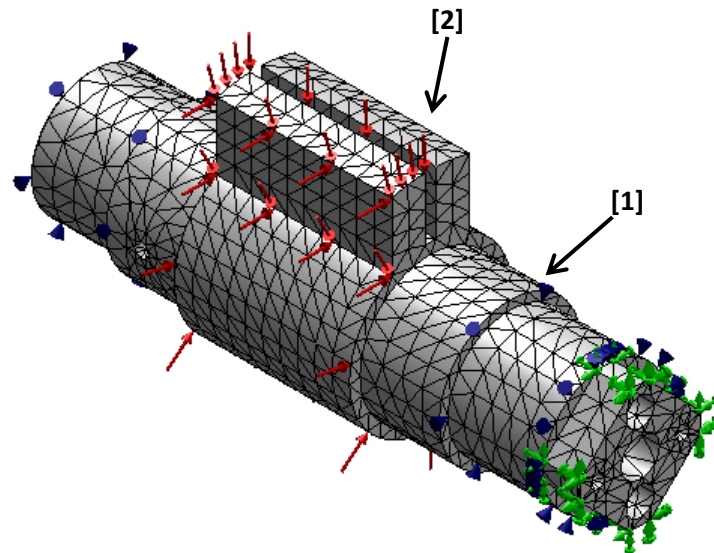



Figure 67: Meshed model with external load and constraints (Shaft and vane actuators J5 and J7).

The materials for the components in the simulation and the values of the external load are shown below. In Figure 67 there are some blue arrows, these represent the bearings.

Table 21: Materials for the components and external loads (Shaft and vanes)

No.	Part Name	Material	Yield Strength [MPa]
1	Shaft	1.4410	590
2	Shaft vanes	1.4410	590
Load Name		Value	Symbol
Pressure		21 MPa	

Next is shown the plots of stress, factor of safety and deformation.

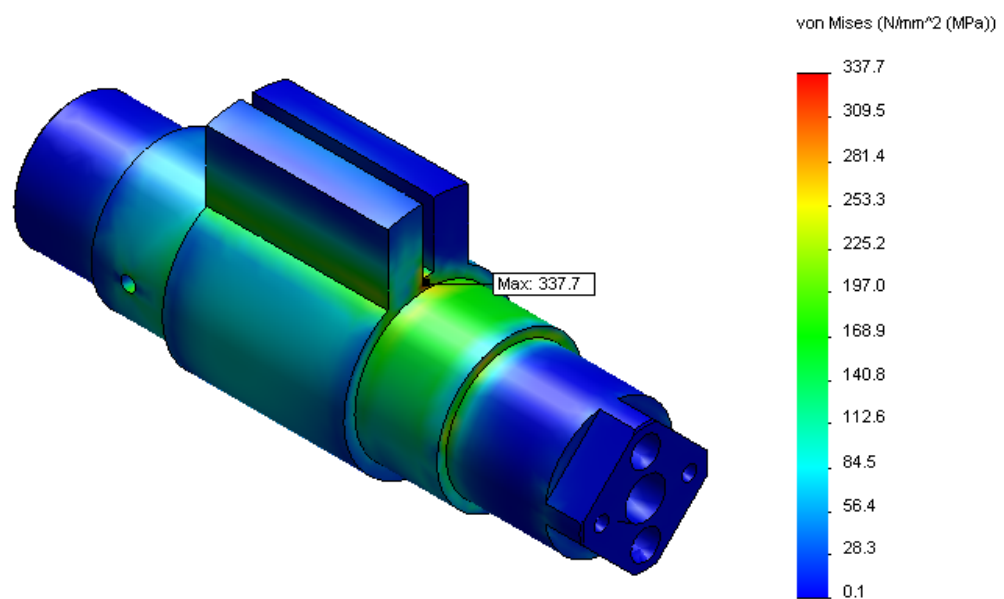


Figure 68: Stress distribution on Shaft and vanes (actuators J5 and J7).

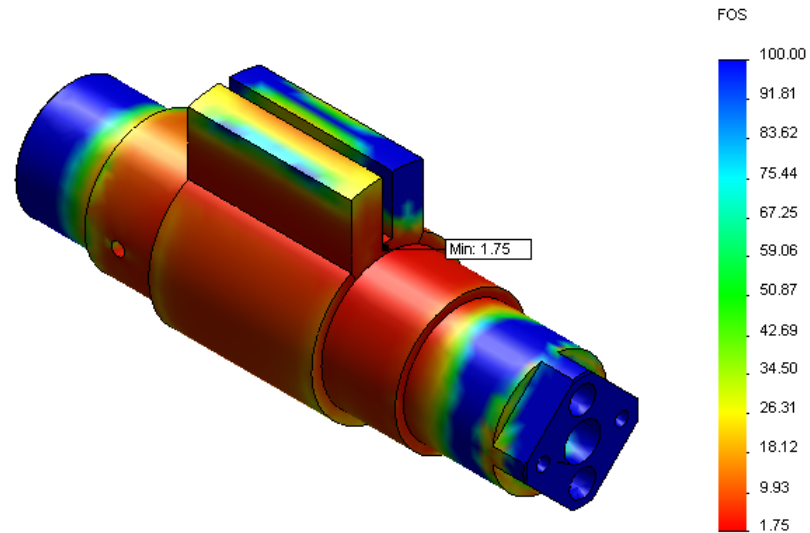


Figure 69: Factor of safety on Shaft and vanes for actuators J5 and J7.

The maximum stress of 337 MPa is located at the bottom of the vanes, in the same place is located the minimum FOS of 1.75. This is because of the same reason as in the chamber and vanes analysis, both components have the same material.

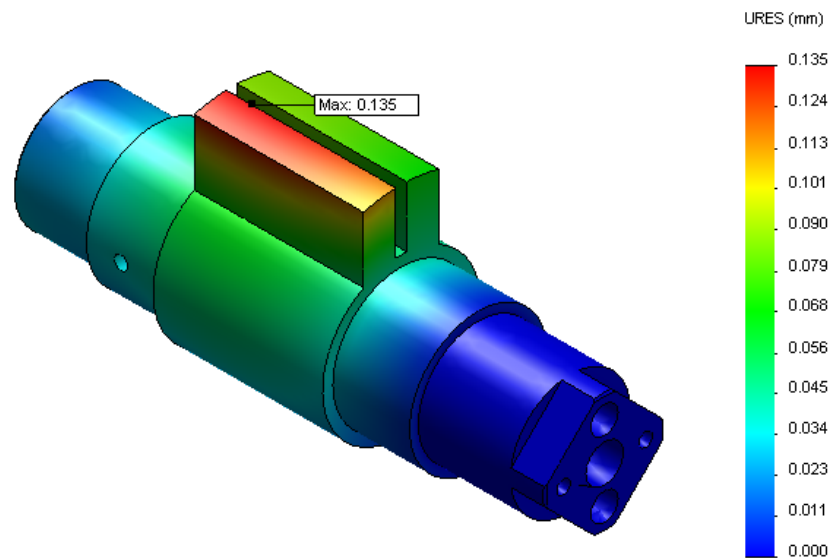


Figure 70: Deformation on shaft and vanes for actuators J5 and J7.

The maximum deformation in this assembly due to the pressure applied is at the top of the vane. Table 22 presents the summary of the results.

Table 22: Summary of the Shaft and vanes (Actuators J5 and J7) FEM analysis results

No.	Part Name	Material	Yield Strength [MPa]	Max. stress [MPa]	FOS	Max. Deformation [mm]
1	Shaft	1.4410	590	273	2.16	6.72e-2
2	Shaft vanes	1.4410	590	337	1.75	1.35e-1

The analysis of the shaft and vanes assembly for the actuator in joint 6 is now presented. As can be seen from Figure 71, the load is the same, as well as the bearings support (blue arrows) but the constraints (green arrows), now are at both ends of the shaft.

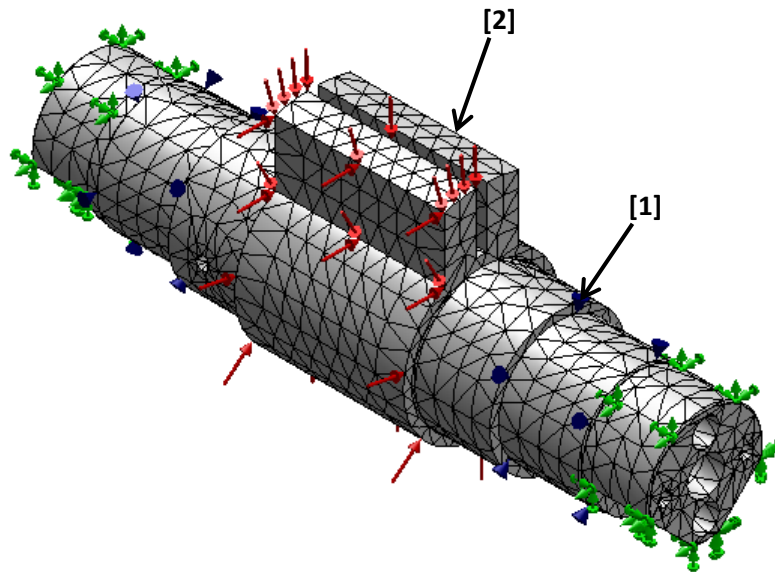


Figure 71: Meshed model with external load and constraints (Shaft and vane actuator J6).

Because the only difference between the shaft vane assemblies is in the shape of the shaft, the information on Table 21 is exactly the same for both assemblies. The plots of stress distribution, FOS and deformation are shown next.

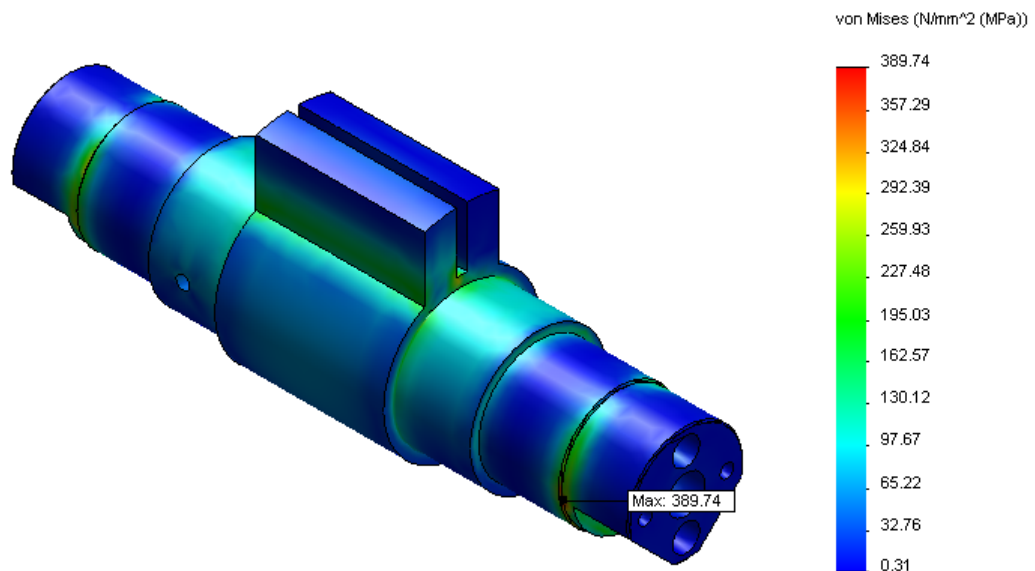


Figure 72: Stress distribution on shaft and vanes (actuator J6).

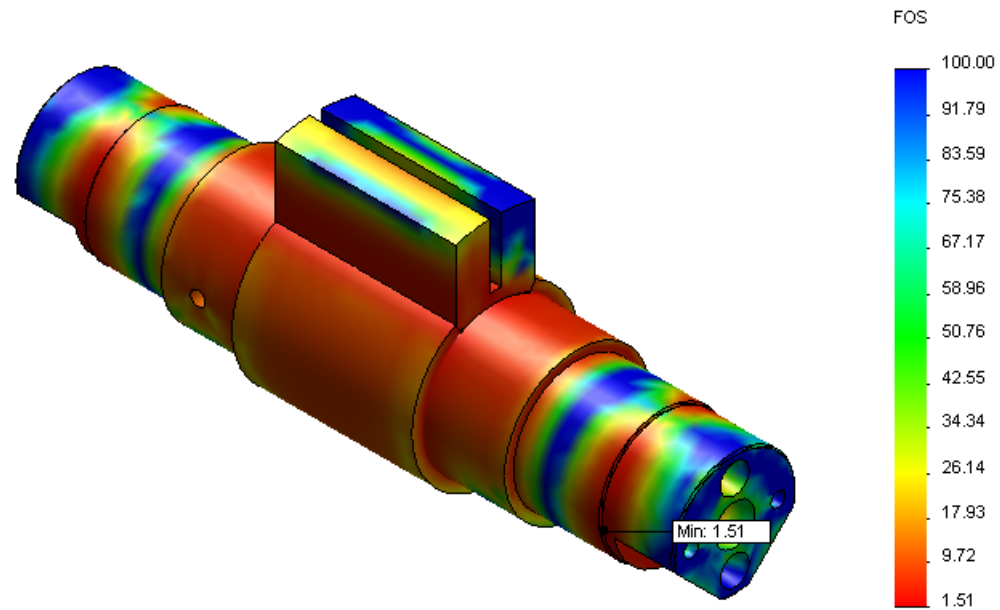


Figure 73: Factor of safety on shaft and vanes for actuator J6.

The maximum stress (389 MPa) is located in the step where there is a change in diameter between the section for the application and the section for the bearings (sections of the shaft in Figure 36). The minimum FOS is located in the same place of the maximum stress as in the previous analysis.

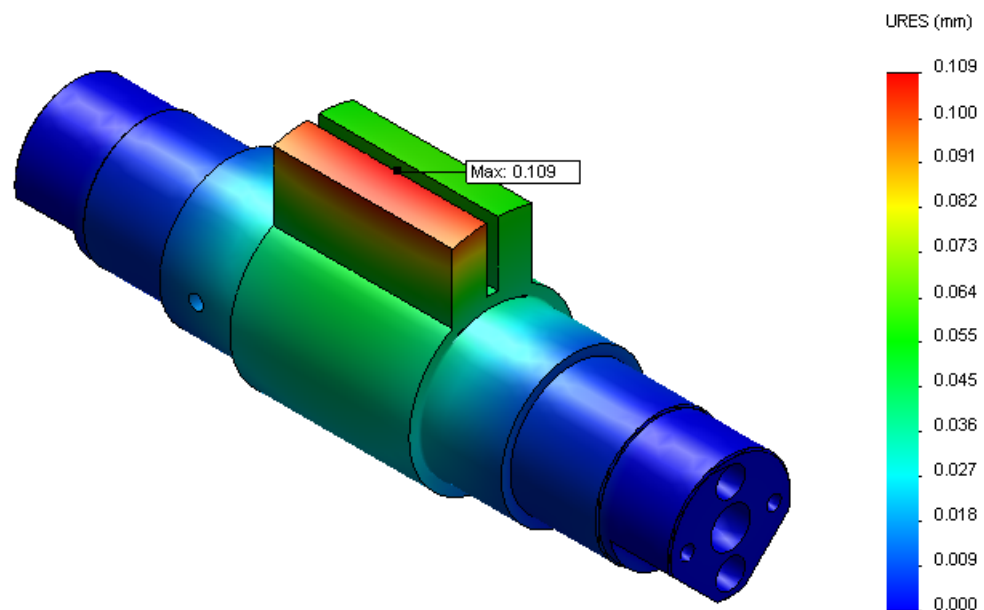


Figure 74: Deformation on shaft and vanes for actuator J6.

Also the maximum deformation is at the top of the vane on which is applied the pressure. Table 23 summarizes the results.

Table 23: *Summary of the Shaft and vanes (Actuator J6) FEM analysis results*

No.	Part Name	Material	Yield Strength [MPa]	Max. stress [MPa]	FOS	Max. Deformation [mm]
1	Shaft	1.4410	590	389	1.51	5.07e-2
2	Shaft vanes	1.4410	590	284	2.07	1.09e-1

The results from the analysis to validate the main components of the vane actuator were described in this section. Next is presented the analysis to validate the links of the new wrist design. Because the actuators are part of the links, the chamber and shaft are also on the analyses for the wrist structures.

6.3. Structural validation of the wrist links

As mentioned before the wrist constitutes part of link 4, the link 5 and link 6 on the WHMAN. The validation of the redesign parts regarding these links is presented in this section. To compute the external loads acting on the links, it was calculated first the forces acting on the tip of the force/torque sensor based on a worst load case scenario presented in APPENDIX C. These forces were used in developing the free body diagrams of the links shown in APPENDIX D. The reactions on the diagrams are the forces and moments acting on each link; these were used in the structural analysis. First is described the structural analysis for link 6, then for link 5 and finally for link 4 (just the redesigned components).

Because the links assemblies are more complex than the ones in the previous section, some modifications were done to the components of the vane actuators to make them simpler in order to decrease the computational time of the results. On the other hand, the 3D models of the links structures have all the details in order to have reliable results about these components.

6.3.1. Link 6 structural analysis

The 3D meshed model of link 6, the external loads (purple arrows) and constraints (green arrows) are shown in Figure 75.

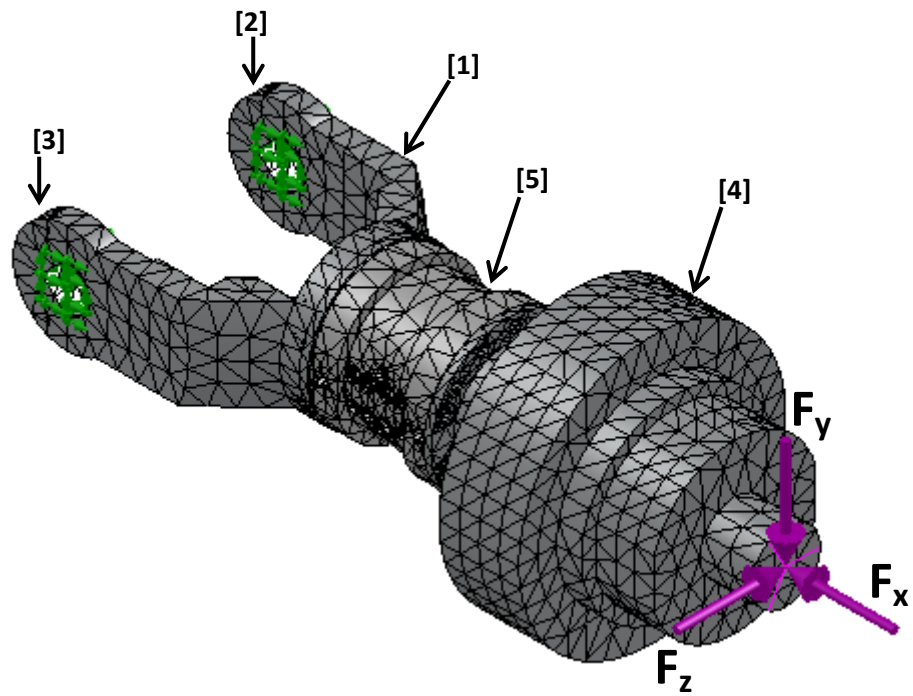


Figure 75: Meshed model with external loads and constraints (Link 6).

Table 24 defines the materials for the components in this analysis and the external loads applied.

Table 24: Materials for the components and external loads (Link 6)

No.	Part Name		Material	Yield Strength [MPa]
1	Link 6 structure		7075-T6	360
2	Link 6 mounting		7075-T6	360
3	Link 6 mounting		7075-T6	360
4	Force and torque sensor		7075-T6	360
5	Vane actuator	Chamber	1.4462	510
		Shaft	1.4410	590
		Bearing housing	7075-T6	360
		Bearing housing one piece	7075-T6	360
	Loads (Axis)		Force [N]	Torque [Nm]
	x		-1859	0
	y		-981	0
	z		-976	0

Following figures presents the stress distribution, FOS and deformation plots.

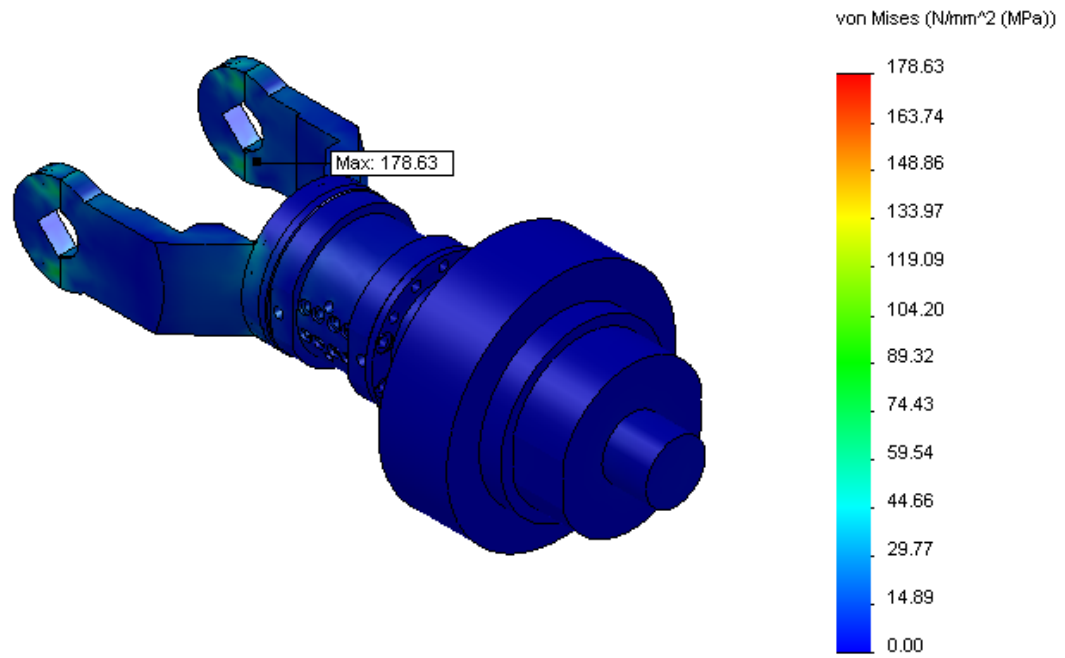


Figure 76: Stress distribution on link 6.

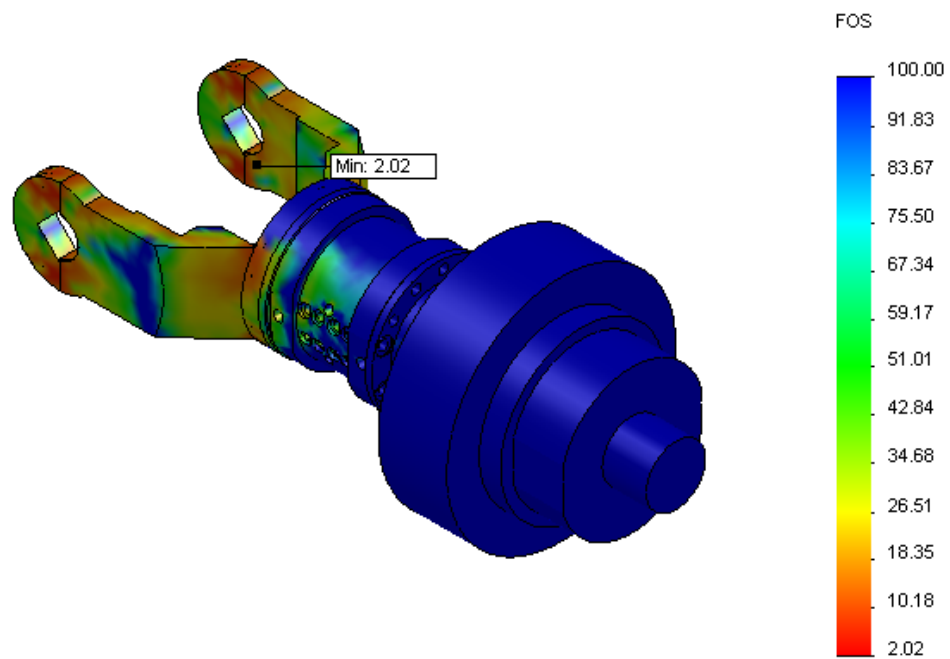


Figure 77: Factor of safety on link 4.

The maximum stress is located at the bolted connection between the link structure and the mounting parts. The minimum FOS of 2.02 is located in the same place of the highest stress because this is generated on the parts with lowest yield strength.

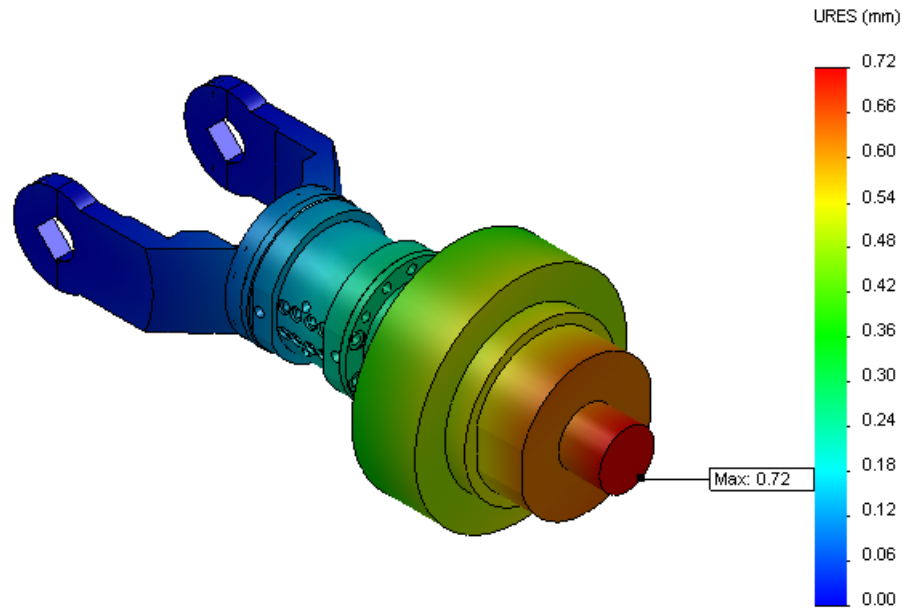


Figure 78: Deformation on link 6 due to the applied loads.

The maximum deformation is about 2.5 times bigger than one calculated in [4] for the current wrist design in a similar analysis. Table 25 shows the summary of the results.

Table 25: Summary of Link 6 FEM analysis results

No.	Part Name	Material	Yield Strength [MPa]	Max. stress [MPa]	FOS	Max. Deformation [mm]
1	Link 6 structure	7075-T6	360	178.6	2.02	1.35e-1
2	Link 6 mounting	7075-T6	360	176	2.04	1.83e-2
3	Link 6 mounting	7075-T6	360	175	2.06	1.96e-2

6.3.2. Link 5 structural analysis

The 3D meshed model of link 5, the external loads (purple arrows) and constraints (green arrows) are shown in Figure 79. For this analysis, there are also moments acting on the y and z axes as external loads.

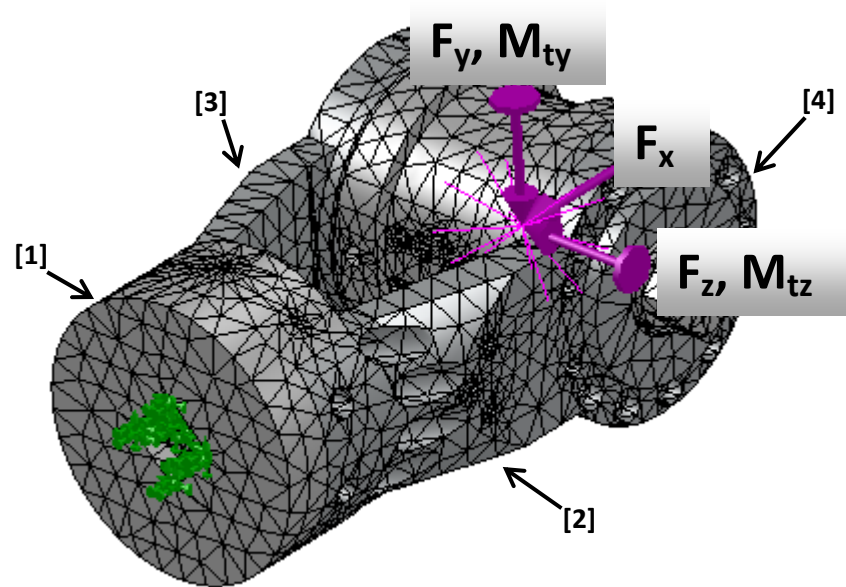


Figure 79: Meshed model with external loads and constraints (Link 5).

Table 26 defines the materials for the components in this analysis and the values of the external forces and moments applied.

Table 26: *Materials for the components and external loads (Link 5)*

No.	Part Name		Material	Yield Strength [MPa]
1	Link 5 base		1.4462	510
2	Link 5 side part		7075-T6	360
3	Link 5 side part		7075-T6	360
4	Vane actuator	Chamber	1.4462	510
		Shaft	1.4410	590
		Bearing housing	7075-T6	360
		Bearing housing one piece	7075-T6	360
	Loads (Axis)		Force [N]	Torque [Nm]
	x		-1859	0
	y		-1208	448
	z		-976	-511

Following the plots of the stress distribution, FOS and deformation of link 5 are presented.

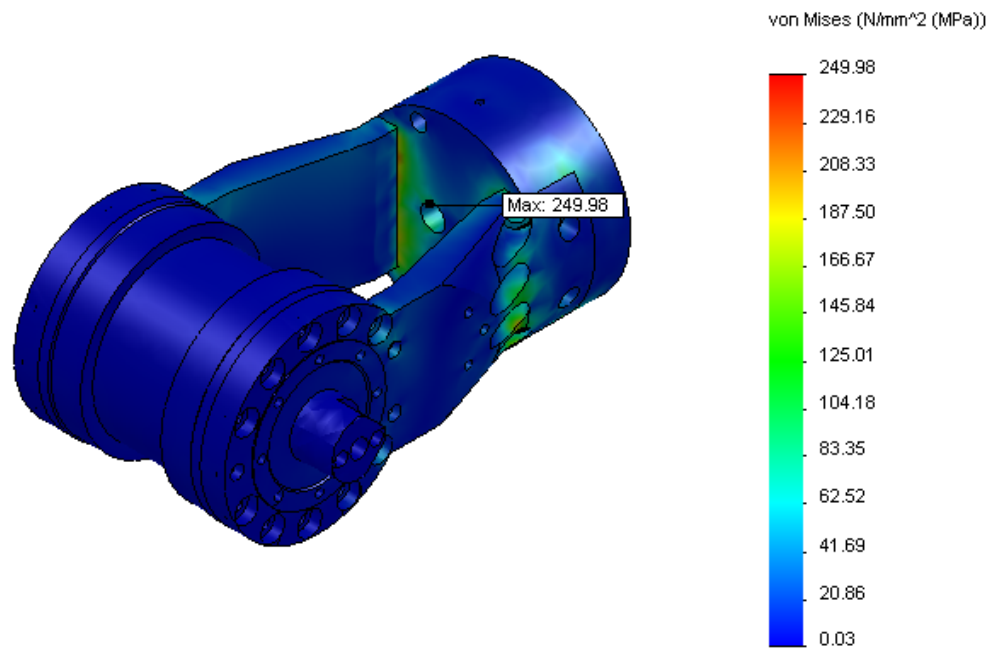


Figure 80: Stress distribution on link 5.

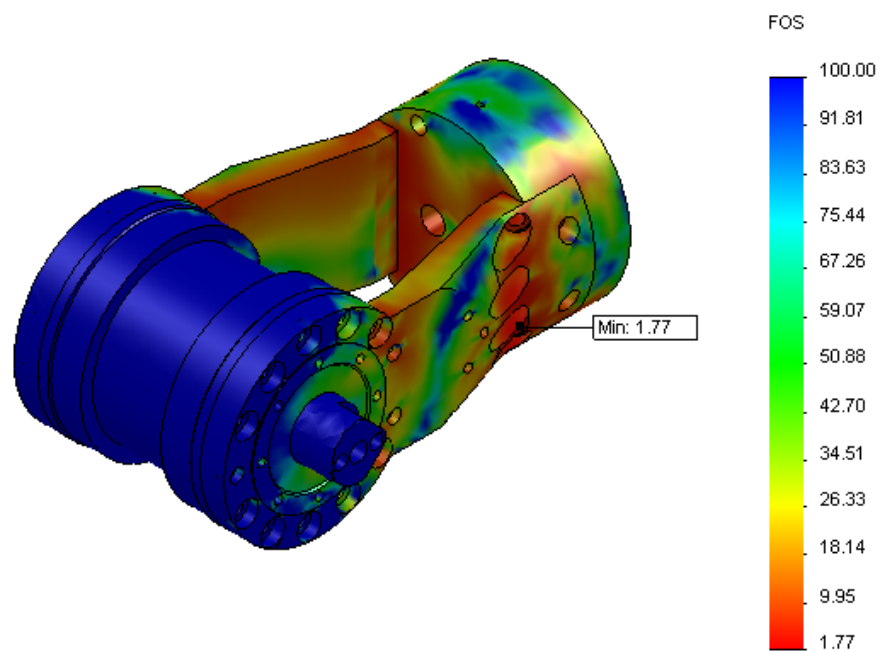


Figure 81: Factor of safety on link 5.

The maximum stress is located on the base at the bolted connection with the side part. In this analysis, the minimum FOS is not at the same place as the maximum stress; in this case is located in a one of the side parts which has lower yield strength and lower stress in comparison to the base of the link, as can be seen in Table 27.

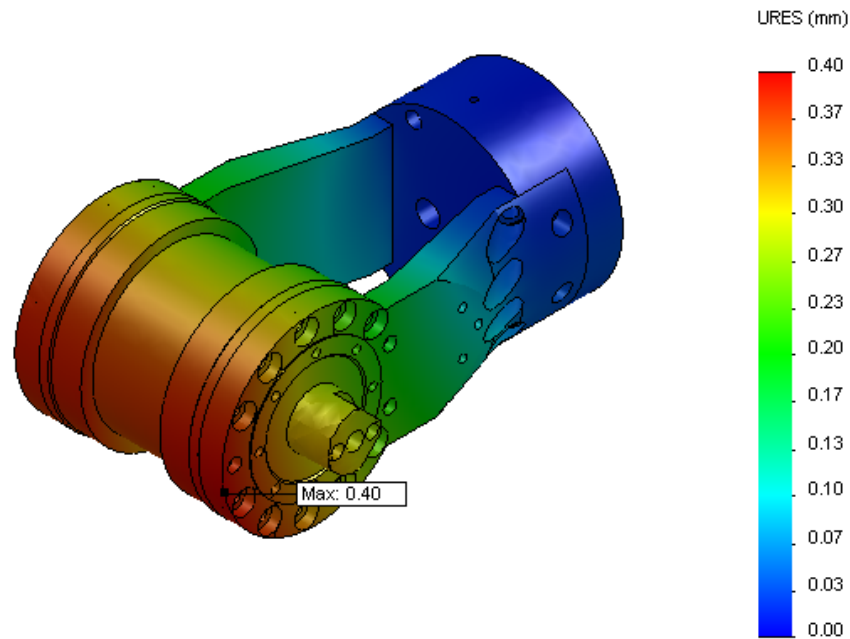


Figure 82: Deformation on link 5 due to the external loads.

In this analysis Link 5 shows a deformation about 3 times bigger than one calculated in [4] for the current wrist design. Table 27 shows the summary of the results.

Table 27: *Summary of Link 5 FEM analysis results*

No.	Part Name	Material	Yield Strength [MPa]	Max. stress [MPa]	FOS	Max. Deformation [mm]
1	Link 5 base	1.4462	510	245	2.04	3.82e-2
2	Link 5 side part	7075-T6	360	190	1.89	3.88e-1
3	Link 5 side part	7075-T6	360	203	1.77	3.99e-1

6.3.3. Link 4 structural analysis (only for the modified components)

The 3D meshed model of the components of link 4 that were modified during this redesign is shown in Figure 83. In this analysis the base of link 5 was used to apply the external loads on it. The external loads (purple arrows) and constrains (green arrows) are also shown.

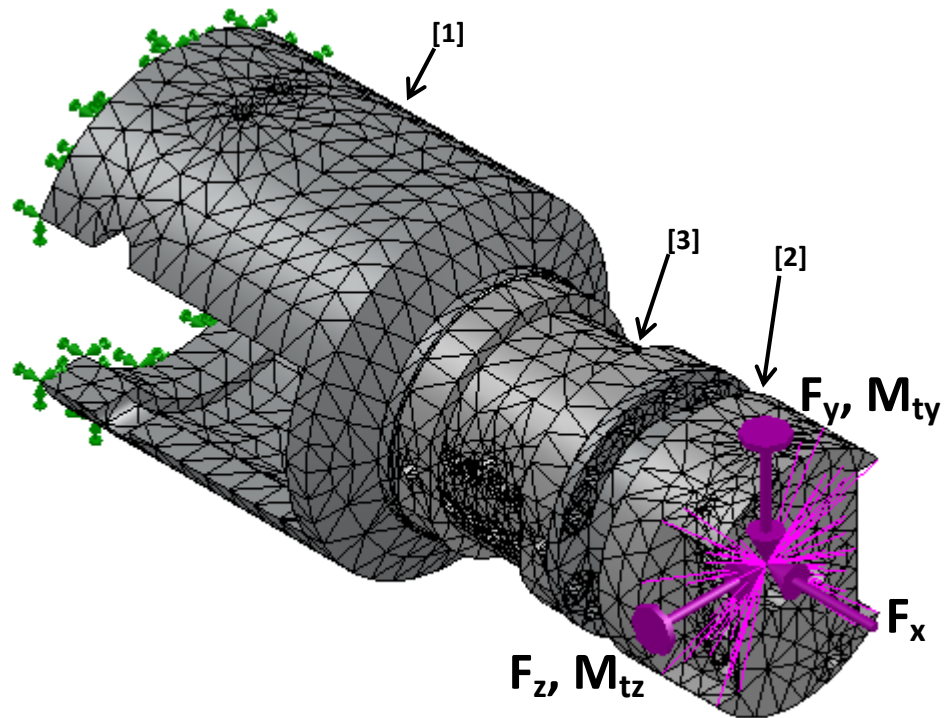


Figure 83: Meshed model with external loads and constraints for the modified components of Link 4.

Table 28 defines the materials for the components in this analysis and the values of the external forces and moments applied.

Table 28: *Materials for the components and external loads (Link 4)*

No.	Part Name		Material	Yield Strength [MPa]
1	Links 4 structure		7075-T6	360
2	Link 5 base		1.4462	510
3	Vane actuator	Chamber	1.4462	510
		Shaft	1.4410	590
		Bearing housing	7075-T6	360
		Bearing housing one piece	7075-T6	360
	Loads (Axis)		Force [N]	Torque [Nm]
	x		-1859	0
	y		-1332	644
	z		-976	-771

Following the plots of the stress distribution, the FOS and deformation for this assembly are presented .

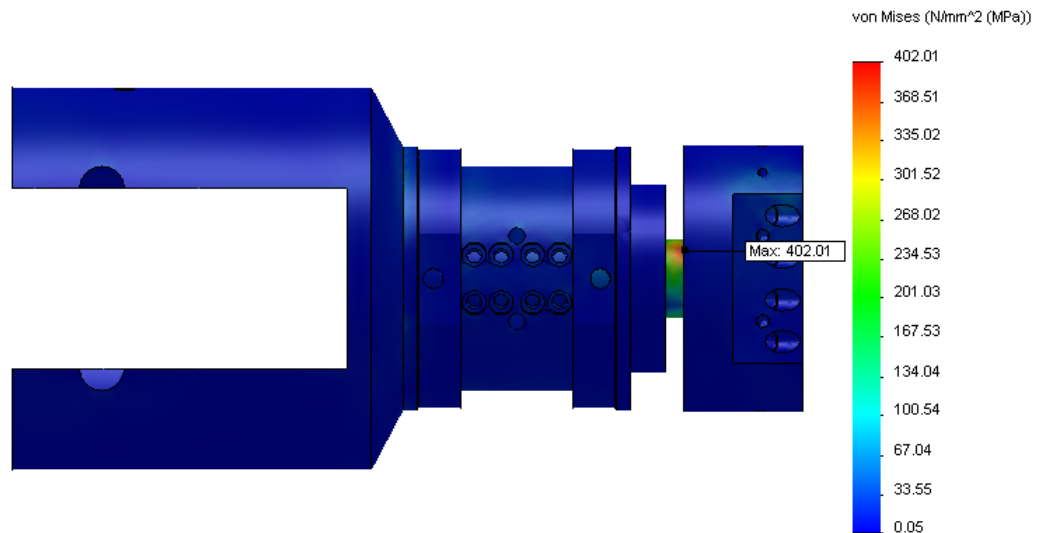


Figure 84: Stress distribution in the assembly.

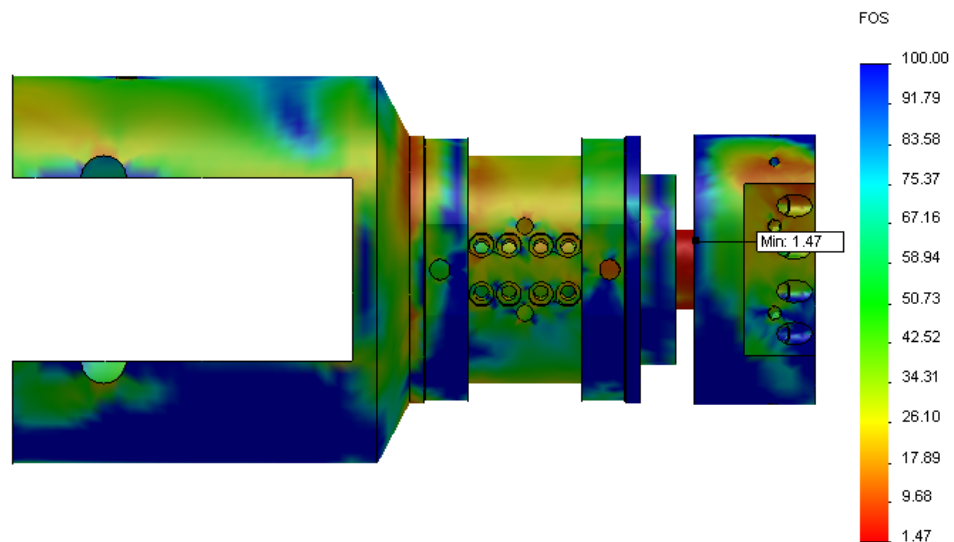


Figure 85: Factor of safety in assembly.

As can be seen in the previous figures the highest stress is generated on the shaft of the actuator. In the simulation of link 6 the stress of the shaft for the actuator in joint 7 is around 100 MPa, the stress on the shaft for the actuator on joint 5 is higher due to the higher forces applied; the stress is about 4 times bigger. The minimum factor of safety is in the same place as the maximum stress. Even as the FOS is 1.47 which is less than the minimum required (1.5), the design is fine because this high stress of 402 MPa is generated according to the analysis in a very small volume of the part.

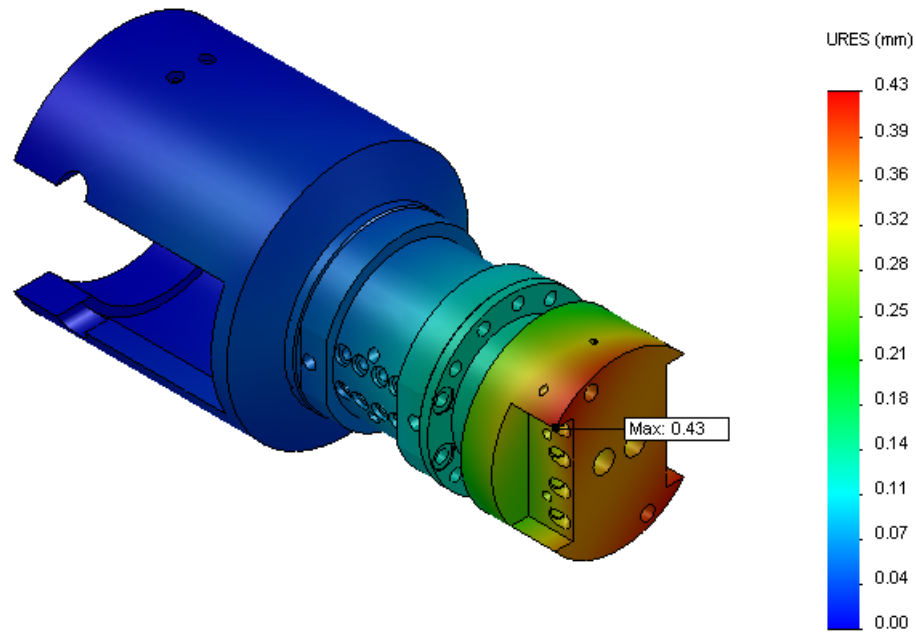


Figure 86: Deformation on the assembly due to the applied loads

The deformation is about 2 times bigger than the one calculated in [4] for the current wrist design. Table 29 shows the summary of the results.

Table 29: Summary of Link 4 FEM analysis results

No.	Part Name	Material	Yield Strength [MPa]	Max. stress [MPa]	FOS	Max. Deformation [mm]
1	Link 4 structure	7075-T6	360	140	2.57	6.13e-2
2	Link 5 base	1.4462	510	217	2.35	4.27e-1
3	Shaft of actuator	1.4410	590	402	1.47	2.10e-1

The previous results from the analyses performed to validate the new wrist design for the WHAMN, shows that the stress level on the components remains under allowed limits, having a factor of safety of 1.5. The only component that is slightly below (1.47), is the shaft of the actuator on joint 5, but the stress is generated in a very small volume of the shaft due to forces calculated in a worst load case scenario. During the normal operation of the manipulator, the external loads are much lower.

7. CONCLUSIONS

A new wrist design for the WHMAN was developed and validated using FEM analysis. The main objective of this work was to design a more compact and lighter wrist. This objective was achieved and based on the 3D models the new design compared with the current wrist weights 50% less.

The payload to weight ratio of the current WHMAN is about 1:1.95 (with a load of 100 kg) with the new design this ratio is decreased to 1:1.65 which is a very good improvement. In order to have a ratio of 1:1 the load capacity has to be increased and the structure of the whole manipulator optimized. To have a lighter wrist, each wrist actuator has to be designed according to specific requirements based on the loads applied on each of them. In this work, the requirements defined are the same for all the actuators in order to have a modularized actuator design. Figure 87 shows the WHMAN with the new wrist. By reducing the hand length of the wrist the dexterity of the robot will increase, this has to be evaluated by simulating manipulator's tasks with the new wrist design.

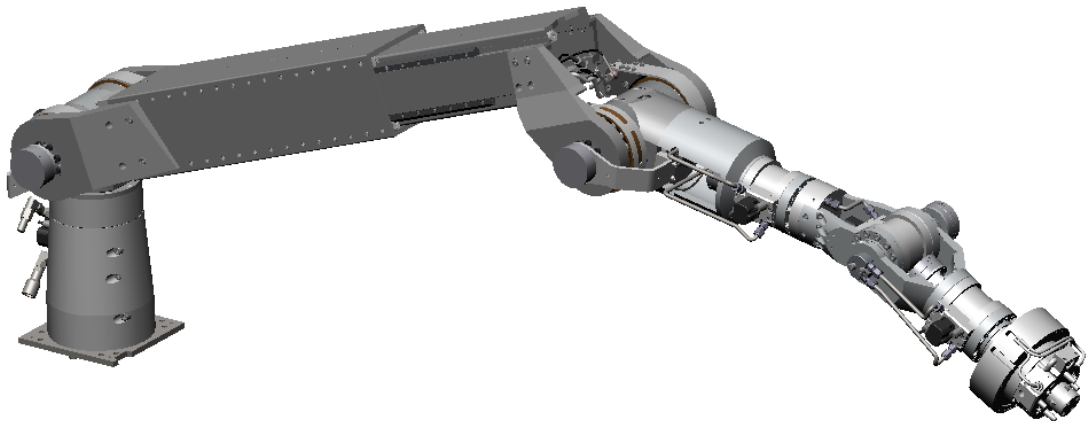


Figure 87: WHMAN with the new wrist design.

The redesign developed in this thesis was also suggested in [4] and an initial sketch for the redesign was presented. In that initial sketch, the wrist looks very compact and the actuators very small, more than in the new wrist design. The main design parameters of those actuators were shown in Figure 35 (the design called initial sketch).

Figure 37 showed a comparison between the main design parameters of the initial sketch design and the optimum design developed in this work (also there are some other designs). From the results presented in Chapter 4 one can appreciate that the size of the shaft radius (R2) in the optimum design is bigger than the shaft radius of the initial sketch design. The chamber length is exactly the same 50 mm and the chamber radius (R1) is just 2 mm bigger on the optimum design.

Based on the comparison of the main design characteristics, the 3D models of the two actuators (optimum and initial sketch design) should have very similar size and shape. However, they don't the main reason is that the initial sketch designs don't have many of the components like the bearings, the fluid passages, the valve block, the resolvers among others. These components have a huge impact into the final dimensioning of the actuators and the wrist.

One of the main tasks in this work was to redesign the wrist actuators, namely the water hydraulic vane actuators. It was noticed that the shaft of the water hydraulic vane actuator is the main component that defines the overall size of the actuator. There are, of course, some other factors but basically by defining the size for the shaft, other components can be developed. Because the shaft is designed based on the requirements, their definition is what determines the size of the actuators. In the current WHMAN wrist design, for example, the actuators are large because they were designed to meet certain requirements.

An approach to define the requirements as well as to resize the actuators is developed and reported in this work. As a result of the developed approach, smaller and lighter actuators were designed.

The actuators have a modularized design to have as many common parts as possible. For the three joints in the wrist there are two different actuators designs, one for joints 5 and 7 and other for joint 6. The only different component between these designs is the shaft. This makes less expensive to manufacture the actuators and reduces the testing time.

The assembly and maintenance process of the wrist were improved by having an easy access to the hydraulic valves and by decoupling the assembly of the actuators from the assembly of the wrist.

The 3D models of the actuators and the wrist were developed into fully detailed design level and have all the components that are required for operation. The detailed development of the models was a demanding and time consuming task. The results obtained in the validation of the wrist and actuators components are very satisfactory. The next step, as a continuation of this work, can be to build and test one of the new actuator designs.

Since this was a redesign work it was quite challenging to proceed with it because first it was necessary to understand the current wrist design and its complex design constrains. In general it was a challenging and time consuming work, but at the end the results are very satisfactory.

REFERENCES

- [1] International Thermonuclear Experimental Reactor, ITER, [website].
<http://www.iter.org/> [Referred 23.05.2011]
- [2] Salminen K., Suiko M., Karjalainen J., Sibois R. & Mattila J., Status of DPT2 – Test Facility for ITER Divertor Maintenance.
- [3] Mäkelä, A., 2006, “Development of Water Hydraulic Rotary Actuators for Robot Joint”, MSc Thesis, TUT, Automation Degree Program [119 p.]
- [4] Valkama, P., 2009, “Design of a six degree of freedom water hydraulic arm for remote handling”, MSc Thesis, TUT, Master’s Degree programme in Mechanical Engineering, [119 p.]
- [5] Marchand F., 2011, “Tooling concepts for WHMAN remote handling”, Msc Thesis [87 p.]
- [6] Parker Mexico [website]. <http://www.parker-mexico.com/hidraulica.html>
[Referred 2.07.2011]
- [7] Hydraulics and Pneumatics [website].
<http://www.hydraulicspneumatics.com/200/FPE/MotorsActuators/Article/True/6426/MotorsActuators> [Referred 31.03.2011]
- [8] R.C. Hibbeler, 2000, “Mechanics of Materials”, Fourth Edition. Prentice Hall.
- [9] Fonselius, J., Rinkinen, J. & Vilenius, M., Servotekniikka, Koneautomaatio, 1998. Helsinki. Oy Edita Ab. [194 p.]
- [10] John J. Craig, 2005, Introduction to Robotics, Mechanics and Control 3th Edition. Pearson Prentice Hall.
- [11] Rivin, Eugene I., “Mechanical Design of Robots”. McGraw-Hill.
- [12] Sciavicco L. and Siciliano B., “Modelling and Control of Robot Manipulator”, Second Edition. Springer.
- [13] Tsai, Lung-Wen, “Robot Analysis: the mechanics of serial and parallel manipulators”. John Wiley & Sons.

- [14] Yang, D.C.H., Rauchfuss J. 2001 “A New Zero-Dimension Robot Wrist: Design and Accessibility Analysis”. International Journal of Robotics Research Vol. 20, No 2, pp. 163-173.
- [15] Chandrupatla T., Belegundu A., “Introduction to Finite Elements in Engineering”, Third Edition. Prentice Hall.
- [16] MatWeb, Material Property Data [website]. <http://www.matweb.com/> [Referred 15.7.2011]
- [17] SKF Group [website]. <http://www.skf.com/portal/skf/home> [Referred 1.03.2011]
- [18] DSTI Dynamic Sealing Technologies, Inc. [website]. <http://www.dsti.com/products/rotary-union/> [Referred 10.04.2011]

APPENDIX A: DESIGN AND SYSTEM CHARACTERISTICS VANE ACTUATORS J5 & J7

Mechanic parameters

Young's Modulus	$E := 200\text{GPa}$	
Poisson's Ratio	$\nu := 0.3$	
Shear Modulus	$G := \frac{E}{2 \cdot (1 + \nu)}$	$G = 7.692 \times 10^{10} \text{ Pa}$
Yield strength	$\sigma := 590\text{MPa}$	
Moment of inertia	$I := 40\text{kg} \cdot \text{m}^2$	

Hydraulic parameters

Bulk Modulus	$B := 2100\text{MPa}$	
Nominal pressure	$p := 21\text{MPa}$	
Nominal flowrate	$Q := 6.8 \frac{\text{L}}{\text{min}}$	
Pipe volume	$V_L := \pi \cdot (1.5\text{mm})^2 \cdot 7\text{cm}$	$V_L = 4.948 \times 10^{-7} \text{ m}^3$
Motion range	$\theta := 280\text{deg}$	

Vane Actuator Main Design Parameters

Chamber Internal Radius	$R_1 := 41\text{mm}$
Shaft External Radius	$R_2 := 23\text{mm}$
Chamber length	$b := 50\text{mm}$

Shaft Design Parameters

Internal shaft radius	$C_{\text{int}} := 5.5\text{mm}$
Ext. shaft radius 1 (Min.)	$C_1 := 17.5\text{mm}$
Shaft length 1	$L_1 := 10\text{mm}$
Ext. shaft radius 2	$C_2 := 17.5\text{mm}$
Shaft length 2	$L_2 := 27\text{mm}$
Ext. shaft radius 3	$C_3 := 20\text{mm}$
Shaft length 3	$L_3 := 22.5\text{mm}$

Vane Actuator System Characteristics

<u>Theoretical output torque</u>	$T_o := 0.5 \cdot (R_1^2 - R_2^2) \cdot b \cdot p$	$T_o = 604.8 \text{ N}\cdot\text{m}$
<u>Max. Actuator speed</u>	$\omega := \frac{2 \cdot Q}{(R_1^2 - R_2^2) \cdot b}$	$\omega = 236.111 \frac{\text{rad}}{\text{min}}$
<u>Shear Stress (T_{xz})</u>	$\tau := \frac{2 \cdot T_o \cdot C_1}{\pi \cdot \left[(C_1)^4 - C_{int}^4 \right]}$	$\tau = 7.255 \times 10^7 \text{ Pa}$
<u>Shaft Factor of Safety</u>	$\text{FOS} := \frac{\sigma}{2 \cdot \tau}$	$\text{FOS} = 4.066$
<u>Mechanical torsion stiffness</u>	$K_s := \frac{1}{\frac{2}{\pi G} \left[\sum_{i=1}^3 \frac{L_i}{(C_i)^4 - C_{int}^4} \right]}$	$K_s = 2.238 \times 10^5 \cdot \frac{\text{N}\cdot\text{m}}{\text{rad}}$
<u>Angle of twist</u>	$\alpha := \frac{T_o}{K_s}$	$\alpha = 2.702 \times 10^{-3} \cdot \text{rad}$
<u>Cross-sectional area</u>	$\text{Area} := \pi \cdot (R_1^2 - R_2^2)$	$\text{Area} = 3.619 \times 10^{-3} \text{ m}^2$
<u>Volume capacity</u>	$\text{Volume} := \text{Area} \cdot b$	$\text{Volume} = 1.81 \times 10^{-4} \text{ m}^3$
<u>Radian volume</u>	$D := \frac{\text{Volume}}{2 \cdot \pi}$	$D = 2.88 \times 10^{-5} \text{ m}^3$
<u>Hydraulic torsion stiffness</u>	$K_h := \frac{4 \cdot D^2 \cdot B}{D \cdot \theta + V_L}$	$K_h = 4.933 \times 10^4 \cdot \frac{\text{N}\cdot\text{m}}{\text{rad}}$
<u>Stiffness Ratio</u>	$\text{SR} := \frac{K_s}{K_h}$	$\text{SR} = 4.537$
<u>Mechanical natural frequency</u>	$\omega_s := \sqrt{\frac{K_s}{I}}$	$\omega_s = 74.805 \frac{\text{rad}}{\text{sec}} \quad \omega_s = 11.906 \text{ Hz}$
<u>Hydraulic natural frequency</u>	$\omega_h := \sqrt{\frac{K_h}{I}}$	$\omega_h = 35.118 \frac{\text{rad}}{\text{sec}} \quad \omega_h = 5.589 \text{ Hz}$

APPENDIX B: DESIGN AND SYSTEM CHARACTERISTICS VANE ACTUATOR J6

Mechanic parameters

Young's Modulus	$E := 200 \text{ GPa}$	
Poisson's Ratio	$\nu := 0.3$	
Shear Modulus	$G := \frac{E}{2 \cdot (1 + \nu)}$	$G = 7.692 \times 10^{10} \text{ Pa}$
Yield strength	$\sigma := 590 \text{ MPa}$	
Moment of inertia	$I := 40 \text{ kg} \cdot \text{m}^2$	

Hydraulic parameters

Bulk Modulus	$B := 2100 \text{ MPa}$	
Nominal pressure	$p := 21 \text{ MPa}$	
Nominal flowrate	$Q := 6.8 \frac{\text{L}}{\text{min}}$	
Pipe volume	$V_L := \pi \cdot (1.5 \text{ mm})^2 \cdot 7 \text{ cm}$	$V_L = 4.948 \times 10^{-7} \text{ m}^3$
Motion range	$\theta := 280 \text{ deg}$	

Vane Actuator Main Design Parameters

Chamber Internal Radius	$R_1 := 41 \text{ mm}$
Shaft External Radius	$R_2 := 23 \text{ mm}$
Chamber length	$b := 50 \text{ mm}$

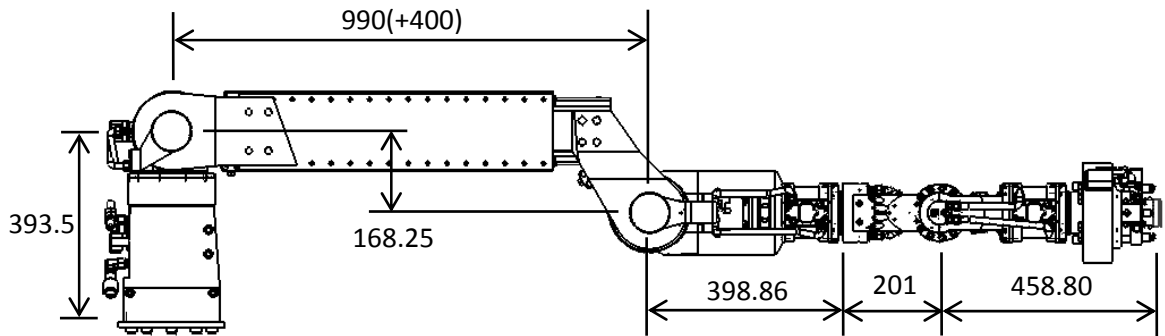
Shaft Design Parameters

Internal shaft radius	$C_{\text{int}} := 5.5 \text{ mm}$
Ext. shaft radius 1 (Min.)	$C_1 := 17 \text{ mm}$
Shaft length 1	$L_1 := 20 \text{ mm}$
Ext. shaft radius 2	$C_2 := 17.5 \text{ mm}$
Shaft length 2	$L_2 := 23.5 \text{ mm}$
Ext. shaft radius 3	$C_3 := 20 \text{ mm}$
Shaft length 3	$L_3 := 22.5 \text{ mm}$

Vane Actuator System Characteristics

<u>Theoretical output torque</u>	$T_o := 0.5 \cdot (R_1^2 - R_2^2) \cdot b \cdot p$	$T_o = 604.8 \text{ N}\cdot\text{m}$
<u>Max. Actuator speed</u>	$\omega := \frac{2 \cdot Q}{(R_1^2 - R_2^2) \cdot b}$	$\omega = 236.111 \frac{\text{rad}}{\text{min}}$
<u>Shear Stress (T_{XZ})</u>	$\tau := \frac{2 \cdot \left(\frac{T_o}{2}\right) C_1}{\pi \cdot \left[(C_1)^4 - C_{\text{int}}^4 \right]}$	$\tau = 3.962 \times 10^7 \text{ Pa}$
<u>Shaft Factor of Safety</u>	$\text{FOS} := \frac{\sigma}{2 \cdot \tau}$	$\text{FOS} = 7.446$
<u>Mechanical torsion stiffness</u>	$K_s := \frac{2}{\pi \cdot G \left[\sum_{i=1}^3 \frac{L_i}{(C_i)^4 - C_{\text{int}}^4} \right]}$	$K_s = 3.796 \times 10^5 \cdot \frac{\text{N}\cdot\text{m}}{\text{rad}}$
<u>Angle of twist</u>	$\alpha := \frac{T_o}{K_s}$	$\alpha = 1.593 \times 10^{-3} \cdot \text{rad}$
<u>Cross-sectional area</u>	$\text{Area} := \pi \cdot (R_1^2 - R_2^2)$	$\text{Area} = 3.619 \times 10^{-3} \text{ m}^2$
<u>Volume capacity</u>	$\text{Volume} := \text{Area} \cdot b$	$\text{Volume} = 1.81 \times 10^{-4} \text{ m}^3$
<u>Radian volume</u>	$D := \frac{\text{Volume}}{2 \cdot \pi}$	$D = 2.88 \times 10^{-5} \text{ m}^3$
<u>Hydraulic torsion stiffness</u>	$K_h := \frac{4 \cdot D^2 \cdot B}{D \cdot \theta + V_L}$	$K_h = 4.933 \times 10^4 \cdot \frac{\text{N}\cdot\text{m}}{\text{rad}}$
<u>Stiffness Ratio</u>	$\text{SR} := \frac{K_s}{K_h}$	$\text{SR} = 7.696$
<u>Mechanical natural frequency</u>	$\omega_s := \sqrt{\frac{K_s}{I}}$	$\omega_s = 97.42 \frac{\text{rad}}{\text{sec}} \quad \omega_s = 15.505 \text{ Hz}$
<u>Hydraulic natural frequency</u>	$\omega_h := \sqrt{\frac{K_h}{I}}$	$\omega_h = 35.118 \frac{\text{rad}}{\text{sec}} \quad \omega_h = 5.589 \text{ Hz}$

APPENDIX C: WORST LOAD CASE SCENARIO



Values regarding each link of the WHMAN

Mass	Center of mass	Link length	
$m_B := 31.6\text{kg}$	$y_{CB} := 137.6\text{mm}$	$y_B := 307\text{mm}$	
$m_1 := 23.18\text{kg}$	$y_{C1} := 89.2\text{mm}$	$y_1 := 393.5\text{mm} - y_B$	
$m_2 := 29.92\text{kg}$	$x_{C2} := 309.45\text{mm}$	$x_2 := 790\text{mm}$	$x_{2\text{offs}} := 140\text{mm}$
$m_3 := 27.53\text{kg}$	$x_{C3} := 650.66\text{mm}$	$x_3 := 850\text{mm}$	$y_3 := -168.25\text{mm}$
$m_4 := 32.46\text{kg}$	$x_{C4} := 98.51\text{mm}$	$x_4 := 398.86\text{mm}$	
$m_5 := 12.61\text{kg}$	$x_{C5} := 137.62\text{mm}$	$x_5 := 201\text{mm}$	
$m_6 := 23.22\text{kg}$	$x_{C6} := 269.08\text{mm}$	$x_6 := 458.80\text{mm}$	

Maximum forces applied to the end-effector

Initial values for the joint variables used in the analysis

$\theta_2 := 45\text{deg}$ Joint 2 variable

$d_3 := 0.2$ Joint 3 variable

$L_{24}(d_3) := (0.990 + d_3)\text{m}$ Length between Joint 2 and Joint 4

X and Y values from the origin of Joint 2 (Shoulder) to the origin of Joint 4 (Elbow)

$$x_{24}(\theta_2, d_3) := \cos(\theta_2) \cdot L_{24}(d_3) - \sin(\theta_2) \cdot y_3 \quad x_{24}(\theta_2, d_3) = 0.96\text{m}$$

$$y_{24}(\theta_2, d_3) := \sin(\theta_2) \cdot L_{24}(d_3) + \cos(\theta_2) \cdot y_3 \quad y_{24}(\theta_2, d_3) = 0.722\text{m}$$

Torque and force generated by the actuators in the analysis

$$M_{tJ1} := 2000\text{N}\cdot\text{m} \quad \text{Torque generated by the actuator in J1}$$

$$M_{tJ2} := 3900\text{N}\cdot\text{m} \quad \text{Torque generated by the actuator in J2}$$

$$F_{J3} := 2000\text{N} \quad \text{Force generated by the actuator in J3}$$

Moments due to the weight of the links

$$M_{tm2}(\theta_2) := m_2 \cdot g \cdot x_{C2} \cdot \cos(\theta_2)$$

$$M_{tm3}(\theta_2, d_3) := m_3 \cdot g \cdot (x_{2offs} + d_3 \cdot m + x_{C3}) \cdot \cos(\theta_2)$$

$$M_{tm4}(\theta_2, d_3) := m_4 \cdot g \cdot (x_{24}(\theta_2, d_3) + x_{C4})$$

$$M_{tm5}(\theta_2, d_3) := m_5 \cdot g \cdot (x_{24}(\theta_2, d_3) + x_4 + x_{C5})$$

$$M_{tm6}(\theta_2, d_3) := m_6 \cdot g \cdot (x_{24}(\theta_2, d_3) + x_4 + x_5 + x_{C6})$$

$$M_{tmtot}(\theta_2, d_3) := M_{tm2}(\theta_2) + M_{tm3}(\theta_2, d_3) + M_{tm4}(\theta_2, d_3) + M_{tm5}(\theta_2, d_3) + M_{tm6}(\theta_2, d_3)$$

$$M_{tmtot}(\theta_2, d_3) = 1192.08\text{N}\cdot\text{m}$$

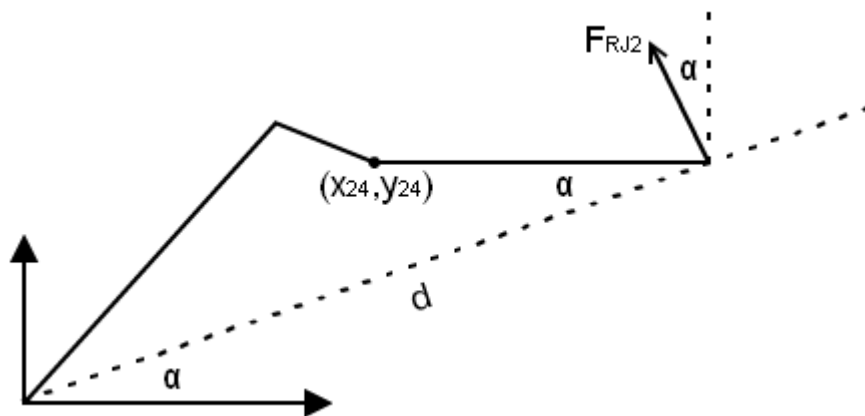
Moment due to the weight of the load

$$L_d := 100\text{kg}$$

$$M_{tLd}(\theta_2, d_3, L_d) := L_d \cdot g \cdot (x_{24}(\theta_2, d_3) + x_4 + x_5 + x_6)$$

$$M_{tLd}(\theta_2, d_3, L_d) = 1980.05\text{N}\cdot\text{m}$$

Force components of the resultant torque in Joint 2 (Shoulder)



Sum of moments in Joint 2 (Shoulder)

$$M_{tRJ2}(\theta_2, d_3, Ld) := M_{tJ2} - M_{tmtot}(\theta_2, d_3) - M_{tLd}(\theta_2, d_3, Ld) \quad M_{tRJ2}(\theta_2, d_3, Ld) = 727.87 \text{ N}\cdot\text{m}$$

$$d(\theta_2, d_3) := \sqrt{(x_{24}(\theta_2, d_3) + x_4 + x_5 + x_6)^2 + y_{24}(\theta_2, d_3)^2} \quad d(\theta_2, d_3) = 2144.46 \text{ mm}$$

$$\alpha(\theta_2, d_3) := \text{atan2}[(x_{24}(\theta_2, d_3) + x_4 + x_5 + x_6), y_{24}(\theta_2, d_3)] \quad \alpha(\theta_2, d_3) = 19.689 \text{ deg}$$

$$F_{RJ2}(\theta_2, d_3, Ld) := \frac{M_{tRJ2}(\theta_2, d_3, Ld)}{d(\theta_2, d_3)} \quad F_{RJ2}(\theta_2, d_3, Ld) = 339.42 \text{ N}$$

$$F_{RJ2x}(\theta_2, d_3, Ld) := -F_{RJ2}(\theta_2, d_3, Ld) \cdot \sin(\alpha(\theta_2, d_3)) \quad F_{RJ2x}(\theta_2, d_3, Ld) = -114.353 \text{ N}$$

$$F_{RJ2y}(\theta_2, d_3, Ld) := F_{RJ2}(\theta_2, d_3, Ld) \cdot \cos(\alpha(\theta_2, d_3)) \quad F_{RJ2y}(\theta_2, d_3, Ld) = 319.57 \text{ N}$$

Force components of the torque generate by the actuator in Joint 1 (Base)

$$F_{J1x}(\theta_2, d_3) := \frac{M_{tJ1}}{x_{24}(\theta_2, d_3) + x_4 + x_5 + x_6} \quad F_{J1x}(\theta_2, d_3) = 990.55 \text{ N}$$

Force components of the force generate by the actuator in Joint 3 (Cylinder)

$$F_{J3x}(\theta_2) := F_{J3} \cdot \cos(\theta_2) \quad F_{J3x}(\theta_2) = 1414.21 \text{ N}$$

$$F_{J3y}(\theta_2) := F_{J3} \cdot \sin(\theta_2) \quad F_{J3y}(\theta_2) = 1414.21 \text{ N}$$

Forces in x, y and z acting in the end-effector

$$F_x(\theta_2, d_3, Ld) := F_{RJ2x}(\theta_2, d_3, Ld) + F_{J3x}(\theta_2) \quad F_x(\theta_2, d_3, Ld) = 1299.86 \text{ N}$$

$$F_y(\theta_2, d_3, Ld) := F_{RJ2y}(\theta_2, d_3, Ld) + F_{J3y}(\theta_2) \quad F_y(\theta_2, d_3, Ld) = 1733.79 \text{ N}$$

$$F_z(\theta_2, d_3) := F_{J1z}(\theta_2, d_3) \quad F_z(\theta_2, d_3) = 990.55 \text{ N}$$

$$F_R(\theta_2, d_3) := \sqrt{F_x(\theta_2, d_3, Ld)^2 + F_y(\theta_2, d_3, Ld)^2 + F_z(\theta_2, d_3)^2} \quad F_R(\theta_2, d_3) = 2382.61 \text{ N}$$

To compute the values of the two joint variables used in the analysis (θ_2 and d_3), which will make to have the worst load case.

Given

$$-30\text{deg} \leq \theta_2 \leq 90\text{deg}$$

$$0 \leq d_3 \leq 0.4$$

$$0\text{N} \leq F_y(\theta_2, d_3, Ld) \leq 981\text{N}$$

$$J_{\text{values}} := \text{Maximize}(F_R, \theta_2, d_3) \quad J_{\text{values}} = \begin{pmatrix} 0.34 \\ 0 \end{pmatrix}$$

$$\theta_{2_} := J_{\text{values}}_0 \quad \theta_{2_} = 19.497\text{deg}$$

$$d_{3_} := J_{\text{values}}_1 \quad d_{3_} = 0$$

$$F_x(\theta_{2_}, d_{3_}, Ld) = 1859.02\text{N}$$

$$F_y(\theta_{2_}, d_{3_}, Ld) = 981\text{N}$$

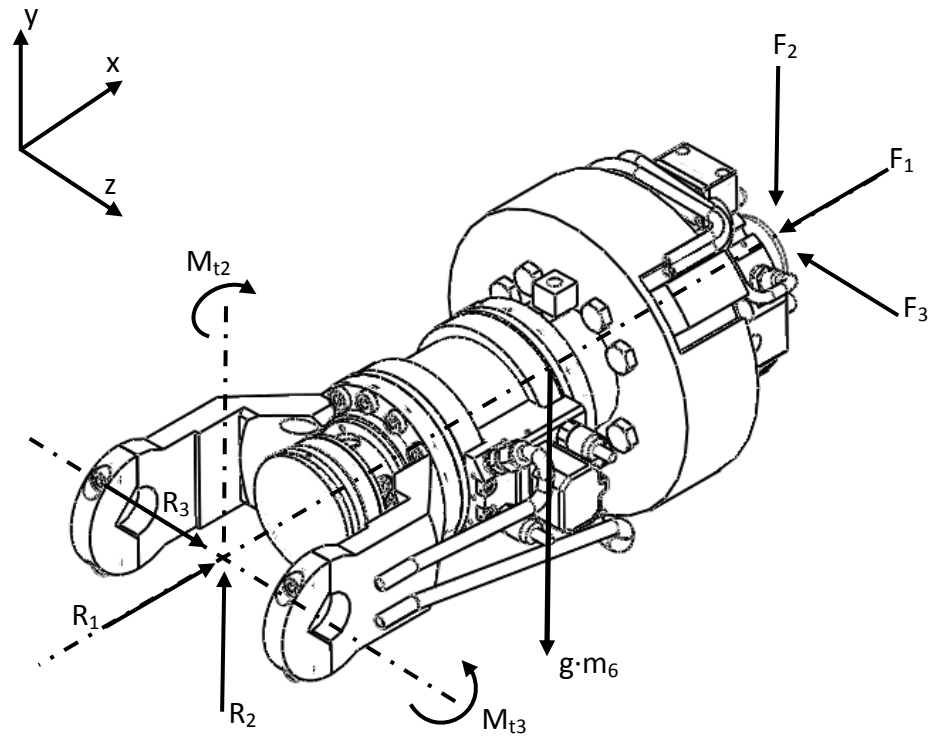
$$F_z(\theta_{2_}, d_{3_}) = 976.54\text{N}$$

$$F_{R_}(\theta_2, d_3) := \sqrt{F_x(\theta_{2_}, d_{3_}, Ld)^2 + F_y(\theta_{2_}, d_{3_}, Ld)^2 + F_z(\theta_{2_}, d_{3_})^2}$$

$$F_{R_}(\theta_2, d_3) = 2317.75\text{N}$$

APPENDIX D: FREE BODY DIAGRAMS

Free body diagram of Link 6 with the force and torque sensor



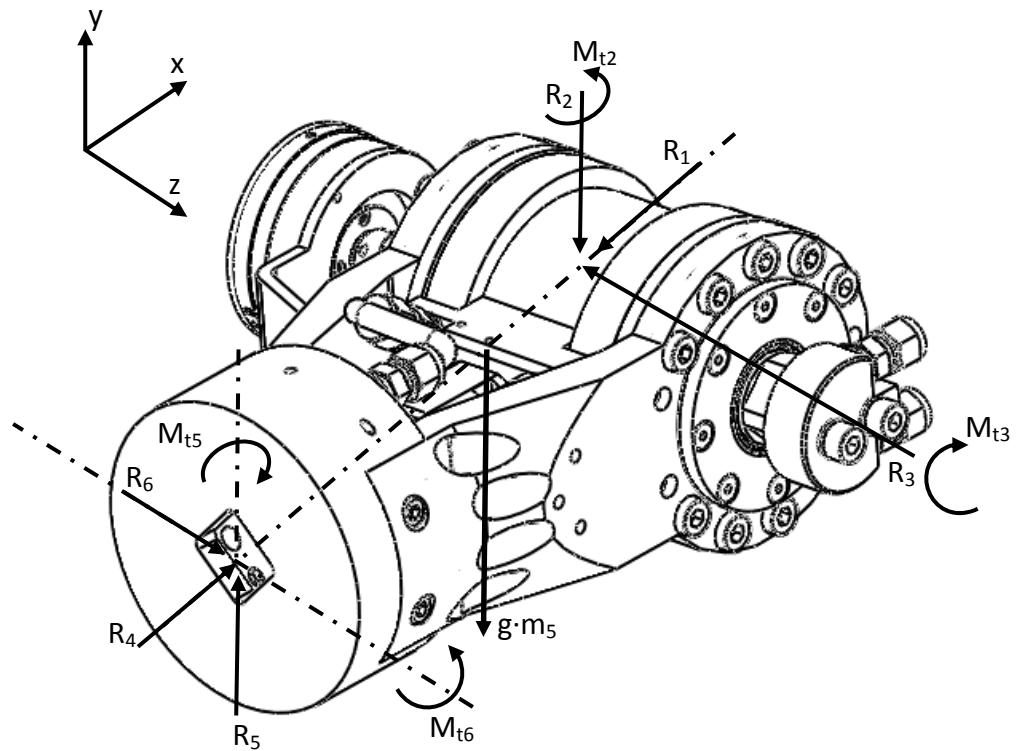
Sum of forces and torques

$$\begin{aligned}
 F_x = R_1 - F_1 &= 0 & M_x &= 0 \\
 F_y = R_2 - F_2 - g \cdot m_6 &= 0 & M_y &= -M_{t2} + F_3 \cdot x_6 = 0 \\
 F_z = R_3 - F_3 &= 0 & M_z &= M_{t3} - F_2 \cdot x_6 - g \cdot m_6 \cdot x_{C6} = 0
 \end{aligned}$$

Reactions

$$\begin{aligned}
 R_1 &= 1859 \text{ N} & M_{t1} &= 0 \\
 R_2 &= 1208 \text{ N} & M_{t2} &= 448 \text{ Nm} \\
 R_3 &= 976 \text{ N} & M_{t3} &= 511 \text{ Nm}
 \end{aligned}$$

Free body diagram of Link 5



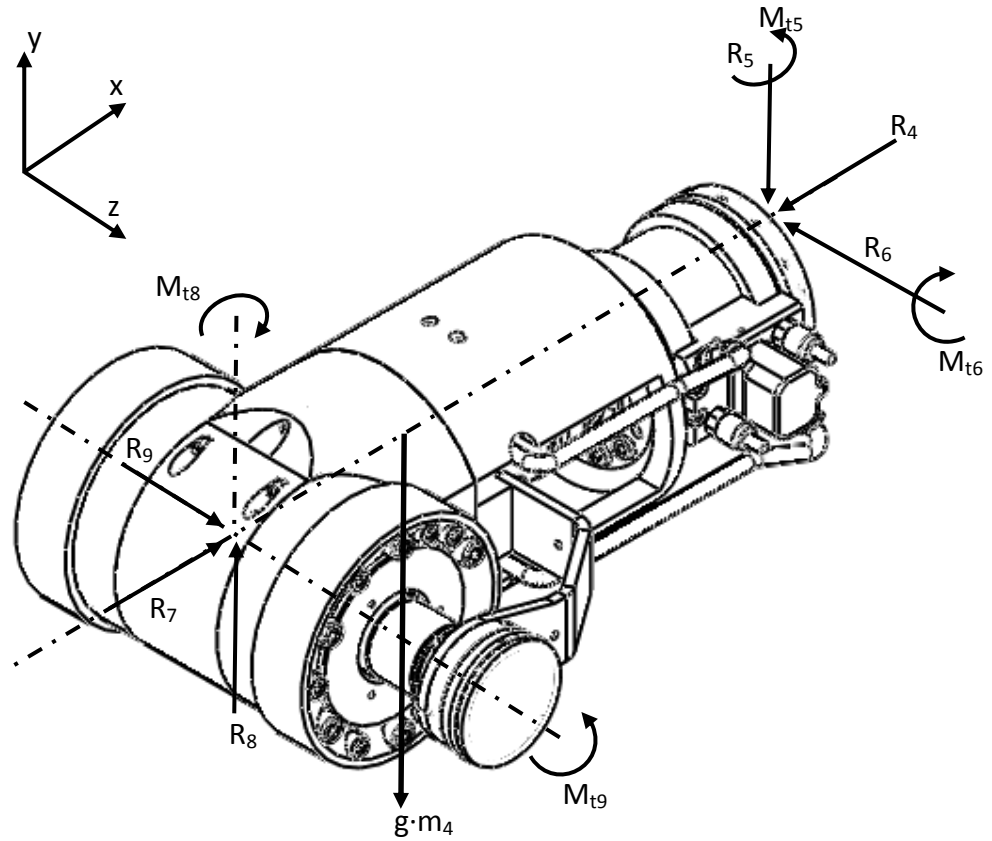
Sum of forces and torques

$$\begin{aligned}
 F_x &= R_4 - R_1 = 0 & M_x &= 0 \\
 F_y &= R_5 - R_2 - g \cdot m_5 = 0 & M_{ty} &= -M_{t5} + M_{t2} + R_3 \cdot x_5 = 0 \\
 F_z &= R_6 - R_3 = 0 & M_z &= M_{t6} - M_{t3} - R_2 \cdot x_5 - g \cdot m_5 \cdot x_{c5} = 0
 \end{aligned}$$

Reactions

$$\begin{aligned}
 R_4 &= 1859 \text{ N} & M_{t4} &= 0 \\
 R_5 &= 1332 \text{ N} & M_{t5} &= 644 \text{ Nm} \\
 R_6 &= 976 \text{ N} & M_{t6} &= 771 \text{ Nm}
 \end{aligned}$$

Free body diagram of Link 4



Sum of forces and torques

$$\begin{aligned}
 F_x &= R_7 - R_4 = 0 & M_x &= 0 \\
 F_y &= R_8 - R_5 - g \cdot m_4 = 0 & M_y &= -M_{t8} + M_{t5} + R_6 \cdot x_4 = 0 \\
 F_z &= R_9 - R_6 = 0 & M_z &= M_{t9} - M_{t6} - R_5 \cdot x_4 - g \cdot m_4 \cdot x_{C4} = 0
 \end{aligned}$$

Reactions

$$\begin{aligned}
 R_7 &= 1859 \text{ N} & M_{t7} &= 0 \\
 R_8 &= 1650 \text{ N} & M_{t8} &= 1033 \text{ Nm} \\
 R_9 &= 976 \text{ N} & M_{t9} &= 1334 \text{ Nm}
 \end{aligned}$$